



8-1999

[Capillary electrophoresis and immobilization strategies research]

Timothy Jack Gibson

Follow this and additional works at: https://trace.tennessee.edu/utk_graddiss

Recommended Citation

Gibson, Timothy Jack, "[Capillary electrophoresis and immobilization strategies research]. " PhD diss., University of Tennessee, 1999.
https://trace.tennessee.edu/utk_graddiss/8823

This Dissertation is brought to you for free and open access by the Graduate School at TRACE: Tennessee Research and Creative Exchange. It has been accepted for inclusion in Doctoral Dissertations by an authorized administrator of TRACE: Tennessee Research and Creative Exchange. For more information, please contact trace@utk.edu.

To the Graduate Council:

I am submitting herewith a dissertation written by Timothy Jack Gibson entitled "[Capillary electrophoresis and immobilization strategies research]." I have examined the final electronic copy of this dissertation for form and content and recommend that it be accepted in partial fulfillment of the requirements for the degree of Doctor of Philosophy, with a major in Chemistry.

Michael J. Sepaniak, Major Professor

We have read this dissertation and recommend its acceptance:

David C. Joy

Accepted for the Council:

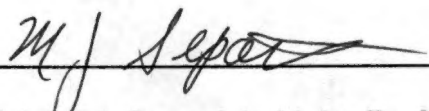
Carolyn R. Hodges

Vice Provost and Dean of the Graduate School

(Original signatures are on file with official student records.)

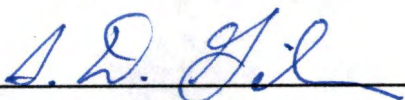
To the Graduate Council:

I am submitting herewith a dissertation written by Timothy Jack Gibson entitled "I. Evaluation of Fundamental Processes and Performance for the Separation of DNA Fragments by Capillary Electrophoresis; II. Evaluation of Immobilization Strategies for Polymeric Stationary Phases for Microsensor Determinations of Semivolatile Organic Compounds". I have examined the final copy of this dissertation for form and content and recommend that it be accepted in partial fulfillment of the requirements for the degree of Doctor of Philosophy, with a major in Chemistry.



Michael J. Sepaniak, Major Professor

We have read this dissertation
and recommend its acceptance:



Accepted for the Council:



Associate Vice Chancellor and

Dean of the Graduate School

- I. Evaluation of Fundamental Processes and Performance for the Separation of DNA Fragments by Capillary Electrophoresis

- II. Evaluation of Immobilization Strategies for Polymeric Stationary Phases for Microsensor Determinations of Semivolatile Organic Compounds

A Dissertation Presented for the
Doctor of Philosophy Degree
The University of Tennessee, Knoxville

Timothy Jack Gibson

August 1999

Dedication

in memory of my mother

Acknowledgments

There are many people to thank for making this possible but most important was the support of my family. My mother's faith and encouragement gave me the determination to undertake this endeavor. I thank my brother Jeff for being there for me, especially at my most difficult times, and my dad for his support and encouragement. I thank my grandparents for always being there, and for being stronger than ever before when I needed it most.

To my friends, I thank you for the occasional intellectual discussions and the frequent "marginal" discussions. I especially thank Mike Stebbins, Brian Clark, Will Nirode, Jeremy Headrick, Kris Scaboo, and Adam Mullenix for their friendship and assistance.

I am very grateful to have a friend like Tracy Staller whose assistance in the lab was far more helpful and appreciated than he realizes. I am also very grateful for Patti Hancock whose enduring friendship through the years and across the miles means a lot to me.

I wish to thank the faculty and staff of the chemistry department for the education, services, and financial support that gave me the necessary resources to pursue my research. I also thank Drs. David and Carolyn Joy in the Biochemistry and Cellular and Molecular Biology Department for their assistance with the scanning electron microscopy work presented in this dissertation.

Finally, I wish to thank Dr. Mike Sepaniak for his advice, ideas, guidance, and for providing the supplies, equipment, and financial support which made all of this possible. Thank you.

Abstract

During the past few decades, the development of chromatography and electrophoresis has been an essential factor for the significant advancements achieved in biotechnology. Today, efforts continue to improve upon the accuracy, speed, and precision of these methods. DNA analysis by capillary electrophoresis (CE) is a good example of how the best attributes of different methods can be brought together to develop analytical methodology that offers significant improvements over existing technology. Despite the many attributes of CE, method validation continues to be problematic. In order to reproducibly achieve high efficiency and good resolution of DNA fragments, deactivating the surface of the separation column is essential. There exist many variations to the original method first suggested in 1985 by Stellan Hjerten. In this work, scanning electron microscopy (SEM) was utilized to examine various columns coated with non cross-linked polyacrylamide. At very low concentrations of acrylamide (~2.5%), no noticeable polymer layer is present. However, as the concentration of acrylamide exceeds 2.5%, a noticeable thickness and non-uniformity is observed. The use of coated columns can then be employed for the size-selective capillary electrophoresis (SSCE) separations of DNA fragments. Since the development of this method in the early 1990's, several papers have discussed the theoretical aspects of utilizing aqueous solutions of soluble polymers for the separation of DNA fragments. However, the instrumentation required to directly evaluate fundamental processes such as variance in SSCE

has been limited by the lack of novel instrumentation necessary to perform these experiments. In this work, experimental measurements of variance under static and dynamic conditions are reported. The determination of static diffusion coefficients and their contribution to total band variance is reported. The fact that diffusion accounts for less than half of the total variance observed led to the conclusion that other processes occurring during DNA fragments separations (i.e., DNA – polymer entanglement/disentanglement interactions) contribute significantly to band variance. Upon optimizing conditions for DNA analyses by SSCE, a novel class of cyanine intercalation dyes reported to offer superior fluorescence sensitivity relative to ethidium bromide was also evaluated in this work. Despite an improvement in sensitivity of DNA/dye complexes when employing the cyanine intercalation dyes, the labeling mechanisms and kinetics proved to be problematic in achieving appreciably lower detection limits by CE.

In another area of research, the potential of utilizing modestly selective stationary phases on microsensors was evaluated. Phases commonly employed in gas chromatography (GC) and liquid chromatography (LC) were bonded onto prepared silicon substrates. The relative affinity and selectivity of these phases for semivolatile organic compounds was determined by exposing these “sensors” to solutions followed by analysis by gas chromatography/mass spectrometry (GC/MS). It was found that improving wettability of the substrate prior to phase deposition was essential to achieve uniform films. Although the relative affinity and selectivity of these films are modest, these phases may be suitable for part of a higher-order, generalized approach to sensing.

Organization

In Part I of this dissertation, research describing the evaluation and application of CE for DNA analysis is detailed in Chapter 1-5.

Chapter 1 is intended to introduce the reader to the fundamentals of free-solution CE. Though significant modifications to this method are necessary for DNA analysis, it would be quite confusing to introduce the reader directly to this information without a cursory background. Along this same line, this chapter is also intended to introduce the reader to the fundamentals of DNA analysis by CE; a more exhaustive discussion of this topic will follow in Chapters 3 and 4.

Chapter 2 discusses the preparation of modified columns necessary for SSCE separations for DNA analysis. The major focus of this chapter is the evaluation of coated columns by scanning electron microscopy.

Chapter 3 details an evaluation of the fundamental processes occurring during SSCE of DNA fragments. Various experimental conditions are examined though it is the actual separation process during this technique which is most carefully evaluated; the contribution of this process to variance is discussed.

Chapter 4 details an evaluation of a novel class of DNA intercalation dyes. These dyes are reported to offer superior fluorescence sensitivity relative to such traditional dyes as ethidium bromide. However, the dynamics of a CE experiment may not always make this technique suitable for dyes of unique binding modes. Results from the evaluation of these dyes are presented.

Chapter 5 summarizes key points from the work presented in chapter 2-4 and offers some insight into the future direction and application of CE in biotechnology.

In Part II of this dissertation, the evaluation of modestly selective stationary phases on microsensors for the determination of semivolatile organic compounds is described. Chapter 6 is an inclusive chapter which covers an introduction, experimental procedures, results and discussion, and conclusions from this research project.

Table of Contents

Part I: Evaluation of Fundamental Processes and Performance for the Separation of DNA Fragments by Capillary Electrophoresis

Chapter 1: Introduction to CE and DNA Analysis.....	2
History and development of CE.....	3
Fundamentals of CE.....	7
<i>intrinsic electrophoretic mobility</i>	7
<i>electroosmotic flow</i>	8
<i>observed electrophoretic mobility</i>	9
Separation figures of merit.....	11
<i>efficiency</i>	11
<i>resolution</i>	14
Basic CE experiment.....	15
Electrophoretic separation of DNA fragments.....	20
<i>theory of migration</i>	20
<i>capillary gel electrophoresis</i>	21
<i>size-selective capillary electrophoresis</i>	22
Statement of problem.....	23

Chapter 2: Examination of Non Cross-linked Polyacrylamide

Coated Columns by Scanning Electron Microscopy.....	25
Introduction.....	25
Experimental.....	30
<i>materials</i>	30
<i>column preparation</i>	30
<i>instrumentation</i>	31
<i>SEM micrographs</i>	31
Results and discussion.....	32
Conclusions.....	36

Chapter 3: Examination of Band Dispersion during Size-

Selective Capillary Electrophoresis of DNA Fragments.....	38
Theory of DNA migration.....	38
<i>Ogston migration model</i>	38
<i>biased reptation migration model</i>	39
Theory of polymers employed in SSCE.....	42
<i>effect of concentration</i>	42
Band dispersion during SSCE of DNA fragments.....	45
Experimental.....	50
<i>materials</i>	50
<i>column and solution preparation</i>	50

<i>apparatus</i>	51
<i>methods</i>	53
Results and discussion.....	54
Conclusions.....	65

**Chapter 4: The Use of Cyanine Intercalation Dyes for Laser
Induced Fluorescence Detection of DNA Fragments by**

Capillary Electrophoresis	72
Introduction.....	72
Experimental.....	81
<i>materials</i>	81
<i>column preparation</i>	82
<i>solution preparation</i>	82
<i>instrumentation</i>	82
Results and discussion.....	85
<i>effect of buffer on separation performance</i>	85
<i>sensitivity and LOD</i>	91
<i>evaluation of sheath flow cell for postcolumn labeling of DNA fragments</i>	95
Conclusions.....	101

Chapter 5: Concluding Remarks: Future of CE for DNA

Analysis..... 103

Part II: Evaluation of Immobilization Strategies for Polymeric Stationary Phases for Microsensor Determinations of Semivolatile Organic Compounds

Chapter 6: Evaluation of Immobilization Strategies for

Polymeric Stationary Phases for Microsensor Determinations of

Semivolatile Organic Compounds..... 109

Introduction..... 109

Experimental..... 115

reagents and solutions..... 115

instrumentation and methods..... 116

Results and discussion..... 120

substrate preparation..... 120

vapor-phase deposition of GC phases..... 125

reaction coating of LC phases..... 126

GC/MS analysis..... 127

evaluation of affinity and selectivity of polymeric phases..... 131

Conclusions..... 138

References	141
Appendix	151
Vita	154

Figures

	Page
1.1 Moving boundary electrophoresis.....	4
1.2 Zone electrophoresis.....	5
1.3 Flow profiles in CE and LC methods.....	10
1.4 Instrumental set-up for basic CE experiment.....	16
2.1 Reaction scheme for coating columns with non cross-linked polyacrylamide.....	27
2.2 Computer scanned images of scanning electron microscopy micrographs of capillary columns.....	33
2.3 Additional SEM micrographs of capillary columns.....	35
3.1 Structure of DNA.....	40
3.2 Effect of concentration on polymer entanglement.....	43
3.3 Effect of field strength on peak efficiency.....	47
3.4 Spatial scanning CE instrument.....	52
3.5 SSCE separation of ϕ x-174 Hae III digest.....	55
3.6 Scans performed for the determination of static diffusion coefficients.....	57
3.7 Scans performed for the determination of dispersion coefficients..	58
3.8 Relationship between diffusion of DNA fragments and viscosity of entangled polymer solutions.....	60
3.9 Relationship between mobility and field strength.....	63

3.10	Effect of fragment size on diffusion and dispersion.....	67
3.11	Effect of field strength on band dispersion.....	68
4.1	Absorbance and fluorescence detection of DNA fragments separated by CE.....	73
4.2	Structures of DNA intercalation dyes.....	77
4.3	Sheath flow cell for postcolumn derivitization.....	84
4.4	Separation of DNA digest in methyl cellulose with TBE buffer.....	86
4.5	Separation of DNA digest in methyl cellulose with TAPS buffer.....	87
4.6	Separation of DNA digest in methyl cellulose with PO-PRO-3.....	90
4.7	Effect of laser power and field strength on background fluorescence from unintercalated dye in the running buffer.....	94
4.8	Labeling time for complete intercalation of dyes.....	97
6.1	Two-chamber vapor-deposition apparatus.....	118
6.2	SEM micrographs of films deposited onto silicon substrates.....	121
6.3	SEM micrographs of films deposited onto silicon after extended cleaning for improved wetting.....	124
6.4	Structures of semivolatile organic compounds.....	128
6.5	GC chromatogram of mixture of semivolatile organic compounds..	132
6.6	Calibration curve to correlate GC/MS peak area to quantity injected.....	133

Tables

	Page
3.1 Mobility of DNA Fragments in Methyl Cellulose Solutions.....	62
3.2 Diffusion/Dispersion Coefficients.....	64
3.3 Diffusion/Dispersion Coefficient of 603 bp Fragment in Different Methyl Cellulose Solutions.....	66
4.1 Spectral Properties of Intercalation Dyes and DNA/Dye Complexes.....	78
4.2 Buffer Effects on Separation Performance and Sensitivity.....	88
4.3 Detection Limits of 310 bp Fragment.....	93
4.4 Continuous Infusion of Premixed Sample through Sheath Flow Cell.....	98
4.5 Continuous Injection of DNA Labeled Postcolumn in Sheath Flow Cell.....	100
6.1 Affinity and Selectivity of Stationary Phases on Silicon Substrates...	129
6.2 Film Thickness and Distribution Coefficients for GC Phases	137

Abbreviations and Symbols

		Page
A	absorbance.....	19
a	radius of ion.....	7
AP	ammonium persulfate.....	30
Ar ⁺	argon laser.....	82
b	detection pathlength.....	19
bp	base pairs (of DNA fragment).....	39
C	sample concentration.....	19
C*	polymer entanglement threshold.....	44
CE	capillary electrophoresis.....	2
CGE	capillary gel electrophoresis.....	21
D	diffusion coefficient.....	13
D ⁰	static diffusion coefficient.....	49
D ^E	kinetic diffusion (dispersion) coefficient.....	49
E	applied electrical field.....	7
ε	permittivity constant;	9;
	molar absorbtivity.....	19
EB	ethidium bromide.....	50
EDTA	ethylenediaminetetraacetic acid.....	50
EOF	electroosmotic flow.....	9

f	frictional coefficient.....	8
F'	direct force exerted upon ion.....	7
F''	counteracting force on ion.....	7
GC/MS	gas chromatography/mass spectrometry.....	116
γ -MTMS	γ -methacryloxypropyltrimethoxysilane.....	30
H	plate height.....	11
η	viscosity.....	9
He-Ne	helium-neon (laser).....	51
i.d.	inner-diameter (of column).....	6
I_0	excitation source intensity.....	19
I_f	fluorescence intensity.....	19
k	Boltzmann constant.....	48
L	length of column.....	7
LC	liquid chromatography.....	9
L_d	length to detector.....	55
LOD	limit of detection.....	19
MC	methyl cellulose.....	50
μ_{eof}	mobility of electroosmotic flow.....	9
μ_{int}	intrinsic electrophoretic mobility.....	8
M_n	monomer molecular weight.....	50
μ_{obs}	observed electrophoretic mobility.....	11

N	efficiency;.....	11
	number of DNA base pairs.....	20
NPe ₄ ⁺	tetrapentylammonium cation.....	80
PAGE	polyacrylamide gel electrophoresis.....	21
PMT	photomultiplier tube.....	53
q	charge on ion.....	7
Q	quantity of solute injected.....	17
QCM	quartz crystal microbalance.....	110
R _f	response factor.....	88
R _s	resolution.....	15
S/N	signal to noise ratio.....	89
σ ²	variance.....	11
SEM	scanning electron microscopy.....	28
SGE	slab gel electrophoresis.....	21
SIM	selected ion monitoring.....	119
SSCE	size-selective capillary electrophoresis.....	22
T	absolute temperature.....	48
t	time.....	13
TAPS	N-tri(hydroxymethyl)methyl-3-aminopropylsulfonic acid.....	81
TBE	tris-boric acid-EDTA.....	50
TEMED	N,N,N',N'-tetramethylethylenediamine.....	30

V	volts;	7;
	volume injected.....	17
v	velocity of ion.....	8
w	width of peak at base.....	15
w _{1/2}	width of peak at half-height.....	14
WD	working distance.....	33
ζ	zeta potential.....	9
9-AA	9-aminoacridine.....	79

**I. Evaluation of Fundamental Processes and
Performance for the Separation of DNA
Fragments by Capillary Electrophoresis**

-Chapter 1- Introduction to CE and DNA Analysis

As the demands to solve more complex biotechnological problems increase, the need to develop novel analytical techniques becomes more essential. Today, the demands upon an analytical chemist are to develop techniques that offer improvements in speed, precision, and sensitivity. Pharmaceutical production, forensic analysis, medical research, and environmental assessment labs benefit from the advancement of technology that facilitates higher sample through-put, a high degree of reproducibility, and the ability to explore proteins, enzymes, and nucleic acids at the molecular level.

An excellent example of this complementary relationship between analytical chemistry and associated disciplines of science is the impact that the development and advancement of separation sciences have had on the biological sciences. Chromatography and electrophoresis have been essential factors to the biotechnology boom evidenced in the past few decades. One particular area of research that has especially benefited from the development of separation techniques is the analysis of DNA. The significance of being able to characterize and identify DNA fragments in such areas as disease research and criminal investigations cannot be overstated. For over 25 years, slab gel electrophoresis has been used to separate and aid in the identification of DNA digest fragments. Recently, a significantly modified technique has shown great potential in offering significant advancements in this area of analytical research; this technique is termed capillary electrophoresis (CE).

History and development of CE

The development of electrophoresis may be traced back to 1930 to the work of the Swedish chemist Arne Tiselius who demonstrated that proteins could be separated from mixtures based on the electrical charges on their surfaces (1). The potential of this emerging technology may have first been demonstrated in 1947 when Linus Pauling used electrophoresis to elucidate the cause of sickle-cell anemia, a contribution that many argue should have resulted in Pauling winning a Noble prize in medicine (2). However, in 1948, it was Arne Tiselius who was awarded the Nobel Prize in Chemistry for his electrophoresis technique that was beginning to show great promise as a research tool.

During the early years of electrophoresis, the technique was applied to samples to identify one or possibly two major components (Figure 1.1). In 1958, the theory of applying a potential to a small sample of a solution to separate analytes into distinct zones was introduced by Stellan Hjerten (3). Hjerten reported that under an applied electric field, analytes in solution migrate at different rates and will eventually form distinct zones (Figure 1.2).

Hjerten's method to obtain distinct analyte zones was dependent upon the ability to achieve resolution between different compounds. However, for the electrophoretic separation to occur, one must apply an electrical field to the system to induce a separation between analytes based on a property of the analytes, i.e., their electrical charge to size ratio. In doing so, the system is heated and, as a result, thermal gradients occur within the system and resolution is degraded. For several years, efforts were focused on methods to reduce the

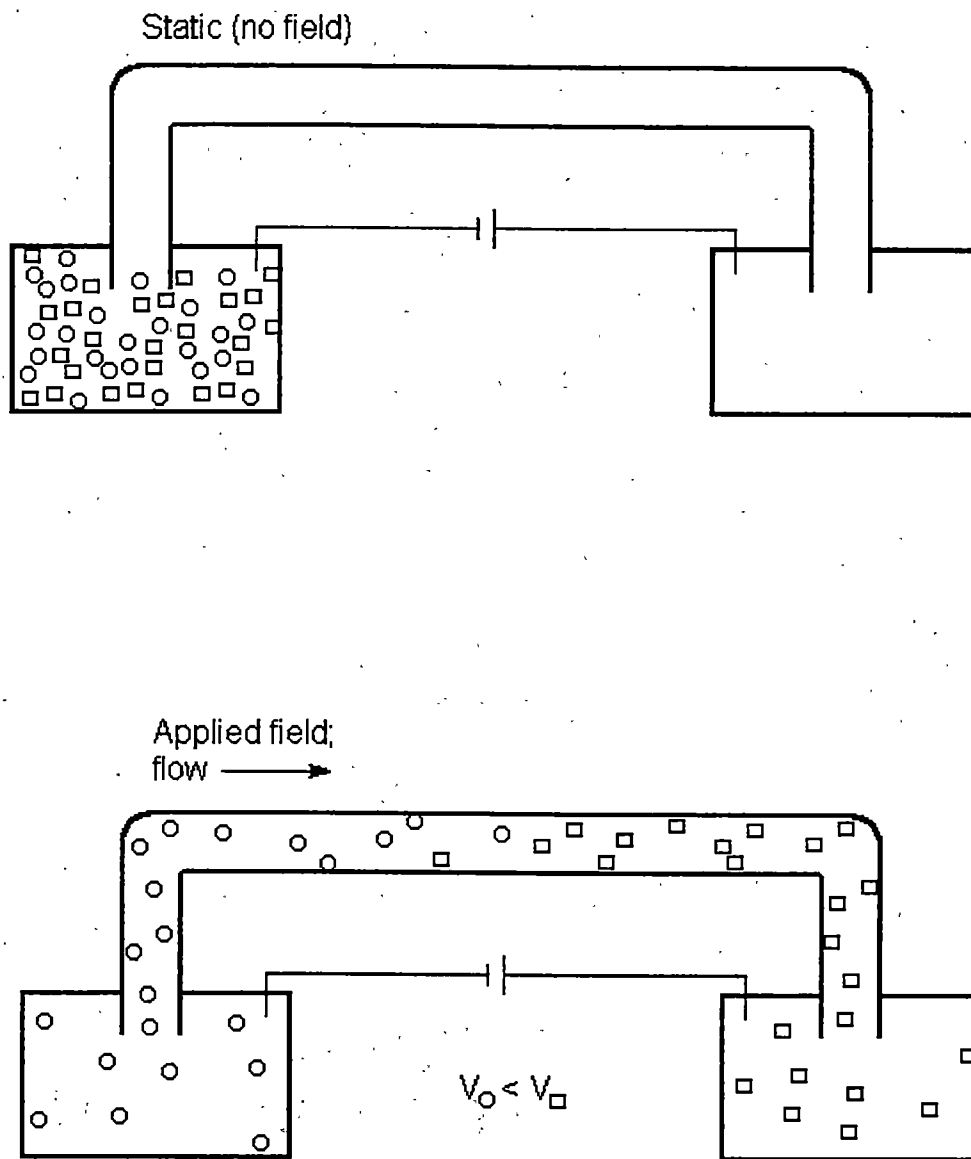


Figure 1.1: Moving boundary electrophoresis. A field is applied to a simple mixture and the components are fractionated based upon the difference in their migration rates.

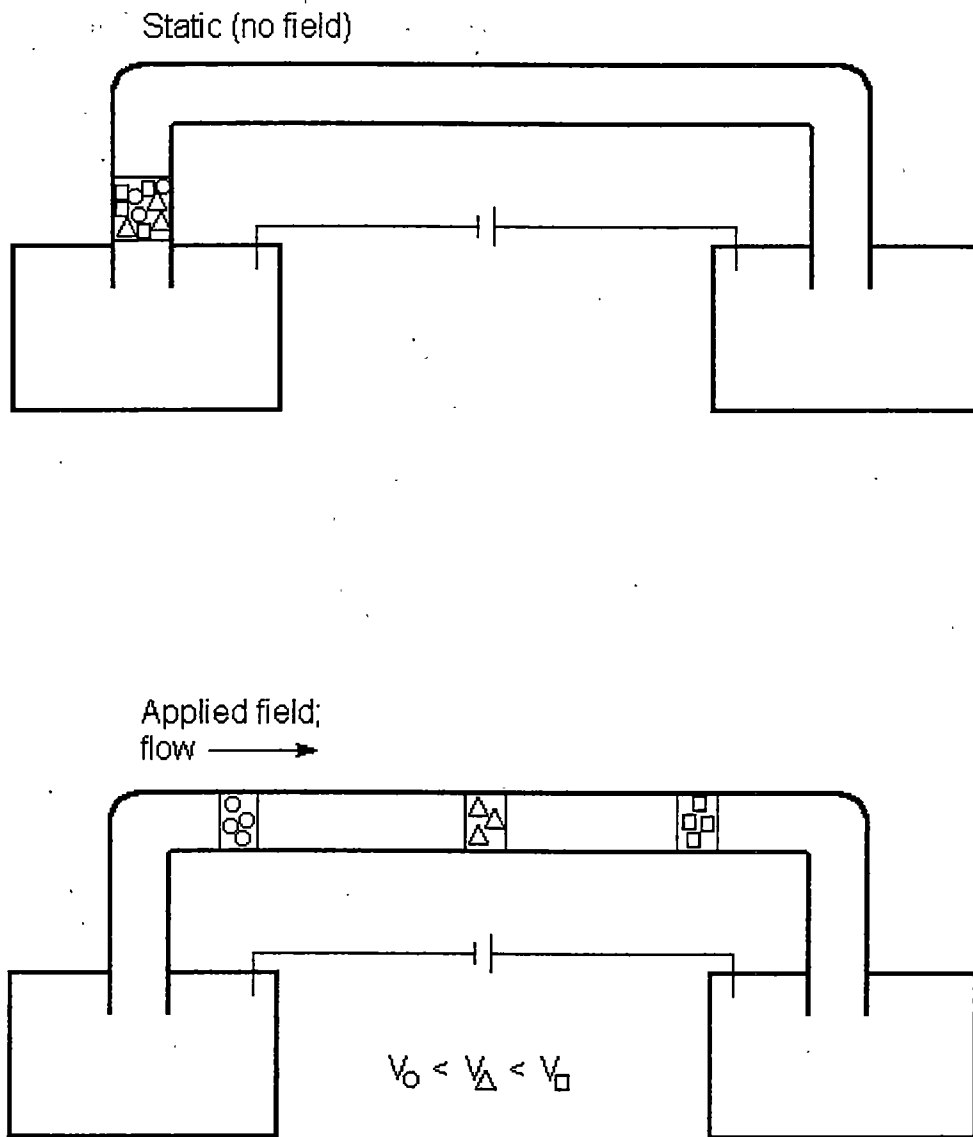


Figure 1.2: Zone electrophoresis. (top) a plug of sample is introduced into the column; (bottom) at some time after applying a field, the analytes form distinct zones based upon their migration rates.

deleterious effects of Joule heating. In 1967, it was Hjerten who again made a major development to this emerging technology. Hjerten proposed the use of columns of smaller inner-diameter (i.d.) so that the increased surface area of the column would permit the efficient dissipation of heat from solution (4). However, column size reduction was limited by detector technology, thus, Hjerten was only able to reduce column size to 3 mm. In the following years, improvements were made such that 200-500 μm diameter glass tubes with potentiometric detection was demonstrated (5) and later UV and conductometric detection was reported (6). Despite the significant improvements in this technology, efficiency and resolution was still greatly limited by the relatively large injection volumes required for detection. In 1981, Jorgenson and Lukacs reported what is often considered the hallmark publication for modern capillary electrophoresis (7). In this work, they reported sensitive fluorescence detection of dansylated amino acids separated in capillary columns with a 75 μm i.d. The excellent heat dissipation of such narrow-bore columns coupled with the very small injection volume required for fluorescence detection resulted in separation efficiencies of 400,000 theoretical plates, more than ten times better than previous attempts.

Since that time, the development and improvement of CE techniques, applications, and detection methods has been remarkable. Today, almost any type of analyte, even compounds without a charge, can be separated by CE. Nearly any optical or electrochemical detection method can be coupled to CE, microchips are employed for CE separations which require only low seconds to

milliseconds for analysis, and single-molecule detection limits have been demonstrated (8-12).

Fundamentals of CE

intrinsic electrophoretic mobility

As discussed in the previous section, electrophoretic separations are generally achieved by exploiting the differences in the charge to size ratio of the ion. The direction and magnitude of an ion's migration rate is dependent upon the magnitude and charge of the ion and the magnitude and direction of the applied electrical field. The directionality of the ion's migration is, of course, to the oppositely charged electrode. The magnitude of the ion's migration rate is dependent upon the force exerted upon the ion by the applied field; this force (F') is described as:

$$F' = qE \quad (1.1)$$

where q is the charge on the ion and E is the applied electric field to the system (13):

$$E = \frac{V}{L} \quad (1.2)$$

where V is the applied voltage (volts) and L is column length (cm). Opposing this directional force is a counteracting force (F'') given by Stokes law:

$$F'' = 6\pi\eta av \quad (1.3)$$

where η is the solution viscosity, a is the radius of the ion, and v is the velocity of the ion (13). Eq. 1.3 can be simplified by replacing $6\pi\eta a$ with the frictional

coefficient f to give:

$$F'' = fv \quad (1.4)$$

The total force (F) experienced by the ion can then simply be derived from Eqs. 1.1 and 1.4:

$$F = F' - F'' \quad (1.5)$$

Assuming a steady-state between the two forces is quickly attained, Eq. 1.6 is derived from Newton's second law of motion (14):

$$F = \frac{dv}{dt} = qE - fv \quad (1.6)$$

As dv/dt becomes zero under steady-state conditions, this term drops out and Eq. 1.6 can be rewritten as:

$$v = \left(\frac{q}{f} \right) E \quad (1.7)$$

The frictional coefficient ratio (q/f) which is proportional to the charge to size ratio and which determines the intrinsic electrophoretic mobility (μ_{int}) of an ion is defined as the velocity per unit field strength and can be derived from Eq. 1.7:

$$\mu_{\text{int}} = \frac{q}{f} = \frac{v}{E} \quad (1.8)$$

It is this intrinsic property that is exploited that enables electrophoresis to be utilized for the separation of ions.

electroosmotic flow

Within a fused silica capillary, solvated cations in solution will accumulate near the negative charges on the surface of the walls. Upon applying an

electrical field, the cations will migrate towards the cathode and, in doing so, will drag along solution within the column; this process is termed electroosmotic flow (EOF) and is depicted in Figure 1.3(A). The velocity of EOF depends on physical parameters of the solution and the capillary and is defined as:

$$v_{EOF} = \frac{E\zeta\varepsilon}{\eta} \quad (1.9)$$

where ζ is the zeta potential of the capillary wall and ε is the permittivity constant of the solution (13). Recalling the relationship derived in Eq. 1.8, the mobility of EOF can be defined as:

$$\mu_{EOF} = \frac{\zeta\varepsilon}{\eta} \quad (1.10)$$

The intrinsicity of this parameter is noted because, again, the mobility of EOF is independent of the applied field. However, even more significant is the fact that EOF has no radial dependence; i.e. EOF results in a flat flow profile as opposed to a parabolic flow profile observed for pressure-driven flow techniques such as liquid chromatography (LC) methods that utilize pumps or gravity to attain flow. Whereas the flat flow profile depicted in Figure 1.3(A) indicates a uniform velocity distribution of analytes in the moving band, the parabolic flow profile depicted in Figure 1.3(B) indicates that the velocity distribution of analyte is not uniform throughout the band and, as a consequence, efficiency is diminished.

observed electrophoretic mobility

It is the combination of the intrinsic electrophoretic mobility and the presence of EOF that determines the rate at which solutes will migrate in free

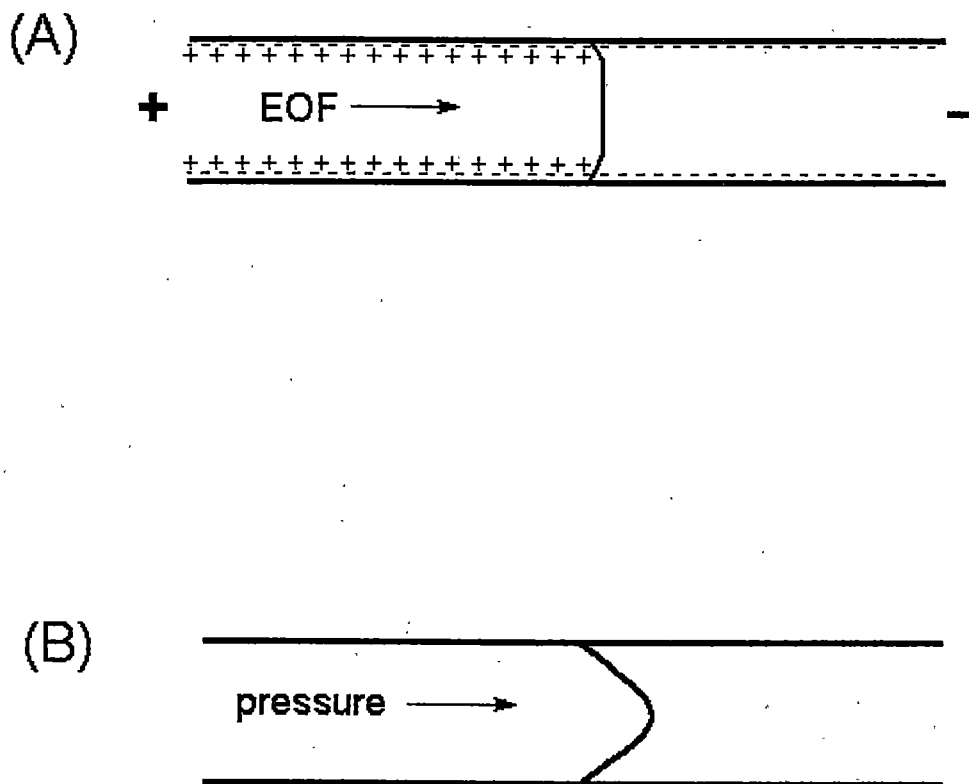


Figure 1.3: Flow profiles in CE and LC methods. (A) plug-like flow profile observed in electrophoretic separations; (B) parabolic flow profile observed in pressure-driven techniques.

solution during electrophoresis. Therefore, the observed electrophoretic mobility (μ_{obs}) is a combination of these two mobilities as shown in Eq. 1.11:

$$\mu_{obs} = \mu_{int} + \mu_{EOF} \quad (1.11)$$

It is important to note that if the μ_{int} and μ_{eof} have the same sign (i.e., are in the same direction), then μ_{obs} is the sum of the two mobilities; conversely, if μ_{int} and μ_{eof} have opposite signs (i.e., are in opposing directions), then μ_{obs} is the difference of the two mobilities.

Separation figures of merit

efficiency

In a well-optimized separation system, the chromatographic band should remain in a narrow Gaussian distribution as it travels through the column. The dispersion, or broadening, of the band is measured by a factor termed variance which is measure of how broad the band becomes distributed from its concentration maximum. A factor called plate height (H) is often calculated to correlate the amount of variance per unit length of separation:

$$H = \frac{\sigma^2}{L} \quad (1.12)$$

where σ^2 is the calculated or measured variance and L is the column length (15).

Efficiency (N) is defined as the number of theoretical plates obtained for a separation (15):

$$N = \frac{L}{H} \quad (1.13)$$

In LC methods, the parabolic flow profile and the use of stationary and liquid phases and the associated slow mass transfer between phases are generally the major sources of variance during separations. In CE, the lack of stationary phases and the radial flow profile eliminate these sources of variance and, thus, usually result in much higher efficiencies relative to LC separations. However, there are several other sources of variance present in CE systems and each of these sources contributes in an additive manner to the total variance observed:

$$\sigma^2_{total} = \sigma^2_{diff} + \sigma^2_{inj} + \sigma^2_{det} + \sigma^2_{thermal} + \sigma^2_{other} \quad (1.14)$$

where these sources of variance are diffusion, finite injection and detection volumes, thermal gradients, and other sources, respectively (16). Other sources of variance may include solute-wall interactions, differences in conductivity between sample plug and buffer, and, in some cases, resistance to mass transfer in techniques which contain complex buffer additives (e.g., micelles). For many of these sources, the variance may be minimized by carefully optimizing conditions of the CE experiment. For example, using lower field strengths so that heat is efficiently dissipated from the column will minimize variance due to thermal gradients. When experimental conditions are optimized, it is then assumed that the major source of band dispersion is due to molecular diffusion of the analyte. Variance from diffusion can be determined from the Einstein equation:

$$\sigma^2 = 2Dt \quad (1.15)$$

where D is the molecular diffusion coefficient (cm^2/s) and t is the time allowed for diffusion to occur (17). Therefore, it becomes apparent that the longer an analyte remains in the column during the separation, more time is permitted for diffusion to occur. Rearrangement of Eq. 1.8 gives:

$$v = \mu E = \mu \left(\frac{V}{L} \right) \quad (1.16)$$

where v is velocity, μ is apparent mobility, and E is the applied field (V/L). We can then determine that the amount of time (t) required for an analyte to migrate along the distance of the column (L):

$$t = \frac{L^2}{\mu V} \quad (1.17)$$

Substituting Eq. 1.17 into the Einstein equation yields:

$$\sigma^2 = 2D \left(\frac{L^2}{\mu V} \right) \quad (1.18)$$

Recall from Eqs. 1.12 and 1.13 that the number of theoretical plates (N) can be given by:

$$N = \frac{L^2}{\sigma^2} \quad (1.19)$$

By combining Eqs. 1.16 and 1.17, we derive that the efficiency of separation may be stated as follows:

$$N = \frac{\mu V}{2D} \quad (1.20)$$

From this equation, one concludes that i) the use of higher voltage results in better efficiency because it causes the migration to proceed more rapidly, thus,

allowing less time for diffusion, ii) ions of greater mobility result in improved efficiency because, again, the ions will proceed more rapidly through the column, thus, allowing less time for diffusion, and iii) ions with a larger diffusion coefficient will result in diminished efficiency. However, in the first conclusion stated above, one must be careful that the applied voltage is not increased to a point at which significant Joule heating occurs; in this case, the improvement in efficiency due to less time for diffusion will be offset by a loss in efficiency due to thermal gradients.

Once data from a separation is recorded, efficiency may be reported by calculating the number of theoretical plates based on peak shape of the electropherogram. The standard equation for this calculation is:

$$N = 5.54 \left(\frac{t}{w_{1/2}} \right)^2 \quad (1.21)$$

where t is retention time of the analyte and $w_{1/2}$ is the width of the peak at half-height (15).

resolution

Resolution is a figure of merit that is strongly dependent upon efficiency. In simple terms, resolution is a measure of the quality of separation between two adjacent peaks. The term "baseline resolution" is often used to state that adjacent peaks do not overlap; i.e. the first peak fully returns to the baseline before the second peak rises. Theoretically, the resolution (R_s) between analytes

can be determined based upon their respective mobilities and the efficiency of separation:

$$R_s = \frac{\sqrt{N}}{4} \left(\frac{\Delta\mu}{\mu_{avg}} \right) \quad (1.22)$$

where $\Delta\mu$ is the difference in mobilities of the two analytes and μ_{avg} is the average of the two mobilities (15). Resolution may also be calculated from experimental data by a simpler equation:

$$R_s = \frac{\Delta t_R}{\left(\frac{w_1 + w_2}{2} \right)} \quad (1.23)$$

where Δt_R is the difference in retention times and w_1 and w_2 are the base widths of the two peaks (15).

Basic CE Experiment

One of the attractive features of CE is that instrumentation can be relatively simple. A fused silica column is placed between two buffer reservoirs and a voltage is applied to the buffer system leading to EOF and migration of ions through the column. Typically, a small detection window is prepared near one end of the column for on-column detection. A typical CE apparatus is depicted in Figure 1.4.

A typical fused silica column is 200-400 μm in total diameter with an i.d. between 25-150 μm . The column is externally coated with polyimide to allow flexibility without breaking the fragile column. For detection purposes, a small

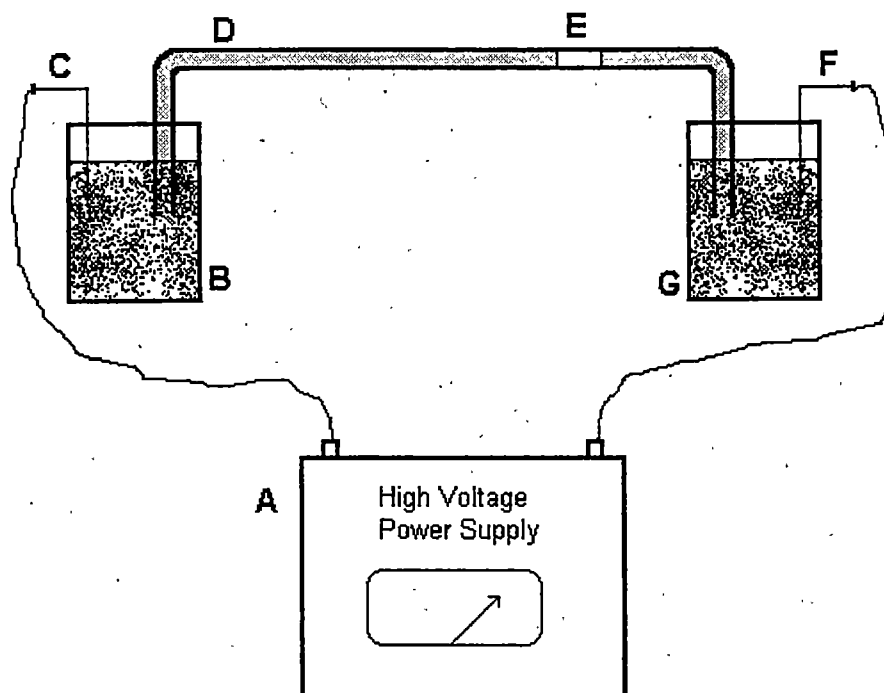


Figure 1.4: Instrumental set-up for basic CE experiment. (A) high voltage power supply; (B) inlet buffer reservoir; (C) lead electrode; (D) column; (E) detection window; (F) ground electrode; (G) outlet buffer reservoir.

portion of polyimide may be removed with warm sulfuric acid in order to obtain a small window for on-column detection.

A sample plug is usually introduced by one of two methods. First, a hydrodynamic injection involves simply placing the injection end of the column into the sample vial and raising the vial 8-10 cm for 10-30 seconds. The hydrodynamic pressure created within the column will siphon a small sample plug into the column. The volume injected (V , nL/s) can then be determined by the Poiseuille equation:

$$V = \frac{\Delta P (i.d.)^4 \pi}{128 \eta L} \quad (1.24)$$

where ΔP is the pressure drop, given as:

$$\Delta P = \rho g \Delta h \quad (1.25)$$

where ρ is density of sample solution, g is the gravitational constant, and Δh is the height difference between the sample vial and outlet vial (18).

A second method of sample introduction commonly used is the electrokinetic injection. In this method, the inlet side of the capillary is placed into the sample vial and an electric field is applied for a brief period of time. The quantity of solute injected (Q) can be determined as:

$$Q = \mu_{obs} \pi r^2 E C t \left(\frac{\kappa_b}{\kappa_s} \right) \quad (1.26)$$

where r is the inner-radius of the capillary, E is the field strength during electrokinetic injection, C is the sample concentration, t is the time of injection,

and κ_b and κ_s are the conductivities of the running buffer and sample, respectively (19).

Following injection, a strong field is applied (typically 100-1000 V/cm) and the injected solutes migrate through the column. The ends of the columns are immersed in buffer reservoirs and the column is filled with buffer as well. Buffers are typically of high buffer strength (10-100 mM) because it is imperative to maintain precise pH in the system. Electrophoretic mobilities of solute ions and EOF are strongly dependent on pH; thus, any change in the background pH of the running buffer could have deleterious effects on the separation. In some types of CE experiments, the buffer may be modified with additives to aid in the separation. For example, zwitterionic buffers may be used to adsorb onto the column walls to eliminate EOF or buffers may contain micelles to aid in the separation of neutral compounds (20, 21). In other cases, chelating agents may be added to the buffer to assist in the separation of metals or fluorophores may be added to the buffer so that the displacement of these fluorophores results in an indirect method of detection (22). A full discussion on the role of the buffer and modifications to aid in separations can be found in the literature (23).

Most detection schemes employ on-column detection methods and the two most common methods of detection are absorbance and fluorescence. Absorbance detection is not very sensitive in CE because of the short pathlengths at the detection window. Recall Beer's law:

$$A = \epsilon bc \quad (1.27)$$

where absorbance is directly proportional to the molar absorptivity (ϵ), the pathlength (b), and the concentration of analyte (c) (24). Given the diminutive size of the i.d. of capillaries used in CE, absorbance detection is simply not very sensitive. Despite this disadvantage, absorbance is still commonly utilized because a large number of analytes intrinsically absorb light.

CE truly became a notable technique when Jorgenson and Lukacs employed fluorescence detection and reported very good efficiency and sensitivity (7). In this method of detection, the fluorescence signal intensity (I_f) is given by:

$$I_f = \theta_f I_0 \epsilon b c k_E \quad (1.28)$$

where θ_f is the fluorescence quantum yield, I_0 is the excitation source intensity, and k_E is the detection efficiency (25). The significant relationship to note in this equation is the direct proportionality between I_f and I_0 . This relationship is often referred to as the "fluorescence advantage"; i.e., the stronger the excitation source, the more intense the resulting fluorescence signal will be. The attributes of lasers make them ideally suited for fluorescence-based CE techniques. Lasers can deliver monochromatic, collimated, high-power light. These attributes result in selective excitation of desired species, a tightly focused beam through the capillary, and a strong fluorescence signal which may lower limits of detection (LODs), respectively.

Despite the several advantages of laser-based fluorescence detection, this is not an universal technique. The number of analytes which exhibit natural fluorescence is limited. Therefore, derivatization of the sample may be

necessary. However, one must be careful that derivatizing sample constituents with fluorescent reagents does not then make the mixture unamenable to CE separation. For example, if a fluorescent chelating agent is added to a mixture of metals prior to analysis, it's possible that the chelated complexes will now all have approximately the same charge to size ratio and, thus, the same electrophoretic mobility, and will not be separated by CE. Several possible strategies have been employed to avoid such problems. In addition to derivatizing samples prior to injection (termed "pre-column derivatization"), samples may also be derivatized on-column by adding complexing reagents into the running buffer (26, 27). In addition, post-column derivatization is often utilized so that labeling of the analyte occurs after the separation is complete (28, 29).

Electrophoretic separation of DNA fragments

theory of migration

It may appear that the structure and properties of DNA would make it impossible to separate fragments by electrophoresis. Recall from Eqs. 1.3 and 1.8 that the intrinsic mobility of an ion is dependent upon its charge and its frictional force; in turn, these factors are dependent upon the size of the ion so that the following relationship is derived:

$$\mu_{DNA} = \frac{q}{f} \approx \frac{N}{N} \approx 1 \quad (1.29)$$

where N represents the length of DNA in number of base pairs. Therefore, in free solution, all DNA fragments would be predicted to have the same electrophoretic mobility and, thus, no resolution of fragments would occur.

In 1967, the combination of electrophoresis with a sieving media was introduced for the separation of polypeptides; this technique was termed polyacrylamide gel electrophoresis (PAGE) (30). Electrophoresis provided the driving force for the fragments to migrate into the gel media but the porosity of the gels is what imparted selectivity based upon the size of the fragments. Whereas small fragments could easily migrate through the porous network, larger fragments can only traverse a limited number of pores, thus, these fragments must weave a more torturous path through the gel.

Capillary Gel Electrophoresis

To perform PAGE, a slab gel must be prepared (also known as slab gel electrophoresis, or SGE). These gels are typically flat, about 20 x 20 cm or larger, and may be several millimeters in thickness. Detection is usually limited to exposing the gel to UV light; sample recovery out of the gel is necessary for other analyses. Another problem with SGE is that gels do not efficiently dissipate heat, thus, very low applied fields (about 10 V/cm) must be utilized in order to avoid the deleterious effects of Joule heating. As a consequence of using such low fields, analysis time may be very slow (hours).

In 1983, Stellan Hjerten first attempted to perform a modified version of this technique in capillaries in a method to become known as capillary gel

electrophoresis, or CGE (31). However, a major impedance to this method was very poor efficiency. Hjerten suggested that the source of the problem was a static attraction between the large biopolymers and the charged walls of the fused silica capillaries. In 1985, Hjerten published what many CE practitioners consider another hallmark publication for CE (32). In this work, Hjerten describes a column-coating regime which effectively coats the walls and, thus, eliminates electrostatic interactions between ions and the fused silica capillary. Another significant effect of this coating procedure is that EOF is also eliminated.

In the following years, the use of CGE resulted in remarkable improvements in the CE separation of biopolymers. Typical results were reports of a 50-fold reduction in analysis time coupled with a 14-fold improvement in efficiencies with low detection limits (33).

Size-Selective Capillary Electrophoresis

Despite the improvements realized with CGE, it was not without faults. Gel-filled capillaries were cumbersome to prepare. The gel must be bonded very strongly to the capillary wall or it may become expelled during electrophoresis. Slight changes in temperature and pH were found to influence the gel's integrity. Also, for all the trouble involved with preparing gel-filled columns, they would last for only a few analyses.

In the early 1990's, a method was introduced that replaced the affixed gels and utilized a solution of soluble polymers as the sieving matrix; this new technique was termed size-selective capillary electrophoresis, or SSCE (34).

This method retained all the positive attributes of CGE (fast analysis time, sensitive detection, excellent heat dissipation, and small sample requirements) but also alleviated many of the problems associated with CGE. Changing the buffer or sieving matrix is as easy as flushing and refilling the column. By being able to flush and store the columns in dilute acid solutions when not in use, column lifetime is greatly extended. Also, there are many types and sizes of polymers available for this technique.

Statement of problem

Despite the many advantages of CE discussed in the introductory chapter, it has been humorously noted that, "There are only three problems with capillary electrophoresis: injection, separation and detection." (35). Though CE has come a long way since this statement was made, there still remain a number of problems which hinder it from gaining wider acceptance. Part of the inability to solve these problems is simply the novelty of this method – much is yet not understood about the underlying fundamental processes of many of these CE applications.

There has been much speculation about the dynamics of DNA separations during SSCE. A significant portion of research involving SSCE of DNA fragments is to simply understand the fundamental processes which are occurring so that experimental conditions may be fully optimized in order to achieve the best results possible. It has been suggested that if reproducibility, sensitivity, and predictability through computer-generated simplex programs

could be demonstrated for the SSCE separation of DNA fragments, this technique could be a major contribution to the bold endeavor to sequence the human genome by the year 2005 (36).

The purpose of the research presented in Part I of this dissertation is to study the fundamental processes occurring during the SSCE of DNA fragments. Once these processes are better understood, the sources of variance become better understood and prospects for developing experimental strategies to minimize these sources of variance during real applications are enhanced.

-Chapter 2-

Examination of Non Cross-Linked Polyacrylamide Coated Columns by Scanning Electron Microscopy

Introduction

In order to achieve efficient separations of DNA by CE, the negative surface charge of fused silica capillaries must be eliminated. One reason for this is to eliminate electrostatic attractions between charged biomolecules and the surface silanols. Even in the case of DNA fragments, static attractions may exist between the negatively-charged fragments and cations adsorbed to the negatively charged surface of the capillary wall. Furthermore, the intercalation of positively-charged dyes may further increase the attraction between intercalated DNA fragments and surface silanols. Such sorption processes would have deleterious effects on retention time, efficiency, and resolution of DNA fragments. Furthermore, as discussed in Chapter 1, the presence of a negative surface charge on the capillary wall results in electroosmotic flow. EOF would oppose the electrophoretic migration of DNA fragments, again resulting in extended retention times and diminished efficiency and resolution.

The combination of sorption processes and the presence of EOF would virtually eliminate the possibility of using CE for DNA analysis. Even if EOF was not completely eliminated from these experiments, the adsorption of DNA fragments would change the zeta potential of the column wall, thus, variations in the magnitude of EOF would result (Eq. 1.10). Such variations in EOF would

result in highly irreproducible retention times of DNA fragments, thus, the use of CE for sequencing applications would not be possible.

In 1985, Hjerten presented a key publication describing the covalent bonding of polymers onto the capillary wall which would alleviate solute-wall adsorption and would also eliminate electroosmotic flow (32). Hjerten's procedure is depicted in Figure 2.1. Briefly, the column is washed with base to remove any impurities adsorbed onto the silica surface. The column is briefly rinsed with water and followed by a wash with acid in order to fully protonate the SiO^- surface of the wall, thus, making it reactive for the silanation step. Next, a bireactive silane is rinsed through the column where one side covalently anchors to the SiO^- surface. In the final step, acrylamide is introduced into the column and, in the presence of an initiator, the acrylamide reacts with the unanchored side of the bonded silane to yield a non cross-linked polyacrylamide coating. After sufficient time has elapsed for *in-situ* polymerization, unreacted reagents are flushed from the columns and the columns are stored in a dilute acid solution. Columns prepared in this manner are typically stable for dozens of separations over 2-4 weeks before performance degradation is observed.

One should not confuse the aforementioned procedure of using non cross-linked polyacrylamide with the CGE method previously described (pg. 19-20). In the former, only the walls of the columns are coated with a thin layer of polyacrylamide. The polyacrylamide is not part of the separation matrix. In the latter, the entire diameter of the column is filled with a solid gel which is used as the separation matrix.

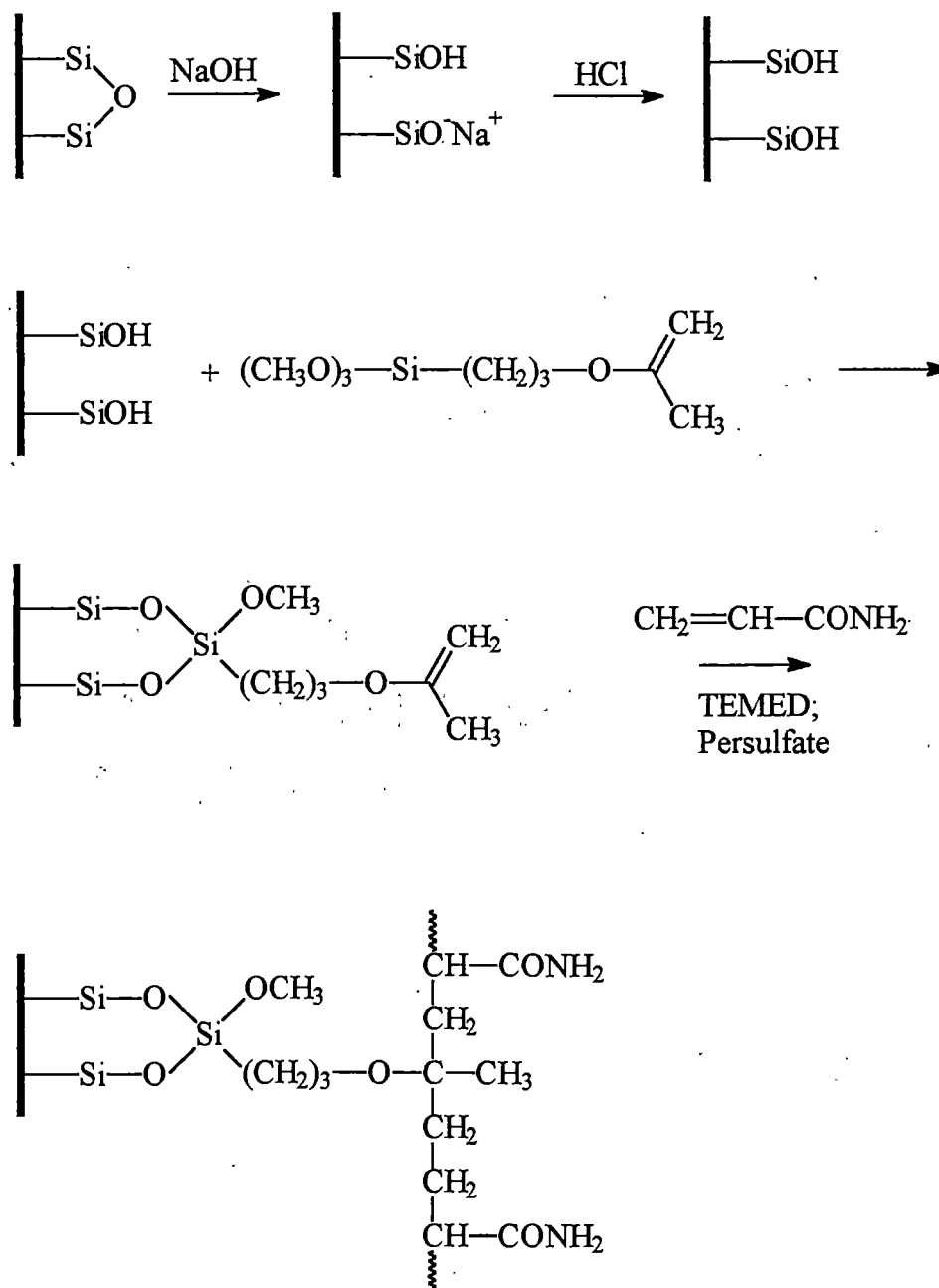


Figure 2.1: Reaction scheme for coating columns with non cross-linked polyacrylamide. Details of the reaction steps are found within the text. Although bis-attachment to adjacent silanols on the surface is depicted, this may not always occur; further cross-linking reactions at these methoxy groups may occur.

Since 1985, numerous publications have appeared suggesting modifications and alternative polymerization regimes. Among these various polymers are poly(vinyl alcohol) (37), epoxy (38), polyether (39), cellulose acetate (40), and polyethylene glycol (41). As alternatives to bonding polymers onto the surface of the capillary wall, some researchers have reported dynamic coatings such as the use of surfactants in the running buffer (42) or the use of highly viscous polymers such as poly(ethylene oxide) (43). However, dynamic regimes may not always reproducibly control EOF as well as bonded polymers.

In many of these reports, careful optimization and control of the polymerization step is reported to be essential to avoid errors such as incomplete polymerization and, thus, insufficient coating. In other cases, clogging of the capillary has been reported when excessive polymerization has occurred (44).

Several papers have appeared in which the efficacy of different capillary coating techniques is evaluated by using the prepared columns to separate complex samples and determining the separation figures of merit (e.g. efficiency and resolution) (45-47). A few studies have actually evaluated the polymerization process occurring during the column coating procedure (48, 49).

The examination of capillary columns by scanning electron microscopy (SEM) was reported by Kaupp et. al. (50). In this work, SEM was utilized to examine surface defects of capillary columns from various batches in order to evaluate batch to batch quality. Etching effects following treatments with HF and HCl were examined. In addition, adsorption phenomena were examined. A correlation of etching (treatment) time with the zeta potential of the column was

made by observing the behavior of protein solutions in the column. It was concluded that incomplete etching treatments resulted in non-uniform zeta potentials as evidenced by the lack of a uniform layer of adsorbed proteins. Rigorous flushing procedures were not effective in removing the adsorbed proteins.

In the work presented in this chapter, columns coated with non cross-linked polyacrylamide were examined by SEM. The effect of polyacrylamide concentration on the thickness of coating was evaluated. If a soluble polymer solution is to be employed as the separation matrix, a thick gel on the column surface is undesirable for several reasons. One of the major advantages of using aqueous solutions of soluble polymers is that these solutions dissipate heat much more efficiently than do gels (51). A thick gel on the column wall could retain heat and lead to increased Joule heating within the capillary. Also, if soluble polymers are to be employed as the sieving agent in the separation technique, a thick gel on the column wall may contribute undesirable sieving effects on the separation. For DNA separations, if the gel protrudes into the separation channel, it's possible that DNA-polymer entanglement interactions could occur which could lead to increased band dispersion and, consequently, a loss in efficiency and resolution. Ideally, a non cross-linked polyacrylamide coating on the capillary wall would be thick enough so that it effectively covers the active sites on the silica surface but so thin (perhaps a monolayer) that it does not affect the separation in any direct manner.

Experimental

Materials

Fused silica capillaries (75 μm I.D. x 365 μm O.D.) were purchased from Polymicro Technologies (Phoenix, AZ). Acrylamide, ammonium persulfate (AP), N,N,N',N'-tetramethylethylenediamine (TEMED), and γ -methacryloxypropyltrimethoxysilane (γ -MTMS) were purchased from Sigma (St. Louis, MO).

Column Preparation

Capillaries were cut to a total length of 20 cm and the walls were deactivated with linear polyacrylamide using a procedure modified from Hjerten's procedure (32). The columns were washed with 0.1 N NaOH for 1 hour, rinsed with deionized water for 10 minutes, washed with 0.1 N HCl for 1 hour and rinsed again with water for 10 minutes. Next, an acidic solution of γ -MTMS (20 ml water + 50 μL 6 M acetic acid + 80 μL γ -MTMS) was flushed through the column for 18 hours followed by a rinse with water for 10 minutes. Solutions of acrylamide (0.25 g for 2.5% acrylamide, 0.40 g for 4.0% acrylamide, and 0.80 g for 8.0% acrylamide) in 9 mL phosphate buffer (9 mL water + 0.087 g K_2HPO_4 ; adjusted to pH 6.8 with HCl) along with a solution of 0.15 g AP in 10 ml water were degassed by bubbling helium through for 30 minutes. Polymerization was initiated by adding 1 mL of the AP solution along with 7.5 μL TEMED to the acrylamide solution; this solution was then quickly introduced into the column to allow *in-situ* polymerization for at least 12 hours. The excess polyacrylamide was removed

by flushing the column with 10 mM H_3PO_4 . When not in use, columns were stored in 10 mM H_3PO_4 .

To prepare the specimens for SEM, 1 cm sections of capillaries were removed from the central portion of the column and coated with a 15 nm layer of gold in order to alleviate charging effects. The specimens were positioned perpendicular to the face of the specimen stage with the use of carbon paste to hold the specimens in place.

In addition to the aforementioned prepared specimens, an untreated bare fused silica column was analyzed as a blank. Also, a column that had been coated with 2.5% polyacrylamide and had successfully been used for several DNA separations before significant performance degradation was observed was included in this study.

Instrumentation

A Hitachi S-3200N Scanning Electron Microscope (Hitachi Scientific Instruments, San Jose, CA, USA) was utilized for all experiments. Operating conditions included a pressure of 20 Pa and a beam voltage of 20 kV. The micrographs presented are backscattered electron images.

SEM Micrographs

The micrographs depicted were obtained with a Polaroid camera attached to the SEM. To aid in preservation, the micrographs were wiped with a dilute acetic acid solution immediately following development. The figures in this

chapter are computer-scanned images using an UMAX Astra1200S scanner (UMAX data Systems, Fremont, CA.) and Presto! Pagemaker software (NewSoft Technology Corp., Seattle, WA.); images were scanned at a resolution of 300 dpi. It is important to note that the software was not used to enhance any features of the images presented in the figures.

Results and Discussion

The specimen obtained from the blank column is pictured in Figure 2.2(A). The bright portion of the image is the fused silica capillary and the dark portion of the image is the inner diameter of the column. This micrograph is included to facilitate comparison with images of coated columns.

Figure 2.2(B) shows a highly magnified view of a column that was coated with a 2.5% polyacrylamide solution. It is not possible to conclude if a very thin coating is present in this specimen. A faint image is evident between the fused silica and the inner diameter of the column but this may be the result of the inability to achieve a better focus. Although a coating cannot be conclusively identified, successful deactivation of the column surface is indicated by the fact that these columns are routinely used for very efficient separations of DNA fragments (52, 53). This indicates that this column is probably coated with a very thin layer of polyacrylamide, perhaps less than 0.1 μm in thickness.

Procedures describing the use of a 4.0% polyacrylamide solution for coating columns have been reported (54). A micrograph of a column prepared at this concentration is depicted in Figure 2.2(C). In this figure, one can clearly see

SOUTHWORTH
PARCHMENT DEED
100% COTTON FIBER

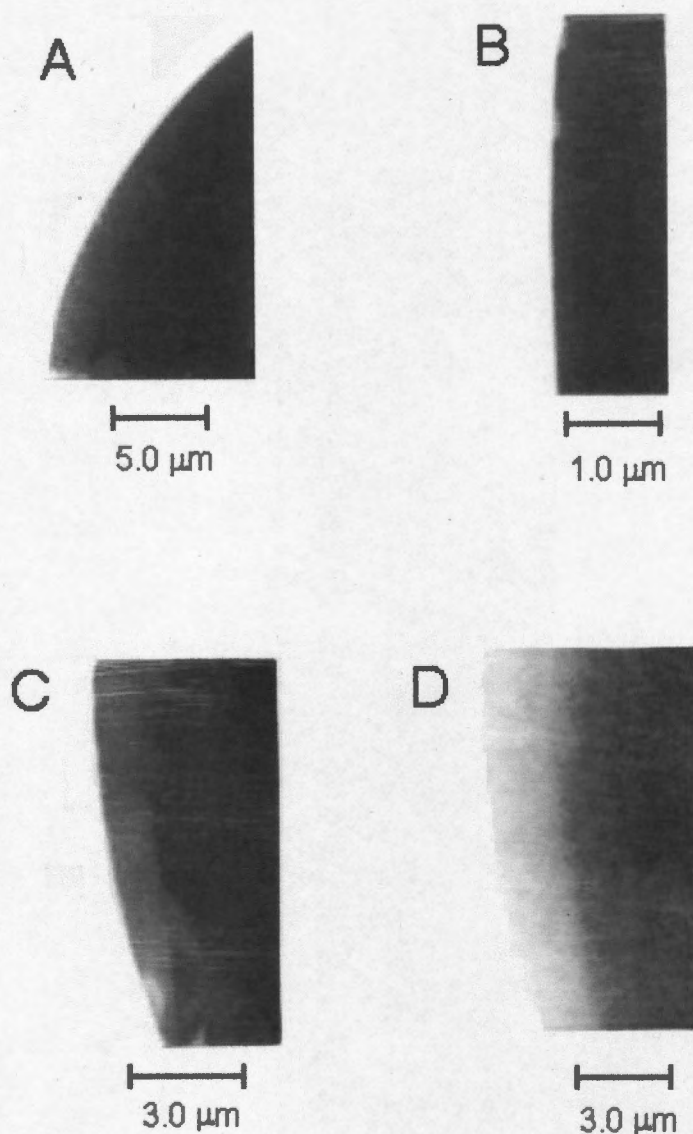


Figure 2.2: Computer-scanned images of scanning electron microscopy micrographs of capillary columns. (A) bare silica column (blank); working distance (WD) = 12 mm; (B) column coated with 2.5% polyacrylamide; WD = 13 mm; (C) column coated with 4.0% polyacrylamide; WD = 12 mm; (D) column coated with 8.0% polyacrylamide; WD = 13 mm.

a layer of polyacrylamide inside the column. It appears that the thickness of this coating is approximately 1.5 μm although it is apparent that this coating is not uniform in thickness.

Examination of the specimen from the column coated with 8.0% polyacrylamide is shown in Figure 2.2(D). Although poor in contrast, a significantly thicker coating on the surface of the column is observed. Further evaluation of this specimen is shown in Figures 2.3(A) and (B). These micrographs clearly show a lack in uniformity of polymer thickness. In Figure 2.3(A), one observes where the coating appears to begin and gradually becomes thicker; in Figure 2.3(B), this gradual increase in coating thickness is even more evident. These micrographs were obtained by examining adjacent regions of the specimen. One possible explanation for the observation depicted in these figures is that while these columns lie parallel on the lab bench during the lengthy polymerization time (12-16 hours), gravity causes the polyacrylamide solution to pool in the bottom of the column, resulting in a thicker layer of coating in this region. It's possible that the orientation of these micrographs depict the position of this column as it sat on the lab bench during polymerization. Possible solutions to this problem include using a syringe pump to continuously force the polymer solution through the column at a constant rate or to rotate the column during the polymerization step.

When a column "dies", this is evidenced by the loss of quality of the separations. For DNA separations, bands become broad and resolution becomes much poorer, indicating fragment-wall adsorption may be occurring.

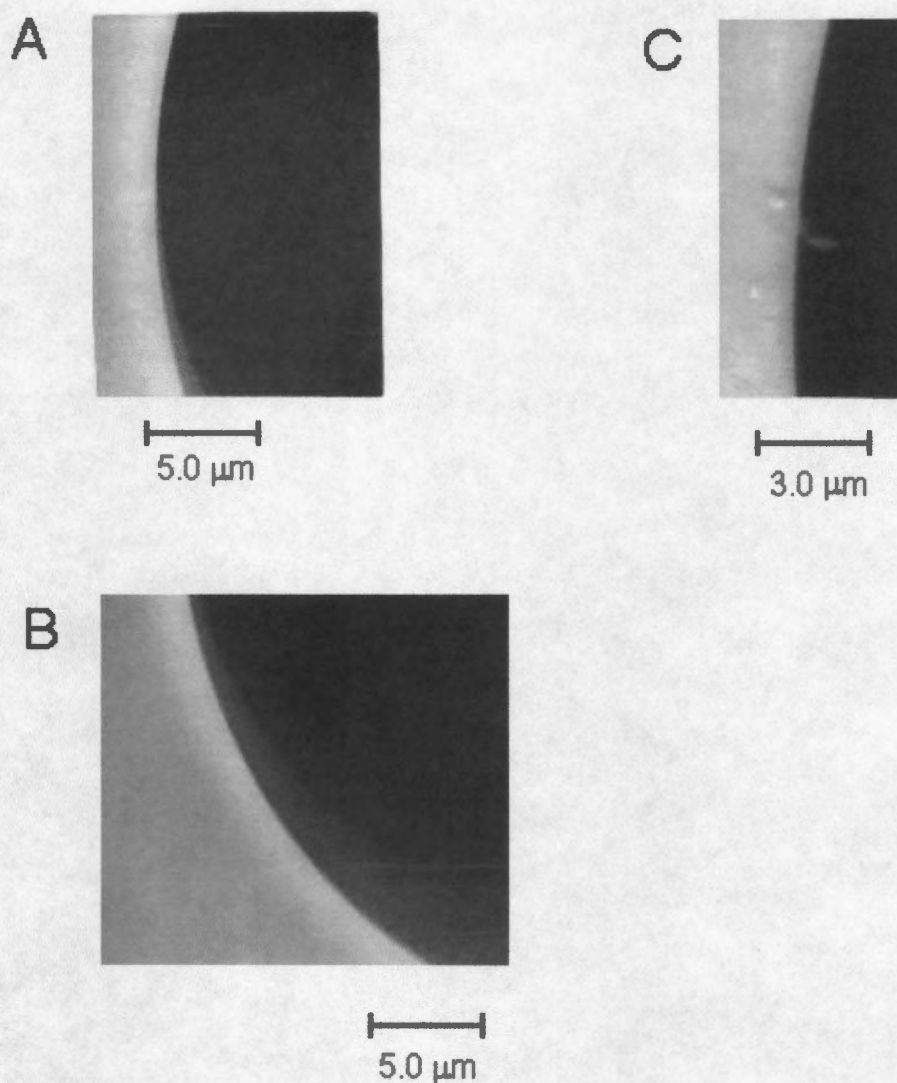


Figure 2.3: Additional SEM micrographs of capillary columns. (A, B) adjacent regions of column coated with 8.0% polyacrylamide; WD = 13 mm; (C) column coated with 2.5% polyacrylamide and used for several successful separations of DNA digests before performance degradation was observed; WD = 14 mm.

Also, retention times increase, indicating the presence of electroosmosis which opposes the migration direction of the fragment bands. Figure 2.3(C) is a micrograph of a column following "column death"; i.e., this specimen is from a column that was coated with 2.5% polyacrylamide and successfully used for several DNA separations before significant performance degradation was observed. Ideally, one would perhaps like to see a micrograph of a dead column which shows patches of the coating removed. However, as was observed in Figure 2.2(B), deactivation with 2.5% polyacrylamide does not result in a clearly visible coating. Unfortunately, Figure 2.3(C) was not as revealing as had been expected during the preparation of specimens for this study. However, this figure does reveal that a loss in the integrity of the coating may have been the source of performance degradation; no obvious visual damage to the column is evident which might have otherwise been used to explain the loss in performance of this column.

Conclusions

Several papers report the successful use of non cross-linked polyacrylamide coated columns to achieve separations that would not be possible in uncoated columns. This demonstrates that this coating is indeed effective. However, the micrographs presented herein illustrate some possible problems that could lead to poor reproducibility that is often problematic in CE experiments.

Columns coated with 2.5% polyacrylamide yield excellent results for DNA separations which would not be possible in poorly coated columns. The fact that this effective coating is so thin that it cannot be seen by SEM at such a large magnification as used for Figure 2.3(B) indicates that this coating is probably less than 0.1 μm in thickness. When using polyacrylamide at concentrations $> 2.5\%$ polyacrylamide, the possibility arises of achieving a non-uniform coating in columns that lie flat on lab benches during the polymerization step. Procedural modifications to ensure a more uniform coating may enhance the performance of coated columns.

-Chapter 3-

Examination of Band Dispersion During Size-Selective Capillary Electrophoresis of DNA Fragments

In Chapter 1, the development of SSCE was described. This technique is now perhaps the most common method employed for DNA analysis by CE. Despite its widespread use, questions remain about the fundamental processes occurring during SSCE of DNA fragments. Several papers offering theories and discussion on this topic have been published yet controversy still remains as many of these manuscripts offer differing fundamental theories on this topic (34, 55, 56).

In this chapter, an exhaustive examination of the electrophoretic process is described. In particular, DNA migration and separation dynamics in SSCE are evaluated. Once these fundamental processes that influence band dispersion are better understood, we can then evaluate the sources of band dispersion in these experiments and optimize experimental conditions so that the full potential of CE may be realized.

Theory of DNA migration

Ogston migration model

A single strand of DNA consists of deoxyribonucleotide bases linked together by phosphodiester bonds. DNA typically exists as a double strand coiled in a helical manner with bases oriented towards the center and the

phosphate backbone oriented towards the exterior of the helix (Figure 3.1). Unperturbed in free solution, DNA fragments tend to "relax" into spheres (57).

The Ogston model of DNA migration assumes that the fragment remains in a spherical shape as it migrates during electrophoresis. The radius of the sphere (R_{DNA}) is related to the fragment length by the following empirical relationship:

$$R_{DNA} = (5.66N)^{1/2} \quad (3.1)$$

where N is the number of base pairs (bp) (56). The assumption that DNA migrates as a spherical entity has been evaluated by gel electrophoresis experiments using charged, solid, non-deformable spherical beads of comparable size to various DNA fragments as determined by Eq. 3.1 (58). In these experiments, the migration rates of the beads and the DNA fragments were compared and, if the DNA fragments indeed behave as spheres during electrophoresis, they would be predicted to have similar retention times as the solid beads. Although the data showed excellent agreement between the migration rates of the beads and the small DNA fragments, this trend rapidly worsened as the size of the DNA fragments exceeded approximately 200 bp. These results suggest a second migration mechanism predominates as the size of DNA fragments becomes larger.

biased reptation migration model

Equation 3.1 predicts that if DNA fragments indeed maintain a spherical shape during migration, the radii of the spheres for fragments of increasing

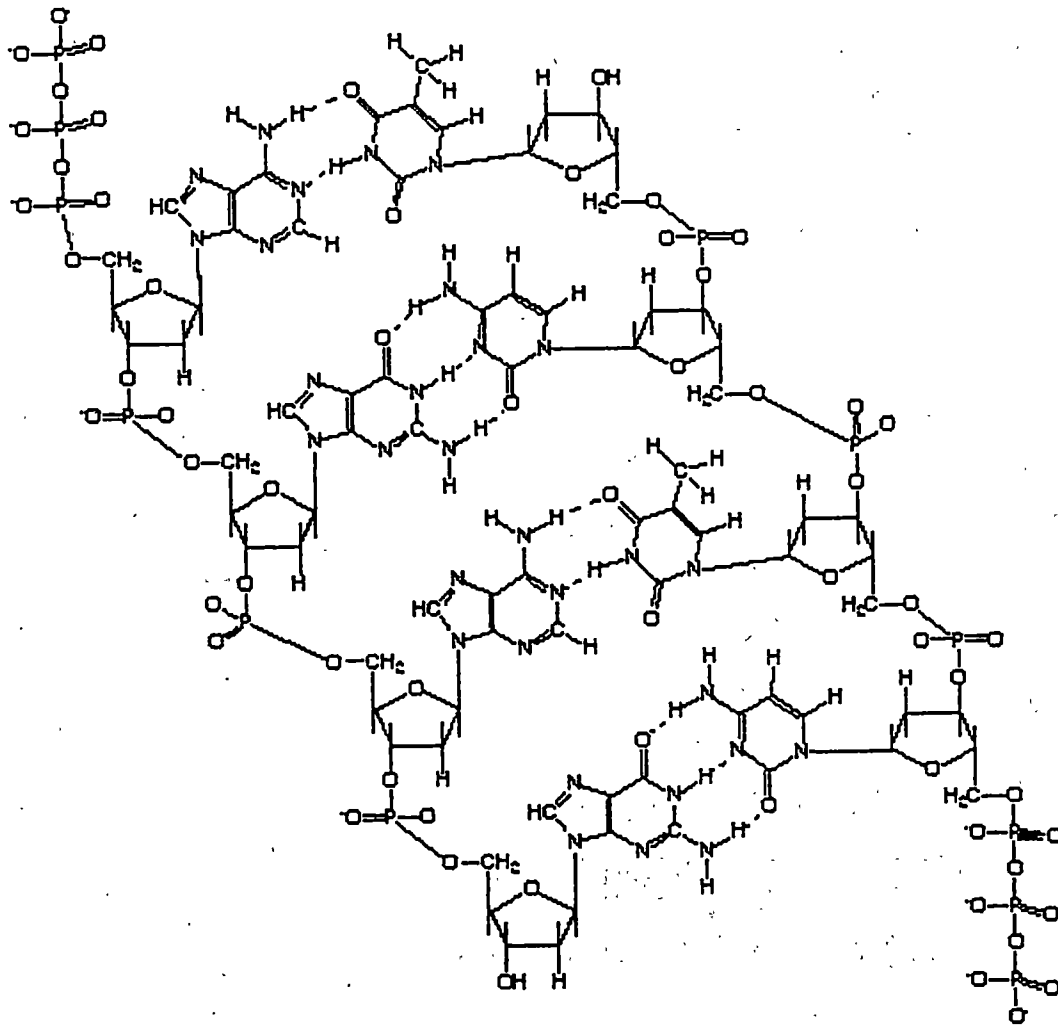


Figure 3.1: Structure of DNA. The four bases depicted (in order from top left) are adenine and thymine (linked by two hydrogen bonds) and cytosine and guanine (linked by three hydrogen bonds).

length become prohibitively large and would be nearly impossible to traverse through a mesh network of reasonable pore size. However, this is not what is observed experimentally as several laboratories report the successful electrophoretic separation of very large DNA fragments in gel and polymer matrices (59, 60). It was postulated that although large DNA fragments may exist as spheres in an *unperturbed* solution, once an electric field is applied and migration begins, the large fragments elongate and are able to reptate through the pores of a mesh network (56). This is the basis of the bias reptation migration model. Experiments show that the mobility of fragments migrating by this mechanism can be quantitatively described as:

$$\mu_{DNA} = \frac{1}{N} + bE^n \quad (3.2)$$

where b and n are constants dependent on experimental conditions.

Despite good agreement of experimental data with these proposed models, there still exist some controversy and uncertainty of the processes of DNA fragments in a complex, dynamic matrix. In reality, an electrophoretic system involves more than just a single DNA fragment migrating unperturbed through a solid, uniform mesh network. Aqueous polymer solutions utilized in SSCE are not rigid but, rather, are dynamic; thus, another model termed "constraint release" has been described (56). In this model, it is suggested that during separations of DNA fragments, the flexible polymers are "pushed away" by the more rigid fragments as they migrate through the polymer solution. Therefore, the pore size of entangled polymers is actually transient during SSCE

of DNA fragments. This proposed model further complicates the effort to provide a definitive description of SSCE.

Several other factors may also influence migration behavior. Such factors include inter- and intra-fragment interactions, change in fragment shape upon insertion of intercalation dye, and effect of pH and other buffer influences. It becomes apparent that understanding the electrophoretic process requires more than simply discussing the proposed models describing the migration dynamics of DNA fragments.

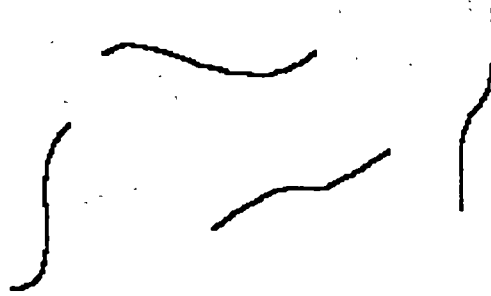
Theory of polymers employed in SSCE

effect of concentration

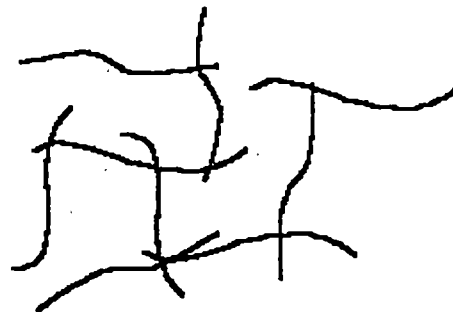
The preceding section suggests that DNA migration through a mesh network is strongly dependent upon pore size of the gel or polymer matrix. If fragments are too large to easily traverse a pore in the mesh, their migration rate is reduced as the fragment must migrate by a more torturous route. In the preparation of gels, the amount of cross-linking initiated during the polymerization of the gel determines the pore size of the separation matrix. When employing aqueous solutions of soluble polymers, it is the concentration of the polymer that will influence the effective pore size encountered by the DNA fragments (Figure 3.2).

At very low concentrations, dissolved polymers are spatially isolated from other polymer strands. As the concentration increases, the likelihood that polymer strands will become entangled with other polymer strands increases.

$C < C^*$



$C = C^*$



$C > C^*$

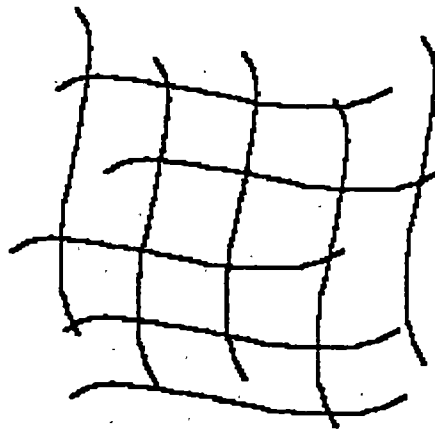


Figure 3.2: Effect of concentration on polymer entanglement. When the polymer concentration is below the entanglement threshold ($C < C^*$), polymer strands are spatially isolated; at the entanglement threshold ($C = C^*$), polymers begin to overlap; as the entanglement threshold is exceeded ($C > C^*$), a mesh network develops.

The concentration at which polymers statistically will be likely to entangle with neighboring polymers is termed the entanglement threshold and can be approximated by:

$$C^* \approx \left(\frac{3M_n}{4\pi R_p^3} \right) \approx \frac{0.6}{[\eta]} \quad (3.3)$$

where C^* is the entanglement threshold concentration, M_n is the monomer molecular weight, R_p is the radius of the polymer "blob", and $[\eta]$ is the intrinsic viscosity of the polymer solution. The latter two terms can be defined by established equations (56); these terms are also proportional to the monomer molecular weight of the polymer. Whereas Eq. 3.3 is a fairly simple mathematical approximation, the equation becomes quite complex as the polydispersity of the polymer increases. In this case, given the relationship between C^* and η approximated in Eq. 3.3, the entanglement threshold can be experimentally approximated by plotting viscosity versus concentration and extrapolating the concentration at which point the slope of the line changes.

Once the polymer concentration exceeds the entanglement threshold, a well-defined polymer mesh develops into an effective sieving matrix for DNA fragment separations (Figure 3.2). As the concentration of polymer increases, the effective diameter of the pores will decrease. Therefore, for the separation of large fragments, polymer concentrations just exceeding the entanglement threshold may be desirable; conversely, the separation of relatively small fragments may require a polymer concentration well above the entanglement threshold in order to obtain pores small enough for effective size discrimination of

fragments. However, one must realize that this is only a qualitative description; the constraint release model previously described introduces uncertainty about the correlation between polymer concentration and definitive mesh size.

Band dispersion during SSCE of DNA fragments

In order to achieve good resolution and efficiency in CE, several sources of band dispersion must be controlled, as previously described in Eq. 1.14. Several of these sources may be reduced or eliminated by careful design of experimental conditions. For example, Chapter 2 discusses the use of coated columns to eliminate band dispersion caused by solute-wall interactions and electroosmotic flow. When experimental conditions are fully optimized, the major contribution to band variance is generally considered to be axial diffusion. Recall from Eq. 1.15 that diffusion is directly proportional to time; i.e., the longer an analyte band remains in the column during electrophoresis, the larger the peak variance becomes due to diffusion. Given the direct relationship between solute velocity and field strength (Eq. 1.7), it may seem that a simple solution to this problem is to increase the field strength, thus, increasing the band velocity and reducing the amount of time the solute band remains in the column. However, the higher field strength also generates more heat which must be dissipated by the column in order to alleviate the deleterious effect of thermal gradients. Therefore, the highest possible field strength that permits rapid velocity of analytes yet does not excessively heat the column must be determined. This optimal field strength can be determined by plotting variance versus field strength

and noting the field strength that corresponds to the minimum of the plot. The increasing variance observed on this plot at field strengths *below* this minimum is due to diffusion while the increasing variance observed at field strengths *above* this minimum is due to Joule heating. A plot to determine the optimal field strength for the experiments described later in this chapter is shown in Figure 3.3.

A method for the direct measurement of diffusion coefficients of proteins was reported by Walbroehl and Jorgenson (61). Briefly, they inject a solute band into a column and perform electrophoresis without pause. A second injection is performed and the solute band is allowed to migrate only a short distance into the column before the applied field is discontinued. After a length of time, the field is reapplied and the solute band migrates past the detector. The difference in peak width from these two injections is attributed solely to diffusion during the period of time the field was discontinued. However, the "stopped migration" method employed requires more than one injection in order to obtain sufficient data. The necessity of performing multiple injections for sufficient data may affect reproducibility. For example, variance due to electrokinetic injections, residual EOF, or changes in the buffer may all increasingly contribute to band dispersion during subsequent injections and analyses.

Clark and Sepaniak describe a novel CE apparatus that permits the rapid and precise translation of the detection zone along a capillary wall (62). This instrumentation facilitates the scanning of a zone under static conditions; thus a static diffusion coefficient may be determined under truly static conditions.

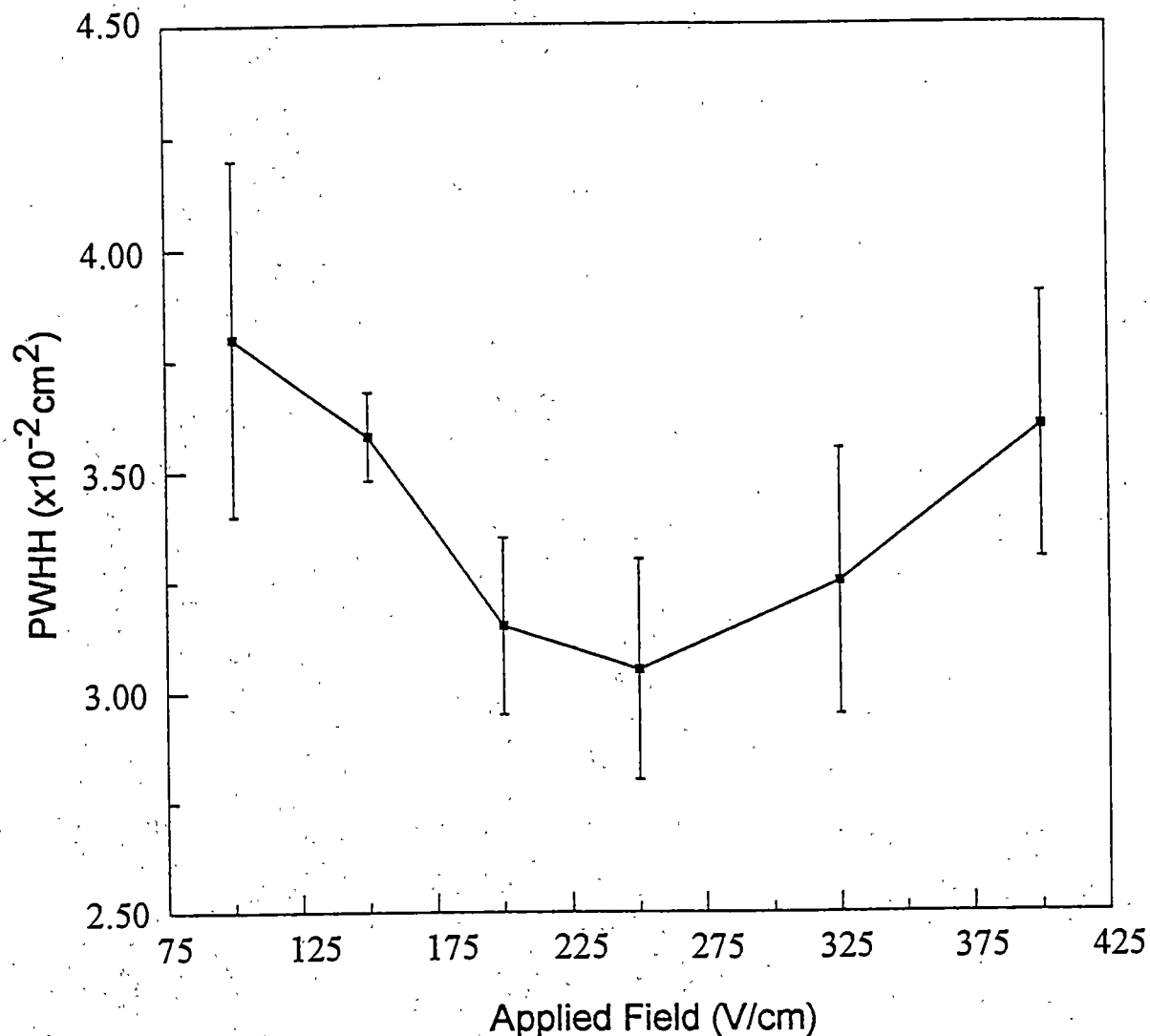


Figure 3.3: Effect of field strength on peak efficiency. A series of separations of ϕ x-174 Hae III digest were performed with increasing field strengths for subsequent trials. Peak widths at half height were measured and the field strength which resulted in the most efficient peaks was determined to be 250 V/cm. The error bars represent the variation of the efficiencies of the four selected fragments used for this study (603, 872, 1078, and 1353 bp).

Furthermore, this determination of a static diffusion coefficient requires a single injection, thus, eliminating the other possible contributing sources of variance present in the aforementioned procedure of Walbroehl and Jorgenson.

Luckey et al. proposed an equation in which the static diffusion coefficient could be utilized to determine a kinetic diffusion coefficient (63). The use of the kinetic diffusion coefficient could then be used to predict the total band dispersion observed during separations of DNA fragments by CE. The Stokes-Einstein equation relates diffusion to the size of molecule as:

$$D = \frac{kT}{f} \quad (3.4)$$

where k is the Boltzmann constant, T is the absolute temperature, and f is the frictional coefficient defined earlier in Eq. 1.4 which includes a , the radius of the ion. Recall from Eq. 1.8 the relationship between mobility (μ) and the frictional coefficient:

$$\mu = \frac{q}{f} \quad (1.8)$$

Combining and rearranging of these two equations indicate the following relationship between mobility and diffusion:

$$D = \frac{kT\mu}{q} \quad (3.5)$$

Given the conformational dynamics of DNA during electrophoresis in a sieving matrix, the electrophoretic mobility of DNA fragments varies with field strength. Therefore, the assumption is made that diffusion must also be dependent upon

field strength. Therefore, when solving Eq. 3.5, it is necessary to specify field strength conditions; for example, at zero-field the equation becomes:

$$D^0 = \frac{kT\mu^0}{q} \quad (3.6)$$

where D^0 and μ^0 are the static diffusion coefficient and the "zero-field" mobility, respectively. Under an applied field (for instance, 50 V/cm), the equation becomes:

$$D^{50} = \frac{kT\mu^{50}}{q} \quad (3.7)$$

where D^{50} and μ^{50} are the kinetic diffusion coefficient and the fragment mobility, respectively, at a field strength of 50 V/cm. Assuming that, at relatively low fields, the temperature does not appreciably change, the following relationship is derived:

$$D^{50} = D^0 \left(\frac{\mu^{50}}{\mu^0} \right) \quad (3.8)$$

In this chapter, static diffusion coefficients of DNA fragments are determined under truly static conditions by use of spatial scanning CE instrumentation. Static diffusion coefficients in various methyl cellulose concentrations are determined and surprising results relating molecular diffusion in polymer solutions are presented. Furthermore, with this novel instrumentation, total band dispersion under kinetic conditions when performing electrophoretic separations of DNA fragments in entangled polymer solutions is also examined. These experimental results are compared with results predicted by calculation of

the proposed kinetic diffusion coefficient in Eq. 3.8. The predicted results from these calculations do not appreciably account for the total band dispersion measured in these experiments. Theories and experimental data for this disagreement are presented.

Experimental

materials

Tris(hydroxymethyl)aminomethane, boric acid, and ethylenediamine-tetraacetic acid (EDTA) were purchased from Sigma (St. Louis, MO, USA) and used to prepare a 45 mM (pH 8.5) Tris-boric acid-EDTA (TBE) buffer. ϕ x-174 Hae III DNA digest, methyl cellulose (MC; $M_n = 100,000$ and $M_n = 20,000$), ethidium bromide (EB), acrylamide, AP, TEMED, and γ -MTMS were also purchased from Sigma. Fused silica capillaries (75 μ m I.D. X 365 μ m O.D.) were purchased from Polymicro Technologies (Phoenix, AZ, USA).

column and solution preparation

Capillaries were cut to give a total length of 40 cm. A large detection window extending from 9-31cm was prepared by removing the polyimide coating with warm sulfuric acid. The capillary walls were deactivated by the procedure previously described in Chapter 2.

DNA samples were prepared by diluting an aliquot from the stock with 45 mM TBE to give a final concentration of 5 μ g/ml. Methyl cellulose (MC) stock

solutions were prepared by heating 100 ml TBE buffer to 90 °C while degassing with helium. Solid MC was then added with stirring until dissolved. Once dissolved, the solution was placed in an ice bath and stirring continued until the solution became clear. Prior to use, EB was added to diluted MC solutions to give a dye concentration of 2.5 μM and then vacuum degassed. Solution viscosities were measured with an Ostwald viscometer.

apparatus

The spatial-scanning capillary electrophoresis instrumentation is depicted in Figure 3.4 and has previously been described in detail (62). Briefly, the capillary column is secured onto a plexiglass stage which is mounted onto an optical sled. The sled is fitted into a dovetail rail table and is equipped with a plastic chain which is connected to a stepping motor. (Boston Gear, Quincy, MA, USA). Motion control of the stepping motor and data acquisition were performed by use of a PS/2 Model 50 IBM computer equipped with a uCDAS-16G data acquisition board (Kiethley Metrabyte, Taunton, MA, USA).

A 1.5 mW helium-neon (He-Ne) laser (Edmund Scientific, Barrington, NJ, USA) at 543.5 nm was used as the excitation source. The laser beam was passed through *f*/1 focusing lens to tightly focus the beam into the inner-diameter of the column. Fluorescence emission was collected by a quartz fiber optic, 200 μm core diameter with a numerical aperture of 0.24 (General Fiber Optic, Cedar

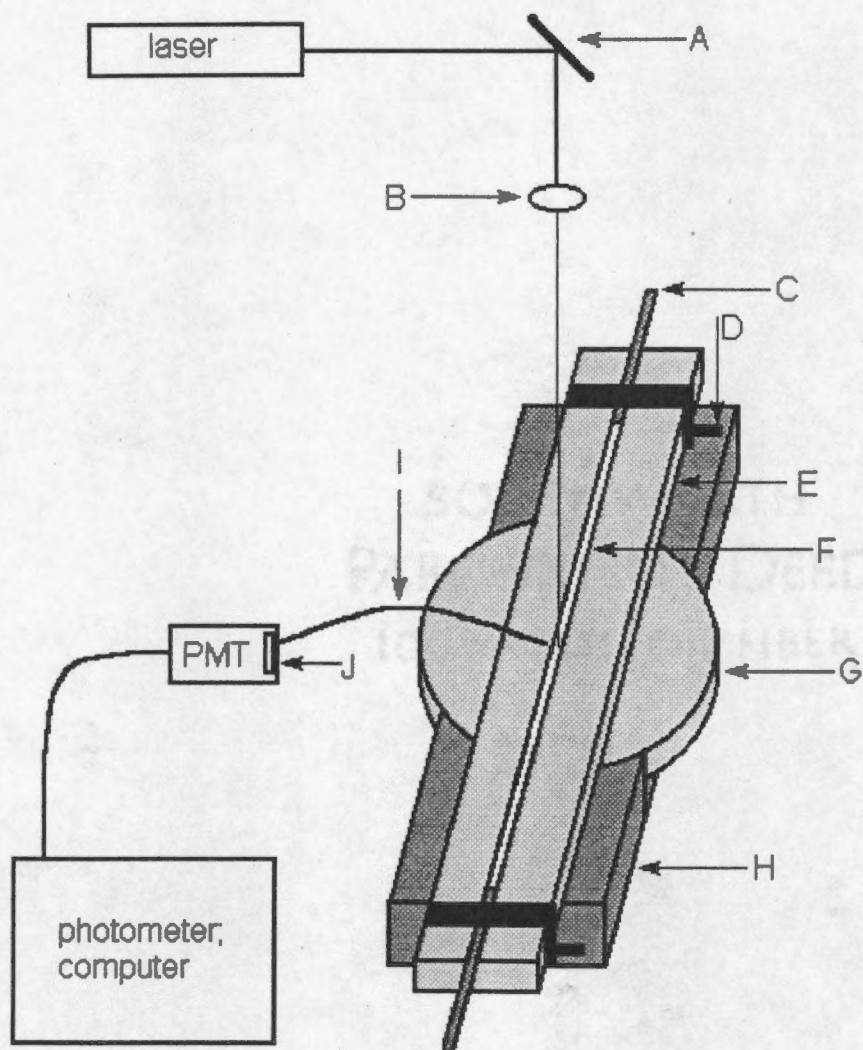


Figure 3.4: Spatial scanning CE instrument. (A) mirror; (B) focusing lenses; (C) needle electrode; (D) high voltage lead; (E) column plexiglass mounting stage; (F) column; (G) alignment stage; (H) grooved aluminum stage, mounted on a chain driver; (I) fiber optic; (J) cut-on filter.

Grove, NJ, USA), arranged 90° to the column, perpendicular to the direction of the incoming laser beam. The fiber optic is directed to a photomultiplier tube (PMT) (Model 282, Hamamatsu, Bridgewater, NJ, USA) which has a 570 nm cut-on filter at the face for optical rejection of scattered light. The photocurrent from the PMT is monitored with a photometer (Pacific Precision Instruments, Concord, CA, USA); the photometer response is directed to a chart recorder (Yokogawa, Atlanta, GA, USA) and computer. Applied fields for electrokinetic injections and electrophoretic separations were performed with a Hipotronics Model 840 high voltage power supply (Brewster, NY, USA).

methods

Before use, air was flushed through the column to remove the H_3PO_4 storage solution. Next, a low viscosity MC solution ($10 \mu\text{M}$ without EB) was flushed through the columns to coat the walls; this was done to prevent air pockets becoming trapped within the column when filling the column with more viscous MC solutions. Next, the column was filled with the MC solution of the desired concentration for studies (e.g., $50 \mu\text{M}$ MC with EB) and the column was equilibrated at -10 kV for 15 minutes prior to sample injection. All injections were performed electrokinetically ($-500\text{V}/10\text{s}$).

For the determination of D^0 , a sample plug was injected and an electric field was applied to allow solute migration past the detector. Once the desired bands passed the detector, voltage was discontinued. The bands were then scanned by the precise translation of the column past the detector at a velocity of

1.0 cm/min. The column was repositioned at its initial detection point and subsequent scans were performed in the same manner at selected time intervals. Variances used to calculate D^0 were determined from measuring peak widths at half height with the aid of LabCalc software (Galactic Industries, Salem, NH, USA).

For the determination of kinetic dispersion coefficients, a sample plug was injected and an electric field was applied to allow solute migration past the detector. Once the bands passed the detector, the voltage was discontinued, the time required for band migration was noted, and the bands were scanned under static conditions. Generally, this required about a three minute pause in kinetic conditions. The field was reapplied and solute migration resumed for a determined period of time. Before the time required for analyte elution, the polarity of the applied field was reversed and the bands continued to migrate in the column now towards the injection side. Once the bands migrated past the detector, the voltage was discontinued, the total time of band migration was noted, and the bands were scanned. This procedure was repeated several more times until a sufficient set of data was obtained.

Results and discussion

Figure 3.5 depicts an electropherogram obtained from the separation of ϕ x-174 Hae III digest fragments. The excellent resolution (2.1 for the 271/281 bp fragments) and efficiency (4.5×10^6 plates/m for the 1353 bp fragment) is typical for a carefully optimized CE experiment.

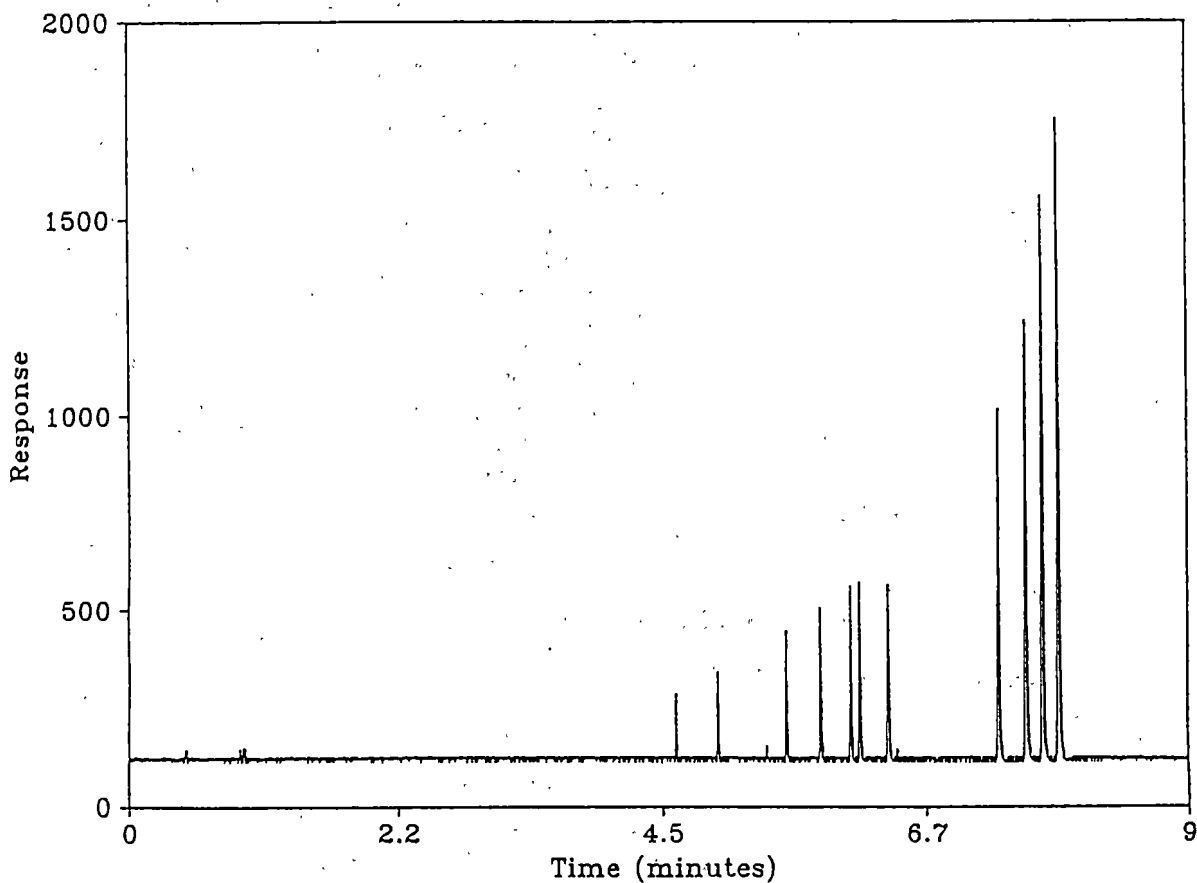


Figure 3.5: SSCE separation of ϕ x-174 Hae III digest. Fragments (in order of elution): 72, 118, 194, 234, 271, 281, 310, 603, 872, 1078, 1353 bp. Conditions: [DNA] = 10 μ g/ml; injection = -500V/10s; E = -10kV/40cm (-250 V/cm); length to detector (L_d) = 20 cm; buffer = 0.5% MC (M_n = 100,000) in 45 mM TBE and 2.5 μ M EB.

Figure 3.6 shows scans of a selected peak from the DNA digest at selected time intervals. The peak depicted was isolated and held under static conditions for the duration of the experiment; i.e., this peak was utilized to determine a static diffusion coefficient. Peak width is measured in centimeters by converting the time axis into a distance axis using the scan rate of 1.0 cm/min. For a Gaussian peak, the peak width at half height is related to variance by Eq. 3.5 which is derived from the formula for a Gaussian peak:

$$W_{1/2} = 2[2\ln 2]^{1/2} \sigma_{total} \quad (3.9)$$

After variance is determined, the slope of a plot of variance versus time yields the diffusion coefficient as shown by Eq. 1.15. The static diffusion coefficients for the last four eluting fragments of the DNA digest (603, 872, 1078, and 1353 bp) are listed later on page 64; the relative standard deviation (R.S.D.) values for these determinations were <10%.

Figure 3.7 depicts scans of a selected peak that was subjected to kinetic conditions as described in the experimental section; i.e., this peak was utilized to determine a kinetic dispersion coefficient. Note that the manipulations required for these measurements do not appreciably alter the Gaussian peak shape and, thus, Eq. 3.5 may also be used to calculate peak variance for these studies as well.

Another paper described a method for determining diffusion coefficients by pumping bands of solutes in water through thin capillaries with the use of a precise syringe pump and then utilizing the Taylor-Aris dispersion equation to determine the diffusion coefficient based on the extent of the laminar flow profile

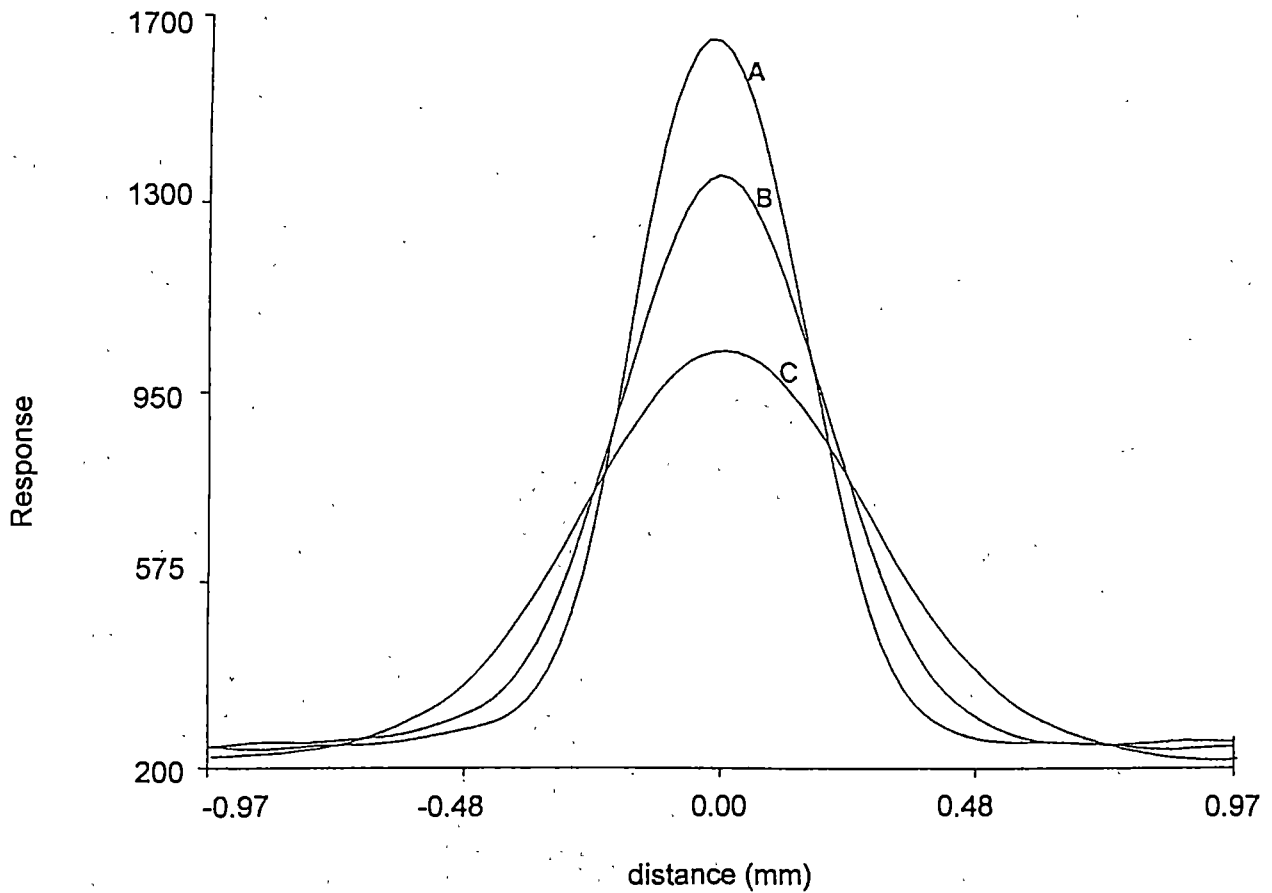


Figure 3.6: Scans performed for the determination of static diffusion coefficients. Scans depicted are of a selected peak (1353 bp); scan rate = 1.0 cm/min. Scans were performed following (A) 0; (B) 27; and (C) 94 minutes of diffusion under static conditions.

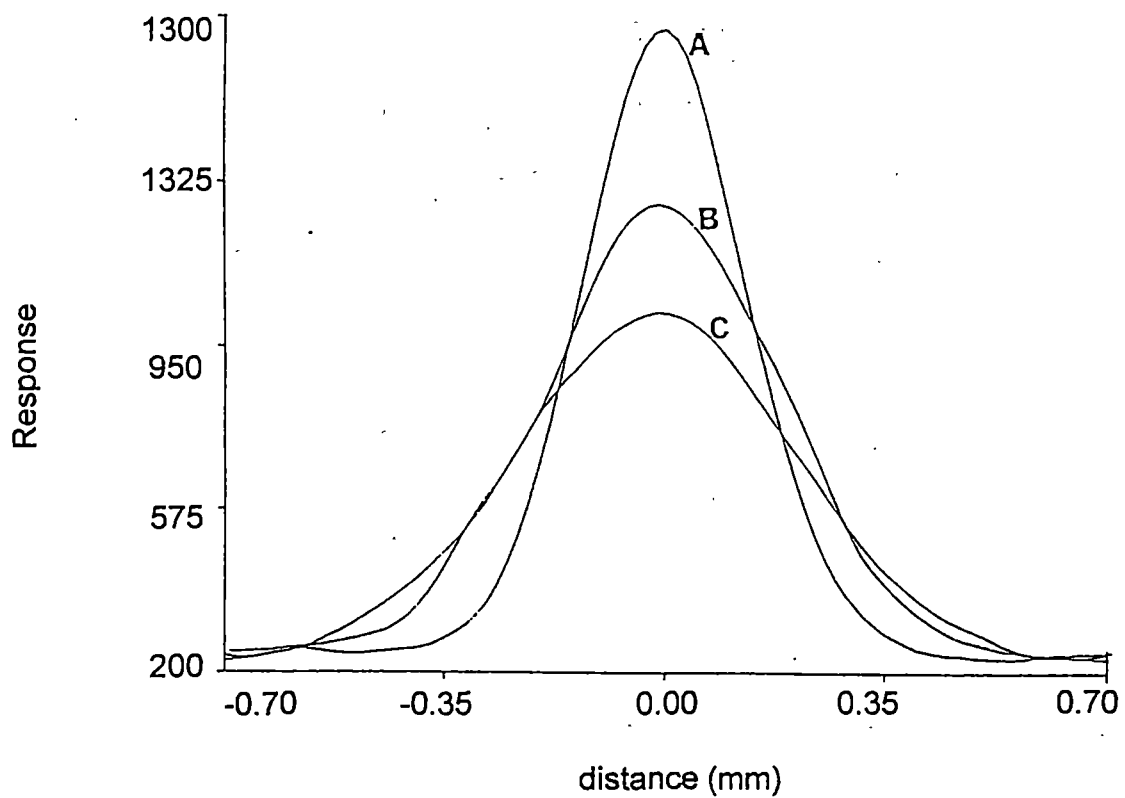


Figure 3.7: Scans performed for the determination of dispersion coefficients. Scans depicted are of a selected peak (1353 bp); scan rate = 1.0 cm/min. Electrophoresis is briefly paused (> 2 minutes) during the scan. Scans were performed following (A) 6; (B) 13; and (C) 20 minutes of electrophoresis.

observed (as depicted in Figure 1.3) (64). This method relies on Fick's law to approximate the diffusion coefficient (D), as stated by:

$$Q = UC_m + D \left(\frac{\partial C_m}{\partial x} \right) \quad (3.9)$$

where Q is the mass flux along the capillary column, U is the mean velocity, C_m is the mean analyte concentration over the tube cross section, and x is the distance along the axis. Though the equation suggests a simple relationship, the determination of the analyte concentration at various points in the capillary is not a trivial calculation (64). Furthermore, it was suggested that results from these experiments could be extrapolated to conditions of other solutions by simply using the Stokes-Einstein relationship and correcting for solution viscosity as "it was assumed that the coefficient of molecular diffusion obeys Einstein's relation and thus is proportional to the absolute temperature and inversely proportional to the solution viscosity." (64).

Based on this assumption that free-solution conditions may be extrapolated to conditions when using entangled polymer solutions, the relationship between the measured diffusion coefficient of DNA fragments and entangled polymer solution viscosities was directly examined and is depicted in Figure 3.8. One can clearly see that this plot indicates that the Stokes-Einstein equation is indeed not valid for oligonucleotides in entangled polymer solutions. In fact, the point at which the slope of the line changes sharply occurs at the entanglement threshold for this polymer. From this plot, one can see the difficulty in predicting the diffusion coefficient based on established equations.

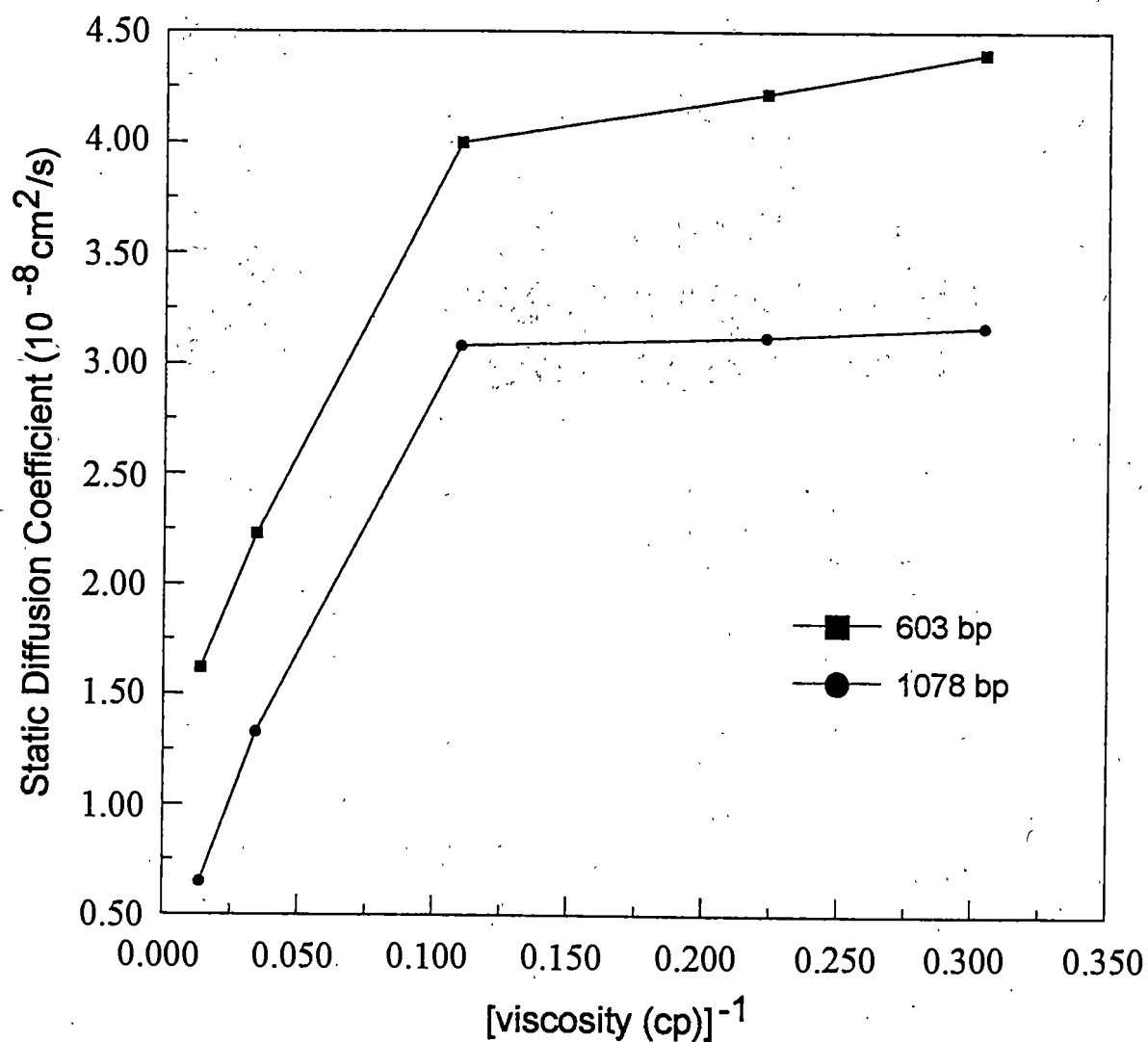


Figure 3.8: Relationship between diffusion of DNA fragments and viscosity of entangled polymer solutions. The static diffusion coefficient for the DNA fragments were measured in the following MC ($M_n = 100,000$) solutions (respective viscosities indicated in parantheses): $20 \mu\text{M}$ (3.29 cp), $35 \mu\text{M}$ (9.13 cp), $50 \mu\text{M}$ (29.2 cp), $70 \mu\text{M}$ (73.1 cp).

Furthermore, the aforementioned procedure of measuring diffusion in free solution would not be a valid method for determining static diffusion coefficients in polymer solutions typically utilized in SSCE. Therefore, the most reliable method to determine static diffusion coefficients when using polymer solutions appears to be experimental measurements as described in this chapter.

Because of the various migration models of DNA fragments in entangled polymers during CE, one would indeed predict that the diffusion coefficients are not the same under kinetic conditions as when under static conditions. The equation derived by Luckey et al. (Eq. 3.8) attempts to correlate the two diffusion coefficients based on a mobility correction factor. Using a 50 μM MC solution ($M_n = 100,000$), the fragment mobilities were measured under various fields and are compiled in Table 3.1 and plotted in Figure 3.9 (A). In this plot, one observes an apparent change in the slope of the line at field strengths between 200-250 V/cm. Therefore, the zero-field mobility used in subsequent calculations is extrapolated from the portion of the graph corresponding to low applied fields (< 200 V/cm). At each field, the expected kinetic diffusion coefficients were calculated and are listed in Table 3.2. The peak variances of these fragments were determined from experimental measurements and one finds that a significant discrepancy between the calculated kinetic diffusion coefficient and the total observed band variance is observed. Therefore, "dispersion" coefficients were determined in the same manner as the diffusion coefficients and are listed in Table 3.2. Two significant trends in this data are observed. First, as the fragment size becomes larger, the percent dispersion accounted for

Table 3.1: Mobility of DNA Fragments in Methyl Cellulose Solutions

(data reported at $10^{-4} \text{ cm}^2/\text{V s}$)

Field (V/cm)	603 bp	872 bp	1078 bp	1353 bp
50 μM MC ($M_n = 100,000$)				
415	2.25	2.20	2.16	2.13
350	2.11	2.06	2.02	1.99
285	2.05	2.00	1.96	1.93
235	2.03	1.97	1.93	1.90
170	1.85	1.77	1.74	1.70
105	1.77	1.58	1.54	1.51
50	1.68	1.51	1.44	1.40
μ^0	1.61	1.45	1.35	1.30
840 μM MC ($M_n = 20,000$)				
415	1.84	1.81	1.78	1.75
350	1.69	1.65	1.62	1.61
285	1.66	1.62	1.59	1.58
235	1.58	1.52	1.50	1.49
170	1.54	1.48	1.45	1.44
105	1.47	1.39	1.36	1.34
50	1.41	1.31	1.26	1.23
μ^0	1.35	1.25	1.21	1.19

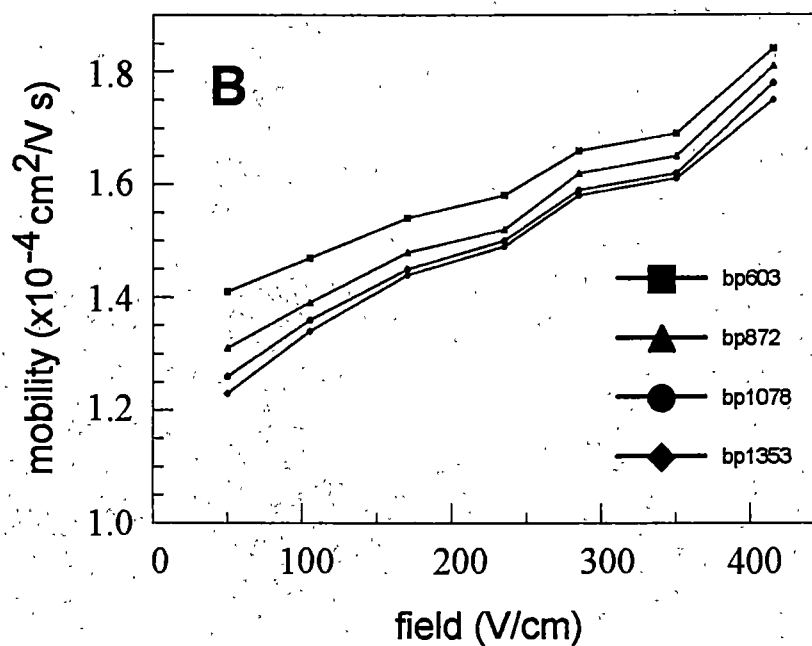
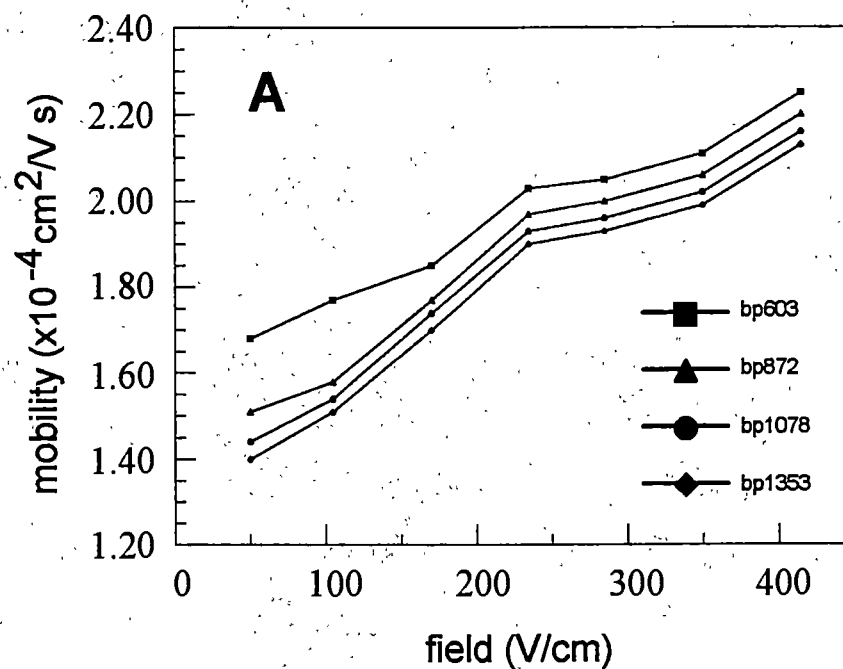


Figure 3.9: Relationship between mobility and field strength. (A) experiments in 50 μM MC ($M_n = 100,000$) and; (B) 840 μM MC ($M_n = 20,000$).

Table 3.2: Diffusion/Dispersion Coefficients ($\times 10^{-8}$ cm²/s)

	603 bp	872 bp	1078 bp	1353 bp
D ⁰	2.20	1.62	1.31	0.868
D ⁵⁰ (c)	2.30	1.71	1.38	0.907
<u>D⁵⁰ (o)</u>	<u>5.85</u>	<u>4.67</u>	<u>5.63</u>	<u>5.40</u>
% acc	47.9	36.6	24.5	16.8
D ¹⁰⁵ (c)	2.43	1.79	1.47	0.978
<u>D¹⁰⁵ (o)</u>	<u>6.88</u>	<u>14.2</u>	<u>14.6</u>	<u>13.0</u>
% acc	20.6	12.6	10.1	7.5
D ¹⁷⁰ (c)	2.53	2.00	1.66	1.10
<u>D¹⁷⁰ (o)</u>	<u>8.85</u>	<u>18.5</u>	<u>14.4</u>	<u>17.5</u>
% acc	15.4	10.8	11.5	6.3
D ²³⁵ (c)	2.78	2.23	1.84	1.23
<u>D²³⁵ (o)</u>	<u>12.3</u>	<u>19.5</u>	<u>19.6</u>	<u>19.1</u>
% acc	15.3	11.4	9.4	6.4
D ²⁸⁵ (c)	2.81	2.26	1.87	1.25
<u>D²⁸⁵ (o)</u>	<u>21.8</u>	<u>27.4</u>	<u>23.9</u>	<u>24.8</u>
% acc	12.9	8.2	7.8	5.0
D ³⁵⁰ (c)	2.89	2.33	1.93	1.29
<u>D³⁵⁰ (o)</u>	<u>23.4</u>	<u>28.6</u>	<u>24.4</u>	<u>24.6</u>
% acc	12.3	8.1	7.9	5.2
D ⁴¹⁵ (c)	3.07	2.49	2.06	1.38
<u>D⁴¹⁵ (o)</u>	<u>36.0</u>	<u>34.6</u>	<u>34.1</u>	<u>33.2</u>
% acc	8.5	7.1	6.0	4.1

D⁵⁰ (c) = calculated dispersion coefficient at a field of -50 V/cm

D⁵⁰ (o) = observed dispersion coefficient at a field of -50 V/cm

% acc = % dispersion accounted for by calculated dispersion coefficient

by the calculated kinetic diffusion becomes less. Also, as the applied field is increased, the percent dispersion accounted for by diffusion becomes less, even at low fields.

The concentration of low molecular weight MC ($M_n = 20,000$) that will give a comparable pore size as a $50 \mu\text{M}$ MC ($M_n = 100,000$) solution was determined to be $840 \mu\text{M}$ based on polymer mesh size equations (56). The same experiment was repeated, again comparing expected diffusion coefficients with observed dispersion coefficients, using the lower molecular weight polymer. Again, the same general trends were observed; i.e., the percent dispersion accounted for by the calculated kinetic diffusion coefficient became less as the fragment size became larger and as the applied field was increased. However, when comparing the data from the two polymer studies, the high molecular weight polymer showed significantly more non-diffusional dispersion than what was observed in solutions of the low molecular weight polymer; data for the 603 bp fragment is included in Table 3.3.

Conclusions

The rapid band dispersion observed during CE is most complex and cannot be attributed solely to longitudinal diffusion. Furthermore, the equation proposed by Luckey, et al. (Eq. 3.8) for kinetic diffusion coefficient determinations in CGE does not appear to account for a significant portion of band dispersion observed when utilizing entangled polymer solutions in SSCE. This is shown graphically in Figures 3.10 and 3.11. Slater et al. further discussed theories of

Table 3.3: Diffusion/Dispersion Coefficient ($\times 10^{-8}$ cm²/s) of 603 bp Fragment in Different Methyl Cellulose Solutions

	840 μ M MC ($M_n = 20,000$)	50 μ M MC ($M_n = 100,000$)
D^0	3.52	2.20
D^{50} (c)	3.68	2.30
<u>D^{50} (o)</u>	<u>5.85</u>	<u>4.80</u>
% acc	62.9	47.9
D^{105} (c)	3.83	2.43
<u>D^{105} (o)</u>	<u>6.88</u>	<u>11.8</u>
% acc	55.7	20.6
D^{170} (c)	4.02	2.53
<u>D^{170} (o)</u>	<u>8.85</u>	<u>16.4</u>
% acc	45.4	15.4
D^{235} (c)	4.12	2.78
<u>D^{235} (o)</u>	<u>12.3</u>	<u>18.1</u>
% acc	33.5	15.3
D^{285} (c)	4.33	2.81
<u>D^{285} (o)</u>	<u>14.0</u>	<u>21.8</u>
% acc	30.9	12.9
D^{350} (c)	4.41	2.89
<u>D^{350} (o)</u>	<u>18.4</u>	<u>23.4</u>
% acc	24.0	12.3
D^{415} (c)	4.80	3.07
<u>D^{415} (o)</u>	<u>27.1</u>	<u>36.0</u>
% acc	17.7	8.5

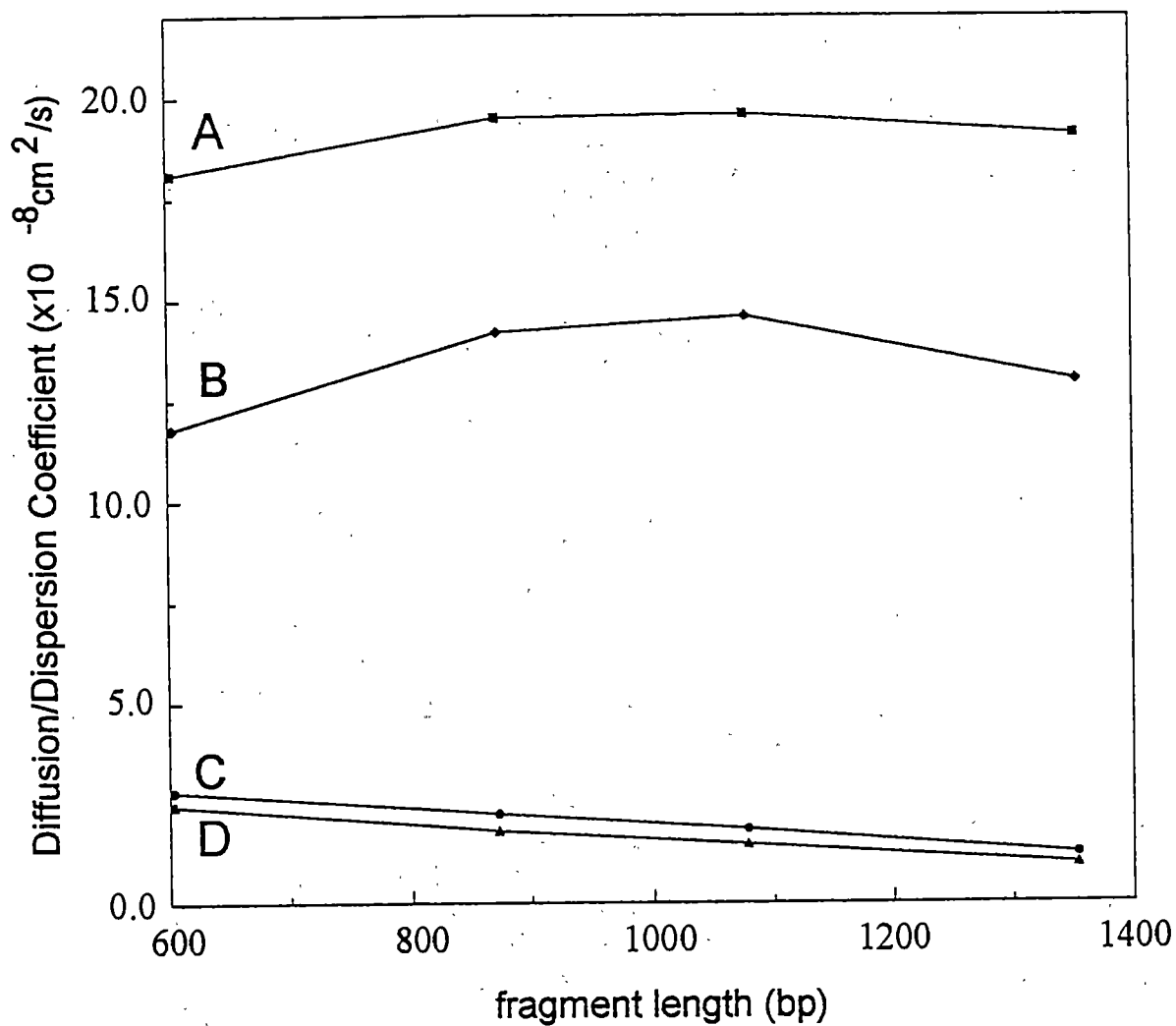


Figure 3.10: Effect of fragment size on diffusion and dispersion. Depicted are measured dispersion coefficients at fields of (A) -235 V/cm; (B) -105 V/cm; and calculated diffusion coefficients at fields of (C) -235 V/cm; (D) -105 V/cm.

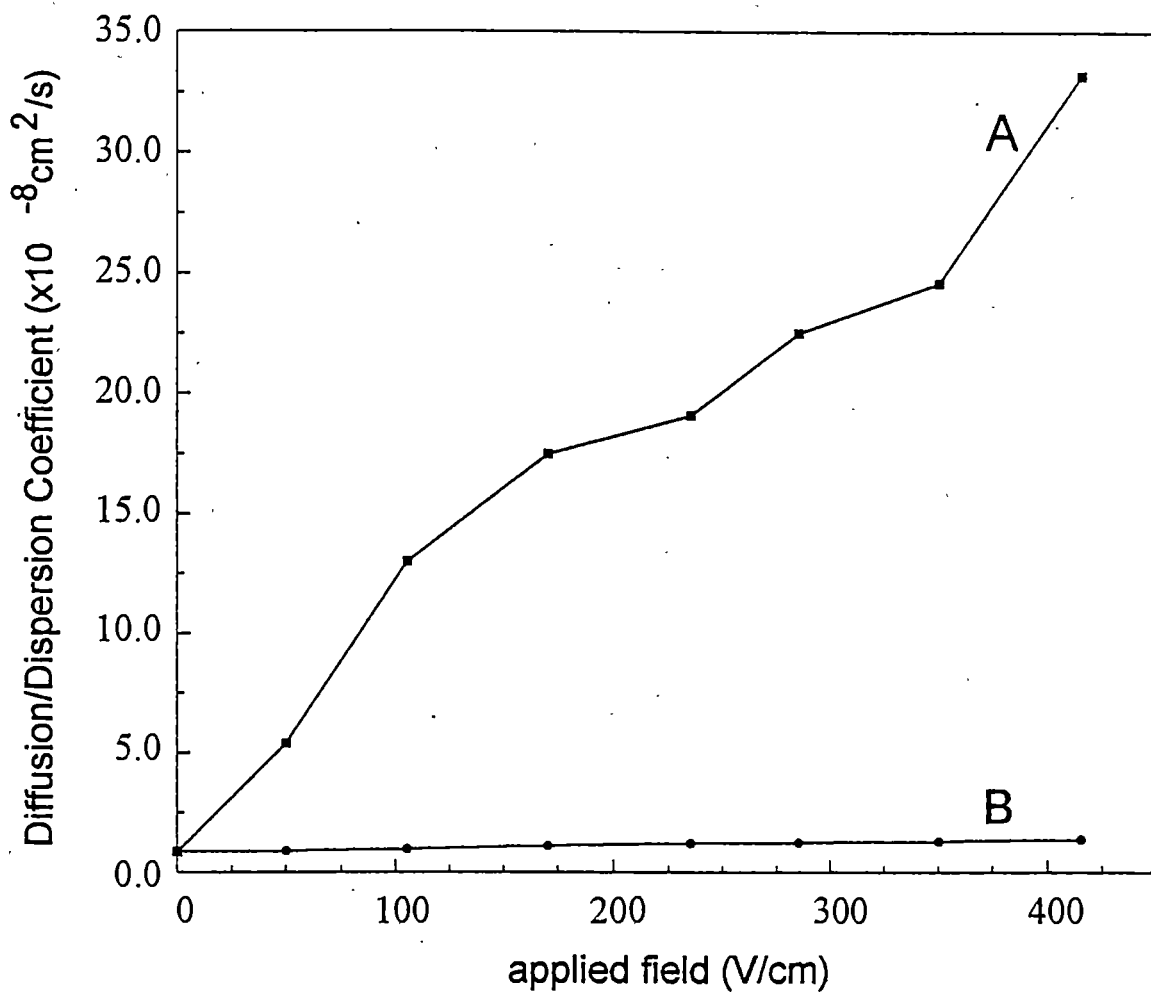


Figure 3.11: Effect of field strength on band dispersion. (A) observed dispersion coefficient; and (B) calculated kinetic diffusion coefficient; versus applied field is depicted for the 1353 bp fragment.

band dispersion in CGE and addressed the validity of the kinetic diffusion expression shown in Eq. 3.8 (65). Their contention is that the Einstein relationship used in the derivation by Luckey et al. is not appropriate for the non-equilibrium events occurring in these CGE separations of DNA fragments. They derive an expression that predicts that the longitudinal diffusion coefficient (D_x) initially increases as the applied field increases; however, as the field becomes stronger, the effect on molecular orientation of the DNA fragments is such that they become more rigidly elongated. This orientation effect begins to cause a decrease in D_x as the orientation becomes saturated. These researchers also present calculations that indicate there is a maximum in D_x when plotted versus base pair number. Slater et al. utilized scaled field and base pair parameters and CGE conditions that cannot easily be extrapolated to SSCE conditions. Nevertheless, the plots of dispersion coefficient versus base pair number for the larger fragments in the test sample appear to exhibit a weak maximum (Figure 3.10; A, B). The plot of dispersion coefficient versus field for the 1353 bp fragment shown in Figure 3.11 A does not exhibit a clear maximum. However, it appears that the slope of that plot decreases for mid-range fields, then increases dramatically for the highest field, presumably due to the onset of severe thermal dispersion.

Luckey et al. contend that as a fragment elongates in an applied field, the transverse diffusion coefficient (D_y , perpendicular to the capillary axis and the applied field) decreases (63). This should exacerbate problems with the thermal gradients that occur at high fields since rapid transverse diffusion reduces the

dispersive effects of thermal gradients. Again, Slater et al. come to a different conclusion concerning the magnitude and trends in D_y (65). Their derivation indicates that D_y can be relatively large and hence thermal gradients are less problematic than predicted by Luckey et al. The experimental results presented in this chapter do not shed much light on this controversy. However, the dispersion coefficient observed at very high fields shown in Table 3.1 and Figure 3.11 clearly indicate the onset of thermal dispersion.

The DNA fragment-entangled polymer interactions which lead to separation in SSCE were discussed by Barron et al. (58). They state that the retardation of mobility caused by these interactions is what actually permits the separation of fragments; thus, the larger the fragments, the more sites for it to become entangled and, consequently, the lesser the observed mobility. They further state that the larger the entangled polymer chain, the more of a frictional drag it exerts on the fragment and, again, the more retarded the mobility will be.

Considering the arguments presented in these references and the experimental data presented in this chapter, it may be concluded that these non-equilibrium interactions involving entanglement-disentanglement are indeed a significant contribution to band dispersion during CE. These fragment-polymer interactions may be considered to be similar to resistance to mass transfer in other chromatography methods. Fragments become entangled and "drag" polymers in various discrete steps during CE. This conclusion is consistent with the trends observed in Table 3.1 and with the hypotheses stated by Barron et al.;

the larger fragments and solutions of higher molecular weight entangled polymers showed the greatest dispersion.

In conclusion, certain assumptions made for CGE may not be valid for polymer solutions. The sources of dispersion that are significant in CGE are also significant in polymer solutions but the dynamics of the separation process in the two systems differ and this causes the extent of dispersion by these sources to not be equal. The trends in the data presented herein show some agreement with derivations offered by Slater et al. However, the trends we observe might also be qualitatively described by a traditional chromatographic resistance to mass transfer argument. Clearly, the issue of band dispersion is scientifically intriguing; however, some CE practitioners such as Pierre Righetti take a lighter view on this topic, "As luck goes, most authors have ignored these issues so far and lived happily with their CZE results." (66).

-Chapter 4-
**The Use of Cyanine Intercalation Dyes for
Laser Induced Fluorescence Detection of
DNA Fragments by Capillary Electrophoresis**

Introduction

A significant problem that is inherent to CE is that the diminutive diameter of capillary columns is not amenable to sensitive detection. Absorbance detection is a common mode of detection because a large number of analytes readily absorb a characteristic wavelength of light. However, given the direct proportionality between absorbance and detection pathlength (Eq. 1.27), the short pathlengths of detection zones of capillary columns limit sensitivity when employing absorbance detection in CE analyses. When Jorgenson and Lukacs first demonstrated fluorescence detection with CE, excellent efficiency and sensitivity were reported (7).

The analysis of DNA fragments by CE may be accomplished by employing absorption detection; however, a significant improvement in sensitivity is realized when DNA fragments are labeled with intercalation dyes and fluorescence detection is employed (67). Furthermore, in some cases, the separation is improved with the intercalation of dyes. For example, when comparing absorbance detection of unintercalated DNA relative to fluorescence detection of DNA fragments intercalated with ethidium bromide (EB), the intercalated fragments exhibit improved efficiency and resolution (Figure 4.1). The most likely reason for this observation is that each positively charged intercalation dye

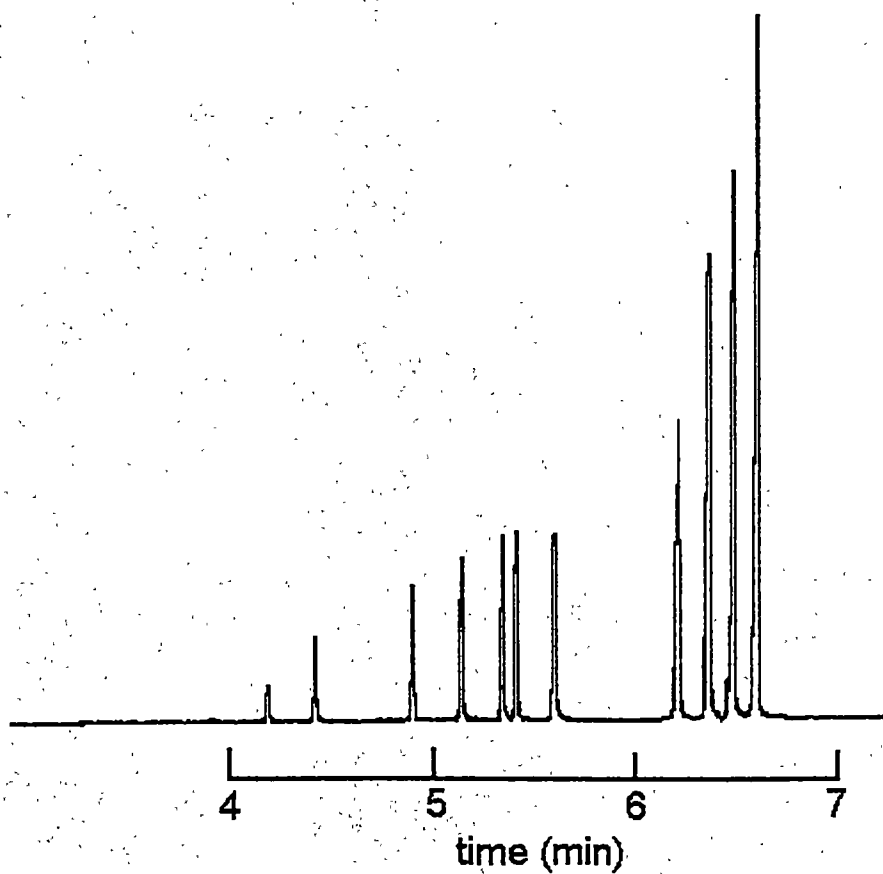
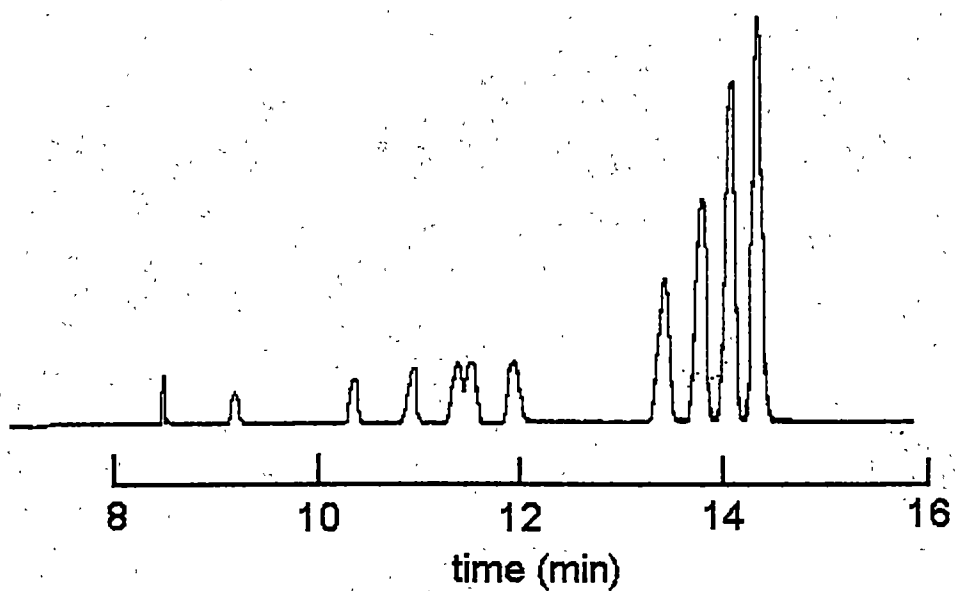


Figure 4.1: Absorbance and fluorescence detection of DNA fragments separated by CE. (top) absorbance detection; $\lambda_{\text{abs}} = 254 \text{ nm}$; $L_d = 32 \text{ cm}$; (bottom) fluorescence detection of fragments intercalated with EB; $L_d = 20 \text{ cm}$.

reduces the overall negative charge of the DNA fragments which retards the mobility of the fragment (as observed in Figure 4.1). This size-dependent modification of charge on the DNA fragment imparts a small degree of selectivity; i.e., a larger DNA fragment is intercalated with more dye molecules and, as a consequence, its mobility is more strongly affected than a smaller DNA fragment intercalated with fewer dye molecules.

There are three strategies which may be employed for labeling DNA fragments with intercalation dyes. First, pre-column labeling is accomplished by mixing the DNA digest with the desired intercalation dyes. However, there are several disadvantages to this approach. If the dye employed is a multi-site intercalation dye (e.g., a bis-intercalator), there is a probability of achieving intrafragment labeling. Also, if the binding affinity is not strong, decomposition of the complex during electrophoresis may occur. In addition, once a DNA digest is labeled in this manner, one cannot "unlabel" the fragment and use a different dye.

Another labeling strategy that may be employed is post-column labeling. In this scheme, DNA fragments are separated by electrophoresis and are labeled with the intercalation dye as it exits the separation column into a post-column reaction chamber (e.g., a sheath flow cell). The most significant problem when employing this strategy is controlling band dispersion which readily occurs from the dead volume and turbulence of the sheathing fluid in the flow cell. Furthermore, a sheath flow cell can be cumbersome to align and to match the flow rates between the separation column and the sheathing fluid. Also, the only

point at which detection may be performed is post-column; this technique is not amenable to multi-point or scanning detection.

The third approach which offers the most simplicity of the three approaches is to employ on-column labeling. This is done by simply adding the intercalation dye to the running buffer and allowing the DNA fragments to become intercalated during electrophoresis. Using this approach, detection may be done at any point along the column and it is very easy to change dyes by simply replacing the buffer with a buffer containing the dye of choice. Also, there is an equilibrium between the dye concentration intercalated into the fragments and in the surrounding running buffer which prevents decomposition of the DNA/dye complex.

Since intercalation alters DNA mobility, the inherent high efficiency of DNA separations by SSCE (as observed in Figure 3.4) can only be maintained if certain conditions are met. First, given the direct proportionality between fragment mobility and charge (Eq. 1.8), the intercalation of charged dye molecules affects the overall charge and, thus, the mobility of the DNA fragment. Therefore, in order to maintain a single migration rate for all fragments of each fragment size, a single labeling ratio must be obtained. Second, if multiple labeling ratios do exist, there must be a rapid on-column equilibrium between the various labeling ratios of DNA/dye complexes in order to achieve an "average" mobility for all fragments of each fragment size. Third, if unequal labeling ratios do exist for fragments of each fragment size, non-specific interactions with

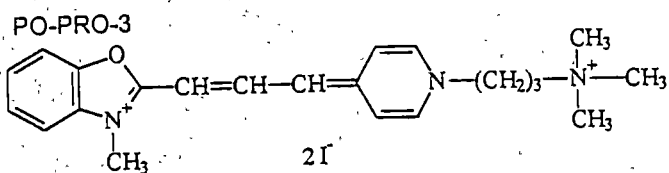
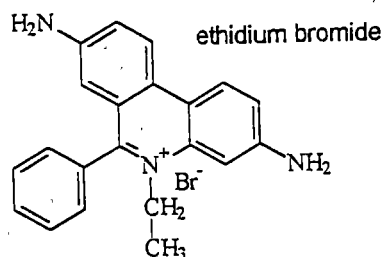
running buffer components must eliminate the differences in migration rates for these DNA/dye complexes.

In choosing an intercalation dye, several factors which influence sensitivity must first be considered. Low levels of detectability benefit from full intercalation (up to the exclusion limit of the dye) with low levels of dye, large dye absorptivities and intercalation-related spectral shift, small free dye fluorescence yields, and large intercalation fluorescence enhancements. Large Stokes' shifts and compatibility with available laser sources and optics are additional desirable characteristics that influence detectability.

Recently, a new series of cyanine intercalation dyes have been developed which are reported to offer superior fluorescence enhancement relative to EB (68). These dyes are offered in either monomeric (e.g., PO-PRO-3 iodide) or dimeric forms (e.g., POPO-3 iodide), as shown in Figure 4.2. The spectral properties of these dyes and the resulting DNA/dye complexes are listed in Table 4.1.

Initially, the use of these dyes for SGE was reported (69-71). Later, attempts to use these dyes for rapid and sensitive DNA detection by CE have been reported but with marginal success (27, 72-74). In these reports, it is typically the dimeric dyes that prove to be the most problematic; Kim and Morris evaluated dimeric dyes in a wide range of polymer and dye concentrations but were unable to achieve efficient, well-resolved separations (74). Several explanations have been presented, including the possibility that intramolecular DNA linkage between different fragments occur, resulting in a distribution of

mono-intercalators:



bis-intercalators:

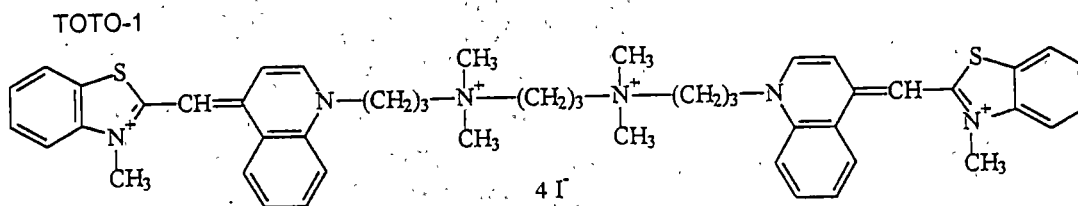
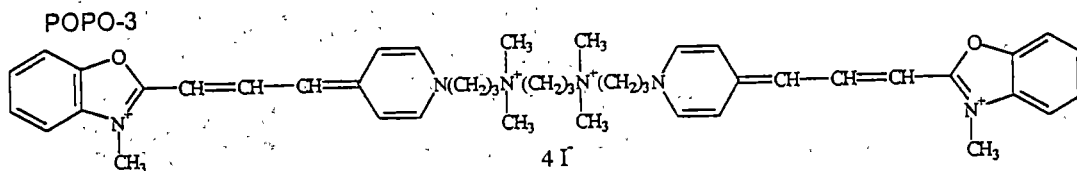


Figure 4.2: Structures of DNA intercalation dyes. Depicted are the monomeric dyes (ethidium bromide and PO-PRO-3) and the dimeric dyes (POPO-3 and TOTO-1) examined in this study.

Table 4.1: Spectral Properties of Intercalation Dyes and DNA/dye Complexes

	λ_{ex} (nm) ^a	λ_{em} (nm) ^a	ϵ (M ⁻¹ cm ⁻¹) ^b	QY ^b
EB	468	615		
DNA/EB	522	605	5,200	0.50
PO-PRO-3	533	556		
DNA/PO-PRO-3	539	567	87,900	0.39
POPO-1	531	561		
DNA/POPO-1	535	572	146,400	0.46
TOTO-1	515	529		
DNA/TOTO-1	520	535	117,000	0.34

^ameasured on fluorometer

^bmolar extinction coefficient (ϵ) and quantum yield (QY) values listed as reported by Molecular Probes

DNA/dye ratios for a single band of fragments; thus, a distribution of mobilities exists for that band of fragments, resulting in broad, inefficient peaks. Another possibility is that partial intercalation of these large dye molecules occurs and the unintercalated portion of the dye molecule may exhibit strong interactions with any exposed area of the capillary wall.

Figeys et al. evaluated the separation of DNA fragments intercalated with dimeric dyes (73). In this report, use of dimeric dyes did not yield the high efficiency and good resolution typically reported for EB. Na^+ was added to the running buffer with the idea that increasing the ionic strength of the buffer would result in the intercalation dye being more tightly held in the complex and that the partition ratio of the dye from the buffer into the DNA fragments would increase. Although an improvement in separation was reported, the data presented does not suggest that an appreciable improvement was realized. Furthermore, increasing the Na^+ concentration to 200 mM as reported by Figeys et al. greatly increases the current during electrophoresis; in order to maintain a desired power density (1W/m), very low fields must be utilized, resulting in longer analyses and increased band dispersion (presumably due to diffusion) (75).

Zhu et al. suggested that adding the monointercalator 9-aminoacridine (9-AA) would improve the separation of these DNA/dye complexes for two reasons (72). First, it is well-reported that cationic monointercalators improve the resolution of DNA fragments (76, 77). Also, it was suggested that 9-AA might fill sites not intercalated by the dimeric dyes, thus, resulting in a more uniform mobility. Although a modest improvement was realized, efficiency was still quite

poor and several fragments (e.g., 271/281 and 1078/1353 bp) remained unresolved.

In 1997, Clark and Mathies published results which finally showed a real improvement in the separation of DNA fragments complexed with dimeric dyes (78). Whereas previous attempts to use these dyes were done with buffers containing Na^+ , tris^+ , and other cations, Clark and Mathies developed a buffer which uses $[\text{CH}_3(\text{CH}_2)_4]_4\text{N}^+$ (referred to hereafter as NPe_4^+) as the sole cation. Although Clark and Mathies report a significant improvement when using these dimeric intercalation dyes in a carefully optimized buffer regime, the goals of their research was to form stable DNA/dye complexes for multiplex sizing of DNA fragments (78). However, separation performance was still poor for fragments > 600 bp and the significant fluorescence enhancement reported for these dyes was not fully realized. Also, given the goals of their research, the DNA fragments were labeled pre-column; thus, no successful use of these dyes for rapid, on-column labeling was demonstrated.

In this chapter, the feasibility of using these cyanine dyes for sensitive on-column intercalation using the buffer regime first reported by Clark and Mathies is investigated. Spectroscopic considerations for achieving better detectability are discussed. Since EB is the most commonly used dye for these types of analyses, a comparison of EB and these cyanine dyes is presented and relative limits of detection (LODs) for a selected fragment are reported. As CE for biotechnology develops, a major goal is to develop applications with ultra-sensitive detection that enable the study of DNA interactions. With this in mind,

the use of a sheath flow cell to label fragments post-separation was evaluated. Furthermore, because of the many difficulties encountered when employing these dyes for on-column intercalation, the use of a sheath flow cell for the post-separation labeling of DNA fragments may prove advantageous if intrafragment interactions or wall adsorption are the limiting factors for effectively using these dyes for CE analyses.

Experimental

materials

Tris(hydroxymethyl)aminomethane, boric acid, and ethylenediaminetetraacetic acid (di-sodium form, Na₂EDTA) were purchased from Sigma Chemical Co. (St. Louis, MO, USA) and used to prepare a 90 mM tris-boric acid-EDTA (TBE) buffer. N-tris(hydroxymethyl)methyl-3-aminopropylsulfonic acid (TAPS) and EDTA (protonated form, H₂EDTA) were also purchased from Sigma. Tetrapentylammonium hydroxide (NPe₄OH) solution was purchased from Fluka (Buchs, Switzerland) and used to make a 160 mM TAPS/1 mM EDTA buffer that was then titrated to pH 8.4 with NPe₄OH. Upon dilution, additional NPe₄OH was added to maintain pH 8.4. ϕ x-174 Hae III digest, methyl cellulose (MC, M_n = 100,000), and ethidium bromide were also purchased from Sigma. POPO-3 iodide and TOTO-1 iodide were purchased from Molecular Probes (Eugene, OR, USA). PO-PRO-3 iodide was a gift provided by Molecular Probes. Fused silica capillaries (75 μ m i.d. x 365 μ m o.d.) were purchased from Polymicro Technologies (Phoenix, AZ, USA).

column preparation

Capillaries were cut to a total length of 40 cm; a small detection window at 20 cm was prepared by removing the polyimide coating with warm sulfuric acid. The capillary walls were deactivated with linear polyacrylamide by the method previously described in Chapter 2.

solution preparation

DNA samples were prepared by diluting an aliquot from a stock sample with either 45 mM TBE or 80 mM TAPS. MC stock solutions were prepared by heating water to 90 °C while degassing with helium and then adding sufficient solid MC to prepare a 1% (w/w) stock. Once dissolved, the solution was placed into an ice bath and stirring continued until the solution became clear. Prior to use, stock solution was diluted to 0.5% MC (w/w) with the appropriate 2X buffer, spiked with intercalation dye (when appropriate), and vacuum degassed.

instrumentation

A He-Ne laser (Edmund Scientific, Barrington, NJ, USA), 1.5 mW at 543.5 nm, and an Ar⁺ laser (Coherent Laser Products, Palo Alto, CA, USA), 10.0 mW at 514.5 nm, were used as excitation sources. An f/1 lens was used to focus the laser through the capillary, and a quartz fiber optic (General Fiber Optic, Cedar Grove, NJ, USA) with a 200- μ m core diameter and a numerical aperture of 0.24 was used to collect fluorescence emission. The fluorescence was passed through either a 570 nm cut-on filter (when using the He-Ne laser) or a 550 nm

cut-on filter (when using the Ar⁺ laser) and into a R282 PMT (Hamamatsu, Bridgewater, NJ, USA). The photomultiplier tube (PMT) photocurrent was monitored with a model 126 photometer (Pacific Precision Instruments, Concord, CA, USA) and computer-aided data acquisition was performed with a program written in-house with LabVIEW (National Instruments, Austin, TX, USA). Applied fields of -250 V/cm were used throughout this study.

The sheath flow cell arrangement used for post-column derivatization studies is depicted in Figure 4.3 and has previously been described in detail (79). Briefly, a He-Ne laser (543.5 nm) was used for excitation and emission was directed by an *f*/2 lens into a PMT. A 1 mm slit and a 570 nm cut-on filter were used for spatial and optical rejection of scattered light.

Fluorometry experiments were conducted with an AMINCO-Bowman Series 2 spectrometer (SLM-Aminco, Urbana, IL, USA). In these experiments, 1.0 µg/ml DNA was combined with buffer/dye in a cuvette and the fluorescence intensity was measured at timed intervals. For DNA/EB, [EB] = 2.5 µM in 45 mM TBE buffer. For DNA/PO-PRO-3, DNA/POPO-3, and DNA/TOTO-1, [dye] = 0.10 µM in 80 mM TAPS/NPe₄⁺. The first data point, at approximately 1 minute following the mixing of DNA and dye, corresponds to the amount of time required to mix the solution and measure the fluorescence spectrum at an acceptable scan rate. In order to duplicate conditions used in the laser-based setup, the excitation source was set at 543 nm and the emission monochromator was set at 570 nm.

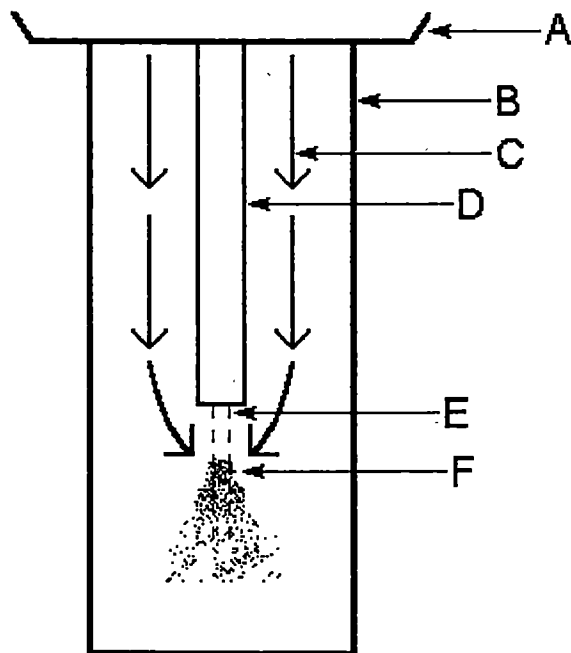


Figure 4.3: Sheath flow cell for postcolumn derivatization. (A) sheath flow cell holder; (B) sheath flow cell cuvette; (C) sheathing fluid flow; (D) separation capillary column; (E) effluent from separation column; (F) detection zone where band exiting the column is labeled; note that efficiency rapidly degrades beyond this point. The field is maintained by submerging the lower portion of the sheath flow cell in buffer solution.

Results and Discussion

effect of buffer on separation performance

One of the many advantages of using EB is that it is compatible with various buffer regimes and separation matrices. Perhaps the most commonly used buffer in DNA analysis by SSCE is TBE. In this work, very good separations with EB in this buffer were achieved (Figure 4.4 (A)). Conversely, on-column intercalation of POPO-3 in TBE resulted in very poor efficiency and resolution (Figure 4.4 (B)). After changing to a TAPS buffer containing NPe_4^+ , a significant improvement in the separation using POPO-3 was achieved (Figure 4.5 (A)); results with on-column intercalation were comparable to separations of prelabeled fragments (Figure 4.5 (B)).

Table 4.2 summarizes data obtained from these separations. Note that even though the separation using POPO-3 was significantly improved when TBE was replaced with TAPS, the separation figures of merit (efficiency and resolution) are still better when EB in TBE is used. Clark and Mathies suggest that this may be due to the labeling kinetics of these dyes. Whereas EB in TBE undergoes rapid on-column labeling, the exchange kinetics for POPO-3 in TBE might be hindered by the presence of other cations in the buffer solution competing with this dye for DNA binding sites. Changing to a buffer system with limited cations (i.e., TAPS) somewhat alleviates this problem. Furthermore, the addition of NPe_4^+ to TAPS provides the buffer with a counterion which effectively buffers the charge of the DNA/dye complexes. As discussed in the introduction to this chapter, migration rates will vary for fragments with different labeling

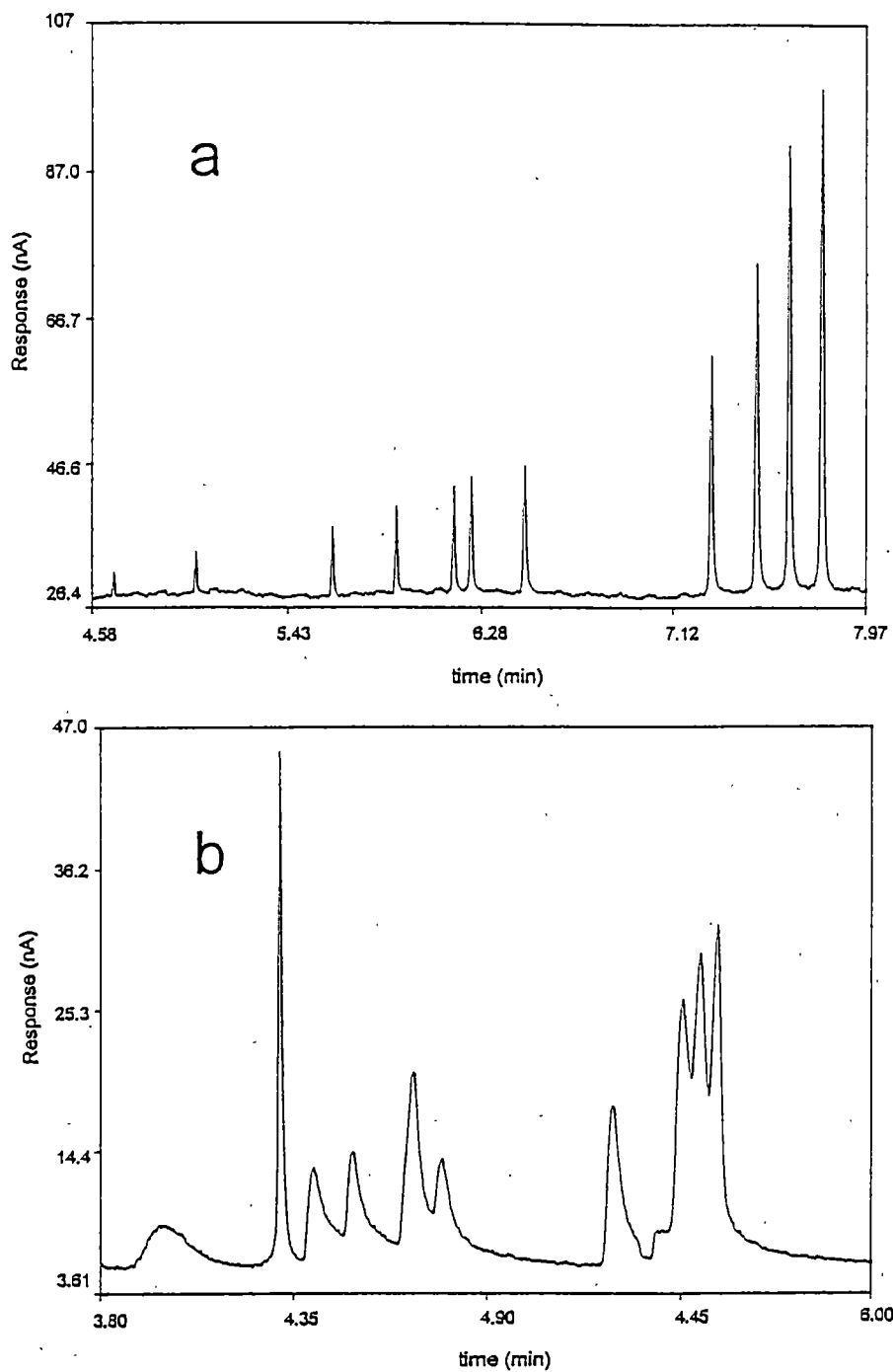


Figure 4.4: Separation of DNA digest in methyl cellulose with TBE buffer. (a) on-column intercalation with $2.5 \mu\text{M}$ EB; 16 pg injected; (b) on-column intercalation with $0.10 \mu\text{M}$ POPO-3; 11 pg injected.

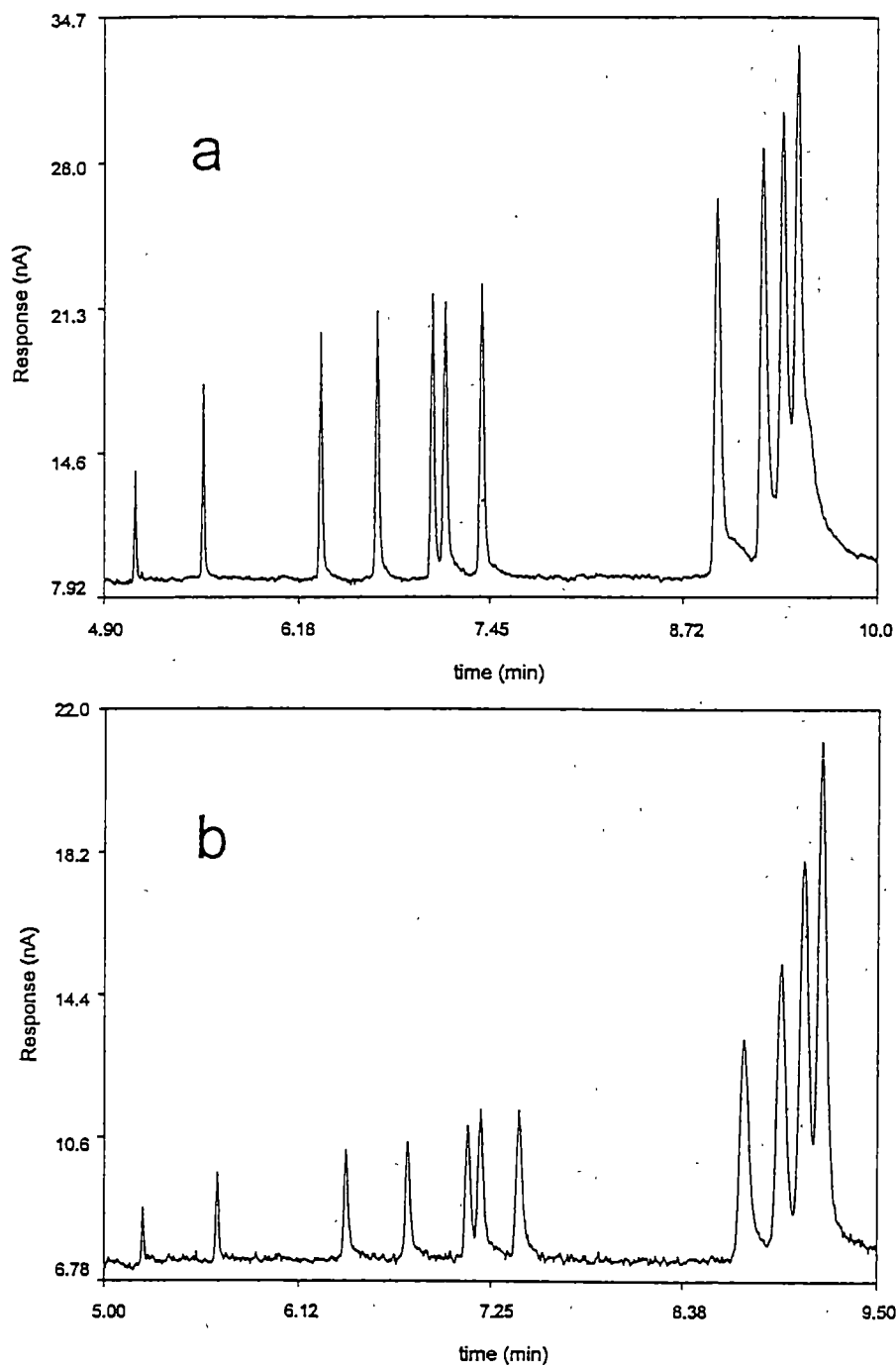


Figure 4.5: Separation of DNA digest in methyl cellulose with TAPS buffer. (a) on-column intercalation with $0.10 \mu\text{M}$ POPO-3; 0.57 pg injected; (b) pre-labeled with $0.10 \mu\text{M}$ POPO-3 (bp:dye = 10:1); 0.72 pg injected.

Table 4.2: Buffer Effects on Separation Performance and Sensitivity

	N_{603} ($\times 10^6/m$)	R_s (271/281)	R_f (nA/M)
DNA/EB in TBE	1.90 (+/- 0.31)	1.9 (+/- 0.2)	7.5×10^7
DNA/POPO-3 in TAPS	0.50 (+/- 0.04)	1.0 (+/- 0.1)	2.1×10^9
DNA/PO-PRO-3 in TAPS	2.60 (+/- 0.20)	2.1 (+/- 0.3)	2.3×10^8

NOTES

- all data shown are from separations performed with on-column intercalation
- N_{603} ($\times 10^6/m$) = efficiency (plates/m)
- R_s (271/281) = resolution between the 271 and 281 bp fragments
- R_f (nA/M) = response factor (nanoamps of signal per molar concentration) of the 310 bp fragment

ratios. It is postulated that the association of the NPe_4^+ counterion has nearly the same effect on fragment mobility as does intercalation by these large dyes. Therefore, for fragments of differing labeling ratios, the association of NPe_4^+ with these complexes compensates for the differences in migration rates and, thus, a more uniform electrophoretic mobility results (78).

The use of TBE with PO-PRO-3, the monomeric analog of POPO-3, also resulted in relatively poor efficiency and resolution but, again, the separation was significantly improved after replacing TBE with TAPS (Figure 4.6 and Table 4.2). Apparently, the role of the buffer counterion is also significant when using the monomeric cyanine dyes. In this case, even when compared with separations using EB in TBE, the best efficiency was obtained when on-column labeling with PO-PRO-3 in TAPS was performed.

The enhancement in separation quality is not only important for complete resolution of fragments but also significantly affects detectability. Established equations (i.e., Eq. 1.26) are utilized to calculate the amount of analyte injected. However, when determining the on-column detectability of a selected fragment, rather than the quantity injected, it is the concentration of analyte at band center that must be considered. This is because the solute concentration is inversely proportional to variance (80); hence, a dye/buffer system that leads to diminished efficiency will also result in diminished detectability in terms of lower signal-to-noise (S/N) ratio. Upon optimizing separation conditions so that efficiency is maximized, an improvement in detectability will be realized as well.

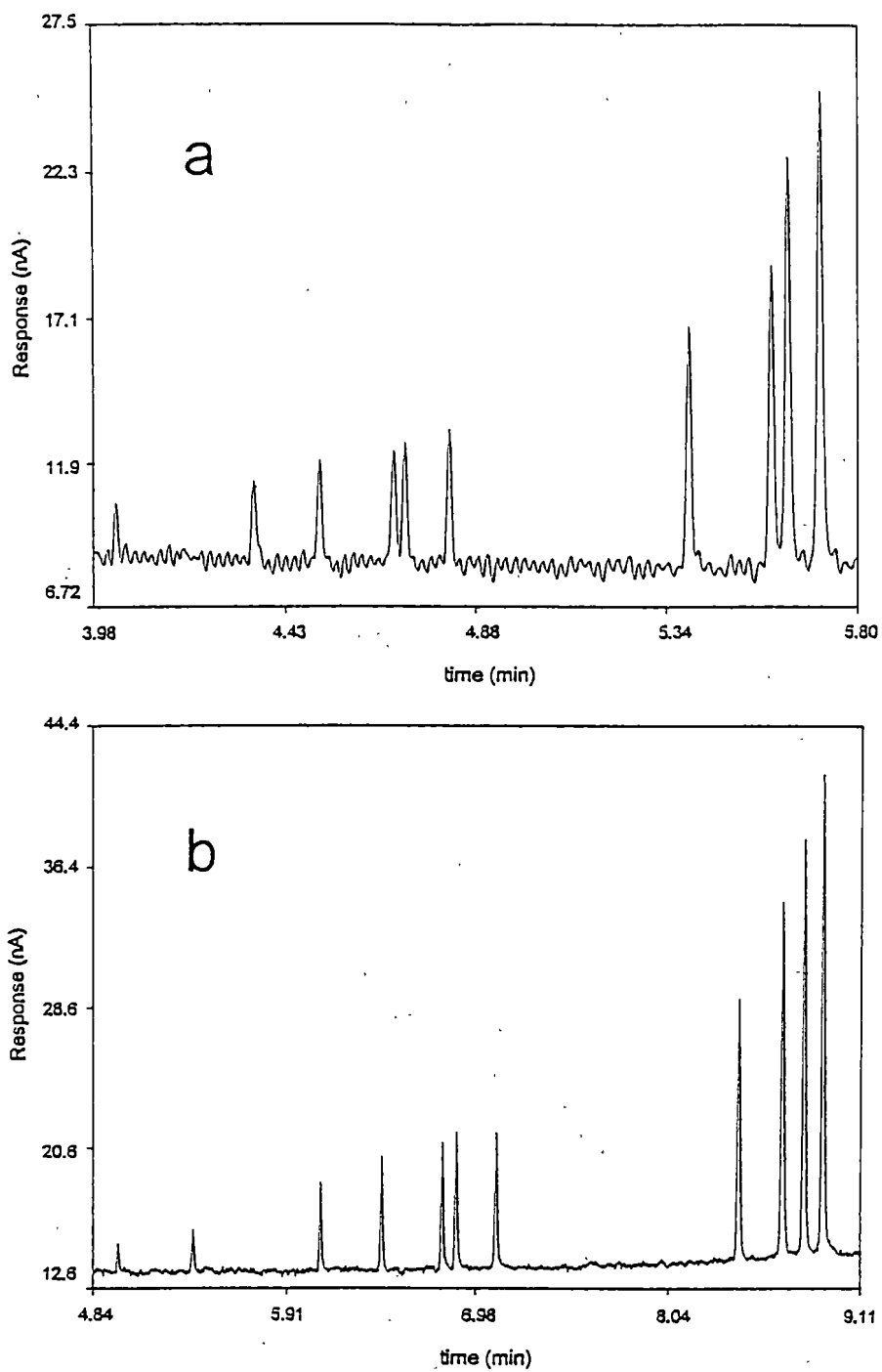


Figure 4.6: Separation of DNA digest in methyl cellulose with PO-PRO-3. (a) on column intercalation in TBE buffer with $0.10 \mu\text{M}$ PO-PRO-3; 8.6 pg DNA injected; (b) on column intercalation in TAPS buffer with $0.10 \mu\text{M}$ PO-PRO-3; 7.2 pg DNA injected.

Sensitivity and LOD

When using POPO-3, replacing TBE with TAPS not only improves the separation but sensitivity appears to improve also. The electropherograms in Figure 4.4 (A) and (B) were obtained by injecting 16 pg and 11 pg DNA, respectively, while the electropherograms in Figure 4.5 (A) and (B) were obtained following an injection of 0.57 pg and 0.72 pg DNA, respectively. To quantitate this improvement in sensitivity, a response factor was calculated (Table 4.2). This factor is calculated by determining the molar concentration of the 310 bp fragment at band center. The signal intensity is determined from the peak height above the baseline and this value is divided by the molar concentration to give the reported R_f . These calculations indicate an improvement in sensitivity when using the cyanine dyes in place of EB that is consistent with differences in the molar absorptivities of these dyes (see Table 4.1). Although the dimeric dye offers the best improvement in sensitivity, this may not translate into improvements in LOD in terms of injected concentration or amount due to the poorer separation efficiency.

Given the apparent separation problems with using POPO-3 and the much better separation performance and modest improvement in sensitivity of PO-PRO-3, the monomeric dye was chosen for LOD evaluations. For these studies, a series of dilutions of DNA samples were prepared in a concentration range to include samples near the expected LOD. The LODs were estimated by using Eq. 1.26 to calculate the quantity injected. This quantity was divided by the measured S/N ratio and an injected quantity corresponding to a S/N of 3 was

extrapolated. Results from experiments using a 1.5 mW He-Ne laser at 543.5 nm for excitation are shown in Table 4.3. Although the use of a laser at 543.5 nm is closer to the excitation maximum for DNA/PO-PRO-3 ($\lambda_{ex} = 539$ nm), these experiments were repeated using the 514.5 nm line of an Ar⁺ laser that may be operated at higher laser powers. Because of the direct proportionality of laser incident power and fluorescence luminescent power, an improvement in the LOD was realized (Table 4.3).

The use of PO-PRO-3 with Ar⁺ laser excitation shows promise for low levels of detectability. However, with increased laser power also comes the undesired effect of increasing the background when using intercalation dye in running buffers. This is illustrated in Figure 4.7 where an increase in laser power results in an increasing background under applied fields. The fact that doubling the laser power does not double the background is largely due to thermal diffusion. The temperature gradient resulting from nonradiative dissipation of absorbed laser radiation results in diffusion of dye from the path of the laser beam. As increasing the field increases the flow rate, this effect is diminished and the background increases. The effect for PO-PRO-3 is greater than for EB due to its 17-fold greater molar absorptivity. However, even with an increasing background, a significant increase in noise was not observed; in fact, the relative noise in the background signal was lower than when experiments were performed at higher laser powers. For experiments using 5 mW and 10 mW of laser power, the relative noise determined from the background signal decreased from 1.4% to 0.9%, respectively, for PO-PRO-3. This may indicate that the flux

Table 4.3: Detection Limits of 310 bp Fragment (fg injected)

	He-Ne Laser	Ar⁺ Laser
DNA/EB in TBE	365 (+/- 10)	46 (+/- 9)
DNA/PO-PRO-3 in TAPS	200 (+/- 40)	10 (+/- 2)

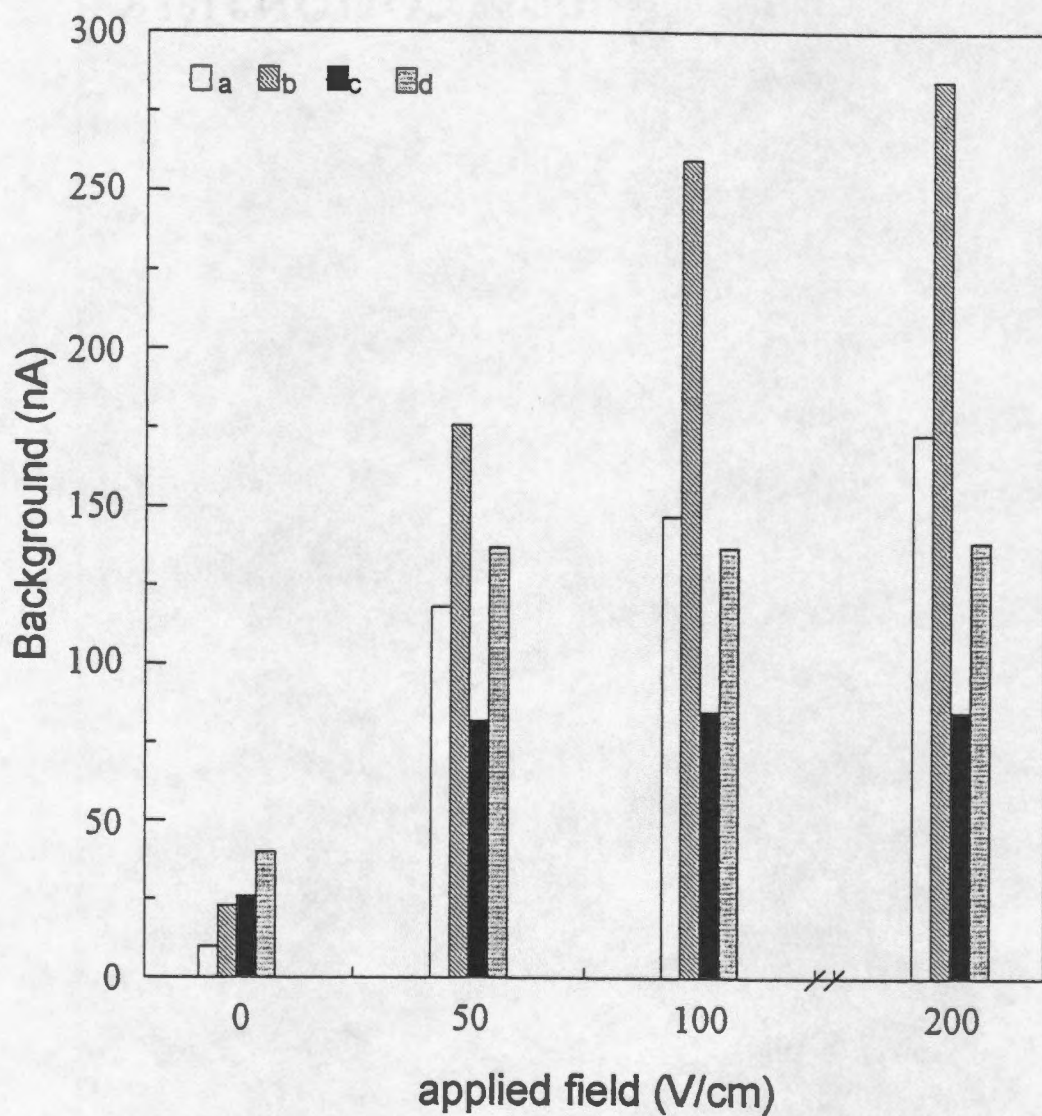


Figure 4.7: Effect of laser power and field strength on background fluorescence from unintercalated dye in the running buffer. (a) 0.10 μM PO-PRO-3 in TAPS with 5.0 mW Ar^+ laser; (b) 0.10 μM PO-PRO-3 in TAPS with 10.0 mW Ar^+ laser; (c) 2.5 μM EB in TBE with 5.0 mW Ar^+ laser; (d) 2.5 μM EB in TBE with 10.0 mW Ar^+ laser.

of dye molecules in and out of the thermal beam path helps compensate for laser noise intensity; i.e., as the laser power fluctuates, so does the flux of the dye molecules. Although the absorptivity of PO-PRO-3 did result in a higher background when this intercalation dye was in the running buffer, the lower relative noise and improved fluorescence enhancement led to a lower detection limit than with EB.

evaluation of sheath flow cell for postcolumn labeling of DNA fragments

The use of a sheath flow cell for the postcolumn labeling of DNA fragments with these cyanine intercalation dyes could be advantageous for both of these dyes. For the monomeric cyanine dye, the reported LODs may be further improved if scattered incident light can be minimized, as has been previously reported for the sheath flow cell (79). This would facilitate this dye being used for ultrasensitive detection in studies in which a sheath flow cell is necessary (e.g., DNA/protein interaction studies such as those discussed in Ref. 79). For the dimeric dye, the primary difficulty in employing this dye for on-column intercalation appears to be the deleterious effects of intrafragment interactions and wall adsorption of partially intercalated dye which leads to significant band dispersion. Conversely, a sheath flow cell scheme would circumvent these problems because the fragment bands may be resolved and the separation complete before the intercalation occurs.

In order for a sheath flow cell to be utilized in this application, intercalation rates must be sufficiently rapid. Intercalation rates were evaluated using a

fluorometer and, whereas the formation of the DNA/EB complex appears to be rapid and stable, the cyanine intercalation dyes may require several minutes or longer to attain the full fluorescence intensity of the DNA/dye complexes (Figure 4.8). However, even within the first minute of mixing DNA into the dye solutions, the fluorescence enhancement appears to be superior to EB.

The intercalation rates were then evaluated using the sheath flow cell in hopes of developing and validating a method utilizing these dyes for ultra-sensitive detection of DNA fragments. A 2.5 μM solution of EB in TBE was pushed through the sheathing capillary and the increase in background fluorescence intensity was measured (Table 4.4). Next, a premixed solution of 2.5 μM EB/1.0 $\mu\text{g/ml}$ DNA was pushed through the sheathing capillary and approximately an 8-fold enhancement was observed. These experiments were repeated with PO-PRO-3 and POPO-3 and approximately a 32-fold and 107-fold enhancement, respectively, was observed (Table 4.4). This experiment generated the amount of signal that ideally should be collected from the sheath flow cell arrangement if a fully formed DNA/dye complex is being detected.

Next, the fluorescence enhancement of these complexes following real-time postcolumn labeling was evaluated. For these experiments, intercalation dye in buffer solution was pumped through the sheathing capillary and a continuous injection of DNA was labeled postcolumn. To help compensate for the reduction in detection pathlength (from 500 μm in the sheathing capillary to 75 μm in the separation capillary), the DNA concentration was increased from 1 $\mu\text{g/ml}$ to 10 $\mu\text{g/ml}$. With the aid of a video microscope, the applied field for the

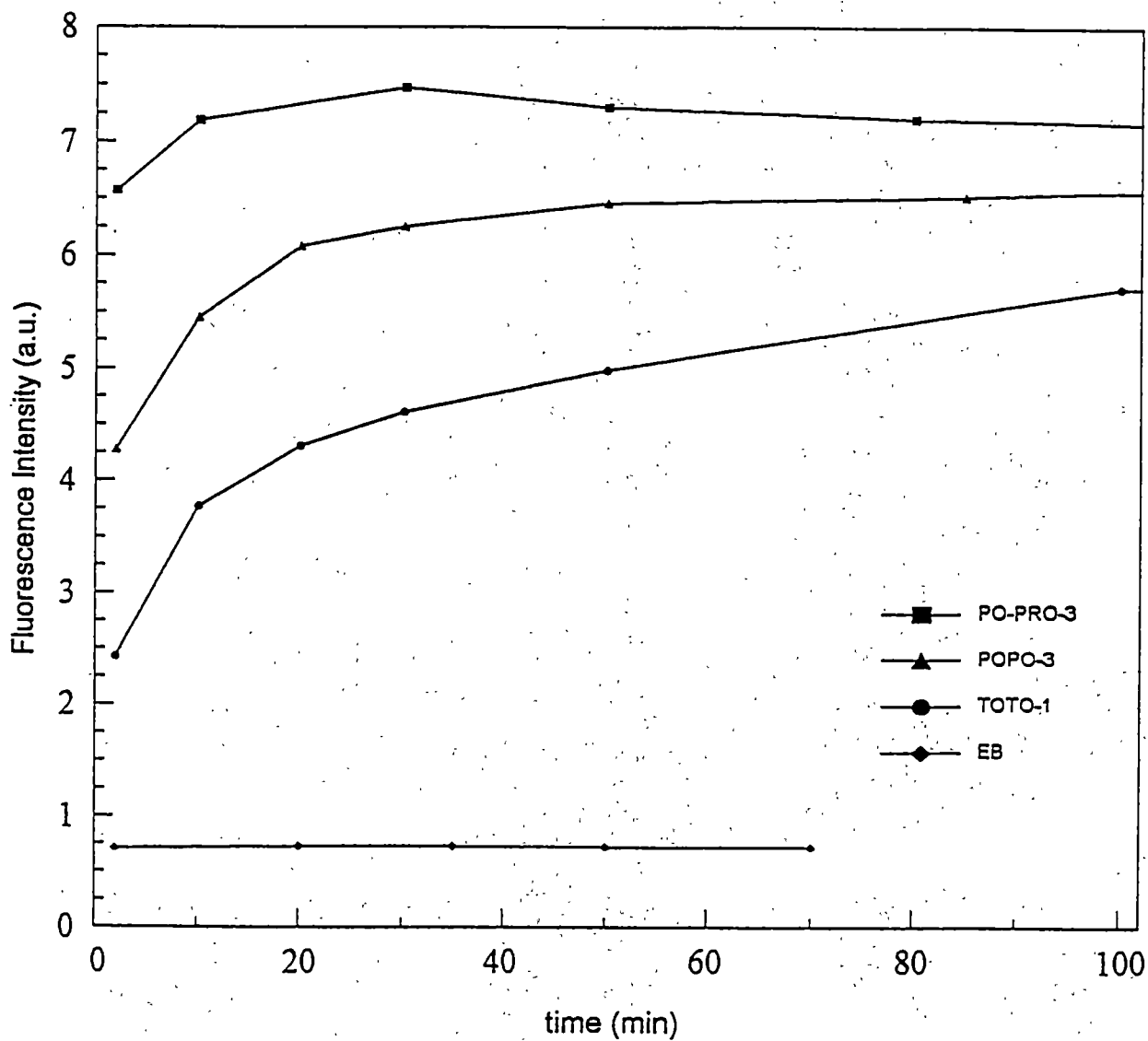


Figure 4.8: Labeling time for complete intercalation of dyes. Details of experimental conditions and procedures are found within the Experimental section of this chapter.

Table 4.4: Continuous Infusion of Premixed Sample through Sheath Flow

Cell

Sample	Signal (nA)	Enhancement
Buffer (background)	24	
EB in TBE	45	
DNA/EB in TBE	185	8x
PO-PRO-3 in TAPS	49	
DNA/PO-PRO-3 in TAPS	820	32x
POPO-3 in TAPS	30	
DNA/POPO-3 in TAPS	670	107x

- Premixed DNA/dye solutions were pushed through the sheathing capillary (500 μm i.d.);
- concentrations: [DNA] = 1.0 $\mu\text{g/ml}$; [EB] = 2.5 μM ; [PO-PRO-3], [POPO-3] = 0.10 μM .

DNA injection and the flow rate of the buffer solution were matched as previously described (79). This is done so that migration of the positively charged dye molecules into the separation capillary is not appreciable. After matching the flow rates, the optimal detection point for focusing the laser excitation source was approximately 0.5 mm from the end of the separation capillary. Fragment band velocities are calculated to be approximately 0.4-0.6 mm/sec (complete elution of the DNA sample from the 40 cm column occurs within about 12-17 minutes) which indicates that fragment bands exiting the capillary would be in the sheathing flow capillary about 1 second before detection occurs. This is sufficient time for intercalation dye to fully permeate the capillary stream by simple molecular diffusion.

Whereas the data in Figure 4.8 indicate that within a minute sufficient intercalation has occurred to result in a large fluorescence signal, the use of a sheath flow cell requires a much quicker intercalation rate; i.e., within a second. Results from these experiments are presented in Table 4.5. The labeling of the DNA with EB resulted in approximately the same fluorescence enhancement whether labeling was performed pre- or postcolumn. However, when evaluating postcolumn labeling with the cyanine dyes, the fluorescence was almost negligible. This indicates that the labeling rates of these dyes, even for the monointercalator PO-PRO-3, is relatively slow and, thus, postcolumn labeling does not appear to be a feasible approach.

Table 4.5: Continuous Injection of DNA Labeled Postcolumn in Sheath Flow Cell

Sample	Signal (nA)	Enhancement
Buffer (background)	24	
EB in TBE	46	
DNA/EB in TBE	190	8x
PO-PRO-3 in TAPS	52	
DNA/PO-PRO-3 in TAPS	145	4x
POPO-3 in TAPS	30	
DNA/POPO-3 in TAPS	46	3x

- Continuous injection of DNA was labeled postcolumn by dye incorporated into sheathing flow;
- concentrations: [DNA] = 10.0 $\mu\text{g/ml}$; [EB] = 2.5 μM ; [PO-PRO-3], [POPO-3] = 0.10 μM .

Conclusions

Fluorometry experiments indicate that when POPO-3 has had time to complex with DNA, the resulting complex fluoresces much stronger than DNA/EB. However, the use of this dye for rapid analysis by CE does not appear possible under typical conditions. Despite a modest improvement in sensitivity when using this dye, this improvement in sensitivity comes at the expense of diminished separation quality. Although Clark and Mathies demonstrated that this dye forms very stable complexes for multiplex DNA analyses, reproducibly obtaining good separation performance in order to achieve better sensitivity appears to be problematic whether prelabeling, on-column, or postcolumn techniques are employed.

The monomeric analog, PO-PRO-3, offered much better results in nearly every aspect investigated in this study. When using TAPS buffer, not only was separation performance as good as or even better than EB in TBE, but the DNA/PO-PRO-3 complex also offers improved LODs. Apparently, this dye can effectively be utilized for on-column intercalation if a carefully optimized buffer regime is employed. However, intercalation kinetics are too slow for the time frame required for postcolumn labeling, thus somewhat limiting the utility of this dye.

Conditions reported herein may possibly be optimized even further. For example, the use of a high-power He-Ne laser at 543.5 nm would result in much stronger excitation (more power absorbed, closer to λ_{max}) and, thus, a stronger fluorescence of the DNA/PO-PRO-3 complex results. The use of a holographic

notch filter would allow a shorter wavelength cut-on filter to be used for dye complexes with small Stokes' shifts such as DNA/PO-PRO-3 ($\lambda_{em} = 539$ nm; $\lambda_{ex} = 567$ nm); thus, nearly full collection of the emission spectrum could be achieved. Also, as detection limits are improved, a lower concentration of dye in the running buffer can be used to achieve full intercalation, hence minimizing problems encountered when performing on-column intercalation.

-Chapter 5- Concluding Remarks: Future of CE for DNA Analysis

Today, the remarkable growth of CE continues as evidenced by the enormous number of published research articles, the increasing number of journals dedicated solely to microcolumn separations and capillary electrophoresis, and the numerous professional organizations and conferences dedicated to CE and associated technology. Much of this ongoing research is directed towards bioanalytical methods and applications. Examples include the use of CE to identify damaged DNA fragments and to identify DNA fragments containing tandem triplet repeats within their sequence (81, 82).

Much effort continues to be directed towards improving upon existing methods for the separation and analysis of DNA fragments. The SSCE method described and used throughout Part I of this dissertation is just one of many variations of CE methods employed for DNA analysis. Many labs continue to use CGE as many aspects of this method are better understood and characterized relative to newer SSCE methods (83, 84). The high speed and sample throughput possible by CE methods has led to significant effort towards producing arrays of capillaries for multiplex applications (85). Although the traditional approach to DNA analysis by CE using capillary columns of approximately 40 cm in length results in much quicker analyses relative to slab gel techniques, methods to perform DNA analysis on microchips is being

developed which further reduces the analysis time to seconds or less (86, 87). Furthermore, the reduced size of microchips may facilitate using this technology in remote locations such as for *in-vitro* diagnostics and field applications.

CE is just one of many analytical methods utilized for DNA analysis. DNA analysis by use of nucleic acid probes has been reported (88, 89). Also, the use of microscopy methods to observe DNA in order to evaluate binding modes of dyes has been reported (90, 91). For many years, the use of mass spectrometry for DNA analysis was not considered to be a feasible method. Given the relatively large size and non-volatile nature of DNA and the necessity to keep DNA in aqueous solution to maintain the integrity of the double-stranded structure, traditional MS techniques could not be used to analyze large biomolecules. With the development of matrix-assisted laser desorption/ionization mass spectrometry (MALDI-MS), the analysis of biomolecules up to 300 kDa is now possible with MS. As a result, an enormous amount of research is now directed towards the use of this method for DNA analysis (92).

As part of the continuing effort in expanding the methods and instrumentation used for DNA analysis, the attributes of CE continues to improve upon traditional methods for DNA separations and analysis. For example, the small sample requirements required for CE with laser-induced fluorescence (LIF) detection reduce the number of amplifying PCR cycles required for analysis of trace amounts of DNA. Also, the speed and, thus, the potential of high sample through-put is a significant improvement realized with CE methods. One such

research area that will greatly benefit from this attribute is the sequencing of the human genome. Yeung puts the enormity of this endeavor in perspective with the following analogies: "The Human Genome Project is an initiative to sequence the entire human genome, which consists of 3×10^9 bp of nucleic acids. Just to read the A, C, T, and G alphabet out loud at four per second will take 24 years. To print one human genome at 60 characters per line and 50 lines per page will result in an encyclopedia occupying 142 ft of shelf space. At the present time, a good molecular biology laboratory can sequence about 3×10^6 bp of genomic DNA per year. This means that it will take 1000 years to sequence the genome once." (36). In addition to the bold undertaking to sequence the human genome, rapid CE methods could become essential for such applications as quickly processing the large number of DNA samples evaluated in crime labs or medical research centers.

The development of SSCE is a good example of the direction of research towards simplifying these methods and reducing overall laboratory time in preparing and processing samples. In the work presented in Part I of this dissertation, modifying the experimental conditions in order to evaluate fundamental processes of DNA separations by CE was greatly simplified by the ability to flush and refill the separation column with polymers of differing concentrations and chain lengths. The on-column intercalation strategy employed reduced the amount of DNA that was needed for these studies. When the study required the evaluation of a new intercalation dye, the buffer was flushed from the column and refilled with the dye of choice rather than discarding

a pre-labeled DNA sample and pre-derivatizing a new aliquot of DNA digest. Furthermore, the reproducible coating of columns used throughout this study generally lasted much longer and for many more studies than a typical gel-filled column; again, reducing the time and cost of this research.

As CE begins to gain wider acceptance and is implemented into more laboratories, the understanding of fundamental processes which occur during CE analyses becomes important as the researcher's goal is to achieve the best efficiency, resolution, and sensitivity possible. The work presented herein identifies experimental conditions which affect these figures of merit. Chapter 2 discussed the importance of column preparation for DNA analyses and presented data depicting the effect of acrylamide concentration in this preparation step. Chapter 3 detailed an evaluation of the effect of sieving polymers on the separation of DNA fragments which not only affects efficiency and resolution but also has consequences on sensitivity as discussed further in Chapter 4. Chapter 4 also indicates potential problems with CE techniques; in particular, the dynamics of the CE process (e.g., effect of DNA fragment mobilities on efficiency; interactions with buffer components) may complicate such simple processes as on-column intercalation of staining dye.

There is always some resistance to implement new methodology over "tried and true" methods. Given that polyacrylamide gel electrophoresis was developed nearly 20 years prior to modern capillary electrophoresis, PAGE is better characterized and understood than CE. Existing written methods are in place which utilize PAGE, thus, implementing CE for the sake of change is not

sufficient; one must be convinced that CE is in fact a *better* method before such acceptance occurs. For this, we must continue to characterize, optimize, and improve upon capillary electrophoresis applications. The purpose of the research presented herein is to work towards that goal.

**II. Evaluation of Immobilization Strategies for
Polymeric Stationary Phases for Microsensor
Determinations of Semivolatile Organic
Compounds**

-Chapter 6-
**Evaluation of Immobilization Strategies for Polymeric
Stationary Phases for Microsensor Determinations of
Semivolatile Organic Compounds**

Introduction

In Part I of this dissertation, the enormous growth in the development and applications of CE was discussed. Another area of analytical chemistry that is experiencing perhaps an even greater rate of growth is the development and applications of chemical sensors. In preparing a review on chemical sensors, Janata et al. report that a search of the Institute of Scientific Information database resulted in 8,278 references for this topic during the period of 1994-1997 (93). Therefore, the extent of this topic necessitates that only a brief overview of sensors be presented.

Sensors can offer numerous advantages over conventional analytical techniques. In many cases, sensors may offer improved sensitivity, low sample requirements, selectivity from complex matrices, the ability to obtain *in-situ* measurements, speed, real-time measurements and process monitoring, portability (field-readiness), and regenerability. Given these attributes, sensors have been developed for a variety of applications. For example, the diminutive size and ability to perform *in-situ* measurements have led to the development of sensors that can be positioned within a single cell to monitor physiological processes as they occur in real time (94). Sensors are used to probe complex hazardous samples, thus, eliminating the need to perform exhaustive extractions

which can generate large amounts of waste while also minimizing worker exposure (95). When coupled to an optical fiber, sensors may be used in hostile environments for remote sensing when it is not possible to directly obtain samples such as an area exposed to biological warfare agents (96).

A typical sensor consists of three elements. First, the recognition element (or selective phase) is used to differentiate between the desired analyte and matrix components. Next, the transducer is the component which transmits the "information" (change in heat, change in mass, etc...) to the third component of the sensor which is the recorder (e.g., photomultiplier tube, frequency counter). The many types of sensors in use today are usually categorized by the transduction principle utilized. For example, in one type of thermal sensor, the sensing face is exposed to a light source and, depending on the properties of the bound analyte, heat may be absorbed or emitted, resulting in the transduction of a thermal signal (97). In another type of thermal sensor, catalytic enzymes are utilized as the recognition element. In the presence of the enzyme's target substrate, the resulting enzymatic reaction generates heat which is measured by a thermistor or thermocouple (98). Examples of enzyme-substrate reactions utilized for these types of sensors include glucose-glucose oxidase, hydrogen peroxide – catalase, and pyruvate – lactate dehydrogenase (98).

Detecting an increase in mass following adsorption of target analytes is the transduction principle for a category of sensors termed mass sensors. Perhaps the most common type of sensor in this class is the quartz crystal microbalance (QCM) (99). In QCM measurements, a resonating frequency is

applied to a crystal (typically gold) which may or may not have an immobilized selective phase on the surface. Following analyte adsorption, the resonating frequency decreases as a result of increased mass on the surface of the crystal. The Sauerbrey equation can then be used to relate change in frequency (Δf) with change in mass (Δm):

$$\Delta f = - \left[\frac{2f_0^2}{A(\mu_q \rho_q)^{1/2}} \right] \Delta m \quad (6.1)$$

where f_0 is the applied frequency, A is the piezoelectric active area of the crystal, μ_q is the shear modulus of the quartz, and ρ_q is the density of the quartz (100).

Optical sensors encompass a wide range of sensors which utilize the interaction of light with matter to gain information about the species being detected. Optical sensors often utilize fibers to direct light to the sensing terminus and also to collect light from the resulting interactions at the terminus and, thus, these types of sensors are termed fiber-optic sensors. Often these interactions between light and analytes result in either absorbance or fluorescence of characteristic wavelengths of light and, thus, are used to directly characterize and identify analytes at or near the sensing terminus; further information about the detected species may be gained from decay time measurements as well (101-104). Unlike gravimetric sensors in which a change in mass can be a non-specific response (i.e., further information is needed to conclusively identify the adsorbed species), optical sensors can offer a very high degree of specificity. For example, optical methods allow chiral discrimination between enantiomers. One example includes a report on receptor molecules

which exhibit a different fluorescent response for the D- and L- form of monosaccharides (105). To present herein a full overview of the expansive topic of optical sensors is not practical; however, extensive reviews are available for further reading (93). In addition to thermal, mass, and optical sensors, extensive designs and applications of electrochemical sensors have also been described in detail (93).

The quintessential feature necessary for an effective sensor is the recognition element. If a sensor cannot discriminate between desired analytes and matrix components, then the attributes of sensors over traditional analytical techniques previously cited cannot be attained in real applications. In recent years, the quest for improved selectivity has been, by far, the "cornerstone of chemical sensing research" (93). This has led to the development and utilization of recognition elements that are indeed highly selective. Examples include the use of immobilized antibodies for the selection of specific antigens (i.e., an immunochemical sensor) (106). Also, the use of size-discrimination recognition elements such as calixerenes have exhibited such a high degree of selectivity that isomers of xylenes can be differentiated (107). A relatively new field of sensors termed biosensors which utilize proteins, enzymes, and nucleic acids as highly selective phases has also received much attention (108-112).

The fabrication of sensors is another interesting aspect of the on-going research of chemical sensors. The drive towards miniaturization continues to be the focus of many research articles as ion, electron, and laser beam patterning of selective layers have been reported (113-115). There are numerous advantages

to be realized upon miniaturization of sensors. Such advantages include the ability to explore microenvironments (such as inside a cell), faster response from rapid kinetics, improved portability for field applications, less materials and lower costs for fabrication, the ability to produce compact sensor arrays, and, in many cases, improved sensitivity.

The use of microcantilevers (100-150 μm) as substrate structures has been reported for the development of microsensors (116). For these devices, the deflection of the cantilever substrate is the physical measurement typically obtained. Bending of the cantilever may result from the stress caused by adsorption of analytes on the substrate (a gravimetric measurement) or cantilever deflection may be the result of a photoinduced stress (a thermal measurement). In the latter case, the amount of photoinduced stress exhibited by the cantilever surface is dependent upon the type and amount of analyte adsorbed on the surface. For example, a bare silicon cantilever may undergo severe photoinduced stress when exposed to a characteristic wavelength of light. Once the silicon substrate is exposed to a sample and is subsequently covered ("protected") by adsorbed analytes, the extent of photoinduced stress may decrease. Upon careful calibration, a correlation of degree of photoinduced stress with amount of bound analyte may be determined. The excellent sensitivity to small changes in temperature and mass exhibited by cantilevers utilized in microsensors has resulted in femtojoule and attomole detection limits (117, 118).

In addition to a drive towards miniaturization, another focus in sensor research is the development of higher-order sensors. In this type of sensor, more than one transduction principle is utilized. For example, a sensor with a resonating frequency will signal analyte adsorption by a mass-induced frequency change. If the surface of this sensor is simultaneously being probed by an optical measurement (e.g., infrared spectroscopy), further characterization of the adsorbed analyte is attained. When utilizing higher-order sensors, a high degree of selectivity may not be necessary. For example, a chemical phase functioning as a recognition element which is modestly selective may differentiate classes of compounds in a sample and further spectroscopic characterization could then be utilized to further characterize the adsorbed species. Modestly selective chemical phases may also serve to simply enhance response factors for classes of compounds. Finally, arrays of microsensors that employ different modestly selective phases on individual sensor elements may be employed with multicomponent analysis techniques to yield quantitative information on mixtures of analytes (119).

This approach to sensing suggests the possibility of using modestly selective GC and LC stationary phases on microsensors which utilize gravimetric and photothermal detection (120). Furthermore, utilizing these phases in the development of higher-order sensors and incorporating them into sensor arrays could lead to the development of microsensors to characterize highly complex matrices such as the hazardous tank wastes currently being stored in such places as Oak Ridge, Tennessee and Hanford, Washington. The use of GC and

LC phases may be well-suited for these types of sensors for several reasons. First, the use of these phases for column chromatography has been extensively evaluated, thus, the bonding chemistry and relative affinities and selectivity of many of these phases are well-characterized; this simplifies the task of selecting an effective phase for certain analytes. Furthermore, these types of phases may be suitable to concentrate semivolatile organic compounds from complex mixtures for enhanced sensitivity and to also provide a moderate level of selectivity as part of a higher-order sensor array (120). The range of analytes probed by the microsensor device can be further expanded by the use of different GC and LC stationary phases on different cantilevers within the sensor array.

The research presented in Part II of this dissertation describes initial evaluations of methods to immobilize polymeric GC and LC onto a microsensor substrate (i.e., silicon) and also includes some characterization studies of selected phases.

Experimental

reagents and solutions

Benzene, toluene, aniline, and phenol were purchased from Fisher Scientific (Pittsburgh, PA, USA) and used to prepare 500 ppm analyte solutions in deionized water. Methylene chloride (CH_2Cl_2) was also purchased from Fisher Scientific. Anhydrous isopropanol was purchased from Sigma (St. Louis, MO, USA). The GC phases OV-25 (75% phenyl/25% methyl) and SP-2340 (100%

cyanopropyl) were purchased from Supelco (Bellefonte, PA, USA). The LC phases phenyltrichlorosilane and octadecyltrichlorosilane were purchased from Aldrich (Milwaukee, WI, USA).

instrumentation and methods

Gas chromatography/mass spectrometry (GC/MS) analyses were conducted with a Hewlett-Packard 6890 GC/ 5973 MSD (quadrupole MS) operated by ChemStation software (Hewlett-Packard, Palo Alto, CA, USA). A Hitachi S-3200N Scanning Electron Microscope (Hitachi Scientific Instruments, San Jose, CA, USA) was utilized for microscopy studies. Typical operating conditions included a pressure of 12 Pa and a beam voltage of 10-12 kV. The SEM micrographs depicted are backscattered electron images. These images were saved as bitmap files and printed directly from Adobe PhotoDeluxe software (Adobe Systems, Inc., Seattle, WA, USA) without any alterations of features.

Test grade, single-side polished silicon wafers (200-300 μm thickness) were purchased from Wafer World (Ft. Lauderdale, FL, USA) and cut to approximately 1.5 cm square sections. Prior to use, the silicon substrates were cleaned with "piranha" solution (3:1 solution of 18M H_2SO_4 + 30% H_2O_2) at 90 $^\circ\text{C}$ for 3 hours. Because piranha solution is a very strong oxidant and reacts violently with many organic materials, extreme caution was undertaken during its use. Fresh solutions were prepared immediately prior to use and immediately discarded down the sink with copious amounts of water after use.

Following this cleaning step, the substrates were dried under helium until all of the visible surface water was removed and then placed in a 120 °C oven for 10 minutes to ensure complete removal of water prior to depositing the polymeric stationary phases.

For the deposition of the GC phases onto silicon, a two-chamber oven apparatus was constructed in-house (Fig. 6.1). The columns and detectors were removed from two Gow-Mac GC instruments (Gow-Mac Instrument Co., Bridgewater, NJ, USA); two aluminum chambers were constructed and connected with stainless steel tubing fitted with ferrules for an air-tight seal. The first oven was set to the maximum operating temperature specified for the phase (300 °C for OV-25; 275 °C for SP-2340). A small dish of neat phase was placed in the sealed aluminum chamber and a gentle stream of helium was used to carry the vapors into the second chamber. The second oven was set to 125-150 °C and the substrates to be coated were placed in the sealed aluminum chamber within this oven.

For the deposition of LC chlorosilane phases, freshly cleaned silicon chips were immersed in a 4% silane in alcohol solution and warmed to 35 °C for 30 minutes. The treated substrates were then cured at 110 °C for 10 minutes (121). Details of these reactions are discussed later.

Contact angles of modified substrates were measured with the aid of a Sony Zoom CCD color video camera microscope and a Trinitron color video monitor (Edmund Scientific, Barrington, NJ, USA). Small aliquots of solution were deposited onto the substrates and the contact angles were directly

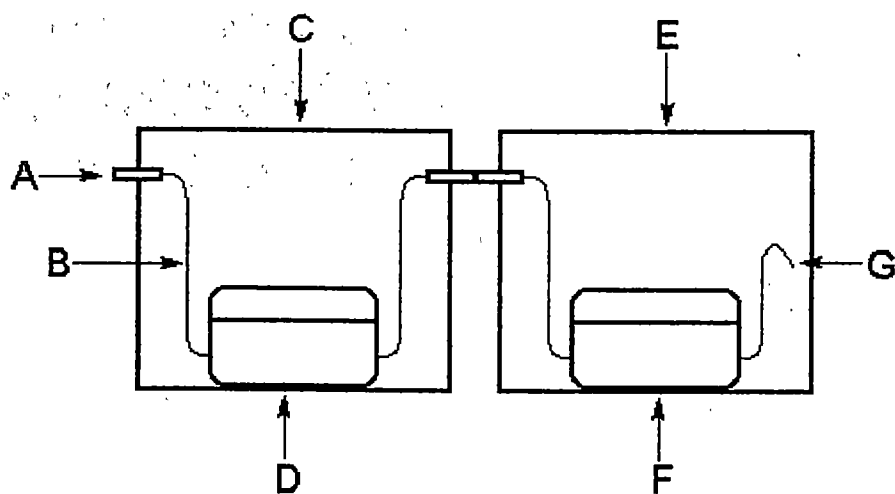


Figure 6.1: Two-chamber vapor-deposition apparatus. (A) inlet for carrier gas; (B) narrow-bore stainless steel tubing; (C) 250-300 °C oven; (D) threaded aluminum chamber for phase being vaporized; (E) 125-150 °C oven; (F) threaded aluminum chamber for placement of substrate being coated; (G) outlet for gas flow.

measured on the video monitor with the use of a protractor. Film thickness on some of these modified substrates was determined by ellipsometry. These analyses were performed by a contracted laboratory.

The modified substrates were exposed to 5 mL of 500 ppm analyte solution for 2 hours. The samples were removed and quickly dipped in water to remove residual analyte solution adhering to the substrate. The samples were then extracted three times with 2 mL volumes of CH_2Cl_2 and the combined extract was concentrated to 1 mL. A 0.5 μL aliquot was then injected into the GC/MS for quantitative analysis.

To increase sensitivity, GC/MS analysis was performed in the selected ion monitoring (SIM) mode. That is, rather than to "scan" a large mass range as is typically done with quadrupole MS, the quadrupole was set to tune only for selected ions. In this case, the parent ions (mass-to-charge; m/z) of the four analytes were selected: $m/z = 78$ for benzene, $m/z = 91$ for toluene, $m/z = 93$ for aniline, $m/z = 94$ for phenol.

The use of temperature programming was necessary to achieve acceptable resolution and efficiency when performing separations by GC. Complete parameters for the GC method developed is provided in Appendix 1. Briefly, the GC oven is initially held constant at 40 $^{\circ}\text{C}$ for two minutes to allow the elution of the solvent (boiling point for $\text{CH}_2\text{Cl}_2 = 40$ $^{\circ}\text{C}$); to protect the MSD, the ionization filament is shut off during this time. Following this solvent delay, a ramp of 5 $^{\circ}\text{C}/\text{min}$ is used to elute benzene and toluene. Next, a quick ramp of 10 $^{\circ}\text{C}/\text{min}$ is used to bring the oven to 75 $^{\circ}\text{C}$ and then the ramp is slowed to 2

$^{\circ}\text{C}/\text{min}$ for 5 minutes to resolve the closely eluting aniline and phenol. The oven is then quickly ramped to 200°C to remove any low-volatility contaminants that may have been injected with the sample.

Results and discussion

substrate preparation

Whichever method of phase deposition is utilized, it was found that completely wetting the surface of the substrate is of critical importance. It has been reported that silicon substrates typically require 30 minutes of cleaning in piranha solution to create a reactive surface that is rich in silanols (122). Therefore, the substrates were cleaned with piranha solution for 30 minutes prior to depositing GC and LC phases. These specimens were then examined by SEM (Figure 6.2). In Figure 6.2(A), a silicon wafer that was cleaned with piranha solution for 30 minutes and uncoated (i.e., a blank) is depicted. Note the relatively dark and featureless surface of this specimen. In Figure 6.2(B), a cleaned substrate that was vapor-coated with OV-25 clearly shows regions of varying contrast and nonuniformity. Similar undesirable features are observed in Figure 6.2(C) which depicts a cleaned substrate which was coated with octadecyltrichlorosilane. Figure 6.2(D) perhaps is the most graphic depiction of a substrate with a poor wetting surface. This specimen is a cleaned substrate that was dip-coated in a 10% OV-25 solution. One can clearly observe the nonuniformity of the resulting film following drying of the solution. Furthermore, edge effects can be observed in the far left portion of the image which is the

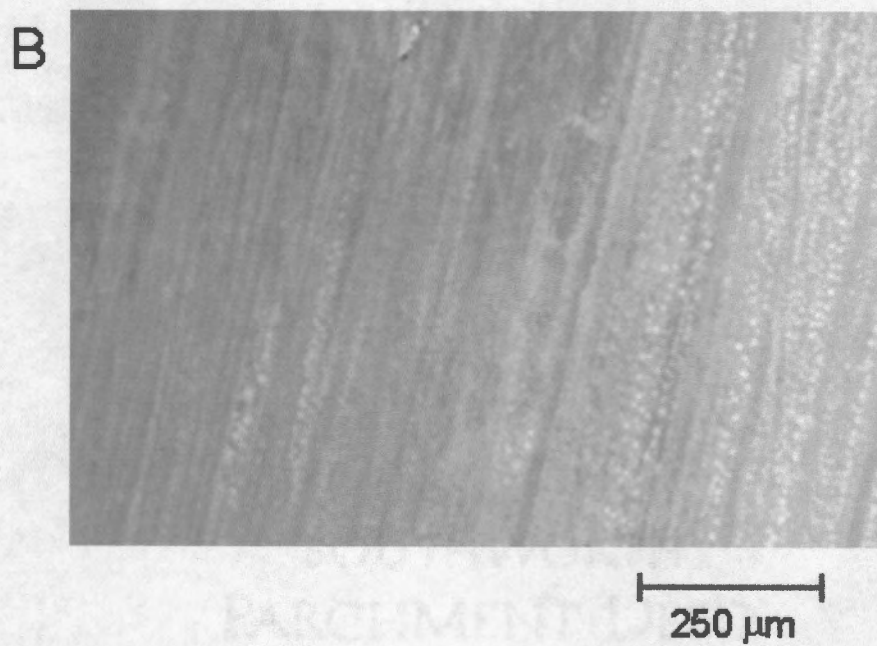
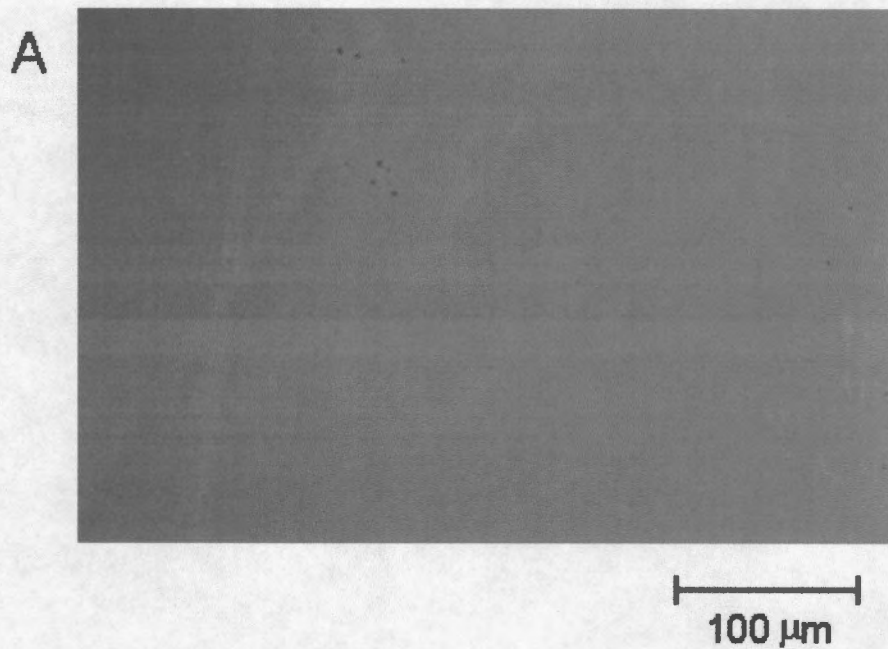
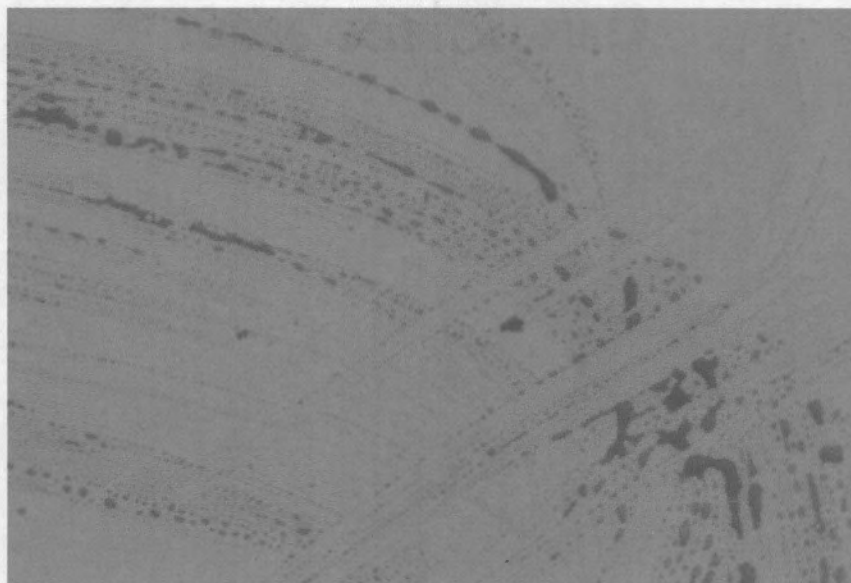


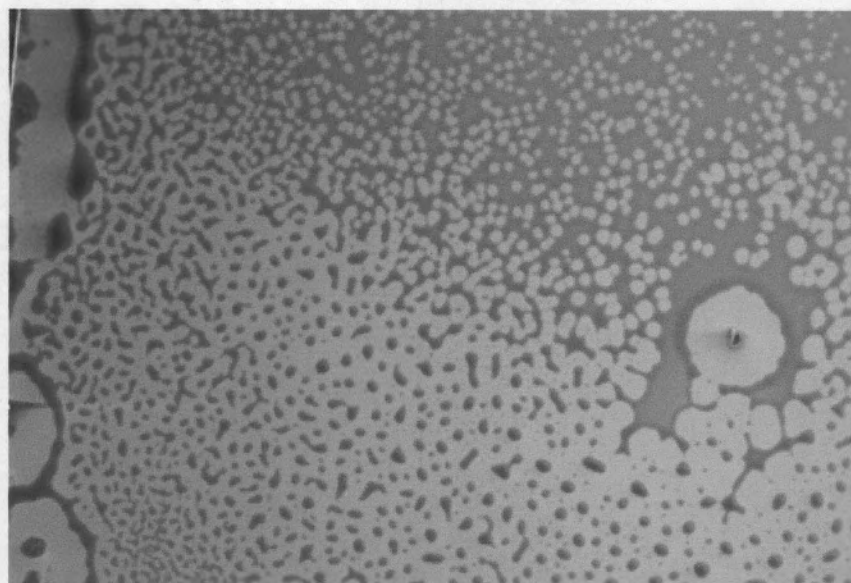
Figure 6.2: SEM micrographs of films deposited onto silicon substrates. (A) blank (uncoated) silicon chip; WD = 9.7 mm; (B) silicon chip vapor-coated with OV-25; WD = 9.7mm.

C



250 μm

D



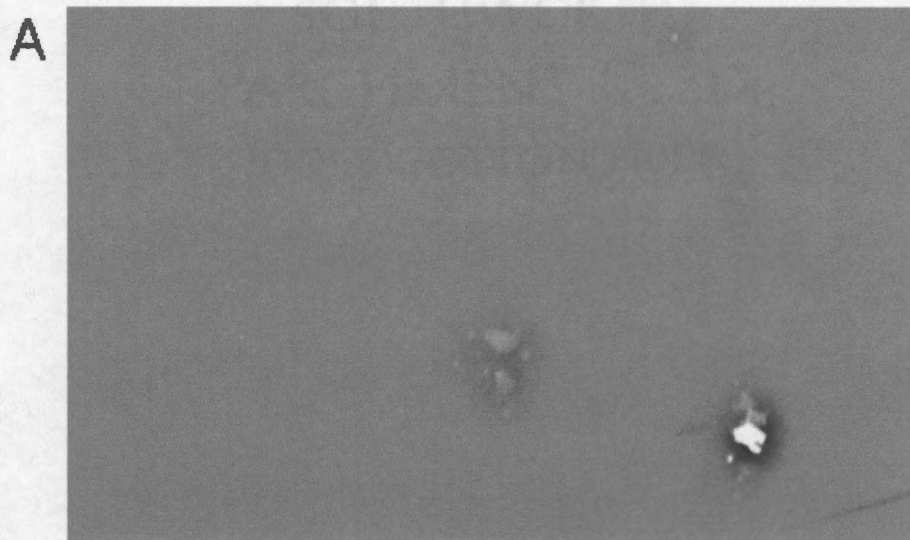
250 μm

Figure 6.2 (cont.): (C) silicon chip coated with octadecyltrichlorosilane; WD = 9.2 mm; (D) silicon chip dip-coated in 10% OV-25 in chloroform; WD = 9.4mm.

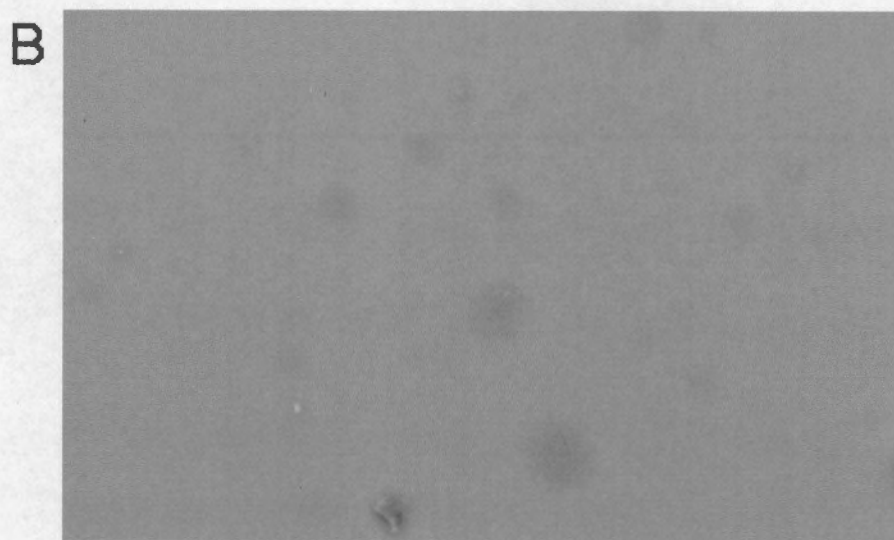
edge of the specimen. This effect is assumed to be the result of increased surface tension near the edge of the substrate.

The efficacy of the cleaning method was carefully evaluated by measuring the contact angle on the substrate following piranha solution treatment. For maximum wettability, the contact angle on a substrate should be less than 5° (123). With the aid of a video microscope, the amount of time required to achieve a contact angle $<5^{\circ}$ with piranha solution was determined to be 3 hours, much longer than had been previously reported (106). In fact, after only 30 minutes of cleaning with piranha solution (as had been done for the specimens observed in Figure 6.2), the contact angle was found to be approximately 24° ; much too large to achieve uniform wetting on a substrate. Therefore, it would appear that the time required for sufficient cleaning on silicon wafers may vary; this may be due to the initial quality and storage conditions of the purchased wafers.

Several new specimens were prepared by first cleaning the substrates for 3 hours before depositing films. These specimens were examined by SEM and much better results were observed (Figure 6.3). Figure 6.3(A) depicts a silicon substrate vapor-coated with OV-25; comparison with Figure 6.2(B) indicates a dramatic improvement in film uniformity following the lengthy piranha cleaning. A substrate coated with octadecyltrichlorosilane is depicted in Figure 6.3(B). Again, upon comparison with Figure 6.2(C), a significant improvement is observed for this film. As a result of these observations, a 3-hour cleaning protocol was adopted for the remainder of these studies.



25 μm



250 μm

Figure 6.3: SEM micrographs of films deposited onto silicon after extended cleaning for improved wetting. (A) silicon chip vapor-coated with OV-25; WD = 10.1 mm; (B) silicon chip coated with octadecyltrichlorosilane; WD = 9.5 mm.

vapor-phase deposition of GC phases

A method commonly used in the forensic analysis of fingerprints is the "fuming super-glue" procedure (124). In this method, the evidence from which fingerprints are desired is placed in a sealed chamber with a small dish of fuming super-glue. Upon condensing, the acrylate compounds in the super-glue fumes, condense onto the substrate surface and the fingerprints are then easily observed and removed. Herein, a similar approach is employed to deposit a thin film of polymeric GC phase onto silicon substrates.

Initially, substrates were cleaned and placed in an oven with a small dish of GC phase. The temperature was set to the maximum operating temperature of the GC phase (specified in the experimental section) and the fuming GC phase was deposited onto the substrates. Although this initial approach is conveniently simplistic, in reality, there is really no means to control or vary the thickness of the films obtained. In this approach, the only time when the GC fumes are being deposited onto the substrate is during the time in which the oven is cooling. A simple solution might be suggested that cycling the chamber through heating and cooling steps may increase the thickness of the deposited film. However, upon each heating step of the cycles, not only are additional fumes generated from the dish of GC phase but may also be regenerated by the thermal desorption of the previously deposited phase from the substrate. Therefore, a two-chamber apparatus was designed and constructed (depicted in Figure 6.1). A small dish of GC phase is placed in the first oven and the temperature is set to the highest operational temperature for the phase in order

to generate fumes. This temperature is specified by the vendor as that at which the vapor pressure of the phase becomes appreciable and/or below the temperature at which the phase may undergo decomposition. The fumes are then swept into a second oven which is set to a cooler temperature so that the fumes will condense. In this second oven is a chamber containing the cleaned substrates to be coated. This apparatus facilitates some experimental control over the thickness of the deposited films by simply controlling the time permitted for fume condensation onto the substrate to occur. Other means to control the thickness may include modifying the carrier gas flow rate and the temperature used for phase vaporization and condensation.

In this evaluation, substrates were exposed to GC phase vapors for 30 minutes and 3 hours. Although one cannot definitively conclude that a 6-fold increase in exposure time will result in a 6-fold increase in surface thickness, one can safely assume that a thicker phase is indeed deposited with increased exposure time.

reaction coating of LC phases

Initially, the trichlorosilanes were coated onto silicon substrates under aprotic conditions by a procedure described by Buszewski (125). In this method, the silane is diluted into a toluene solution within an ampule. The volatile mixture is frozen in liquid nitrogen so that the ampule may be safely flame-sealed. The sealed ampule is slowly thawed and then heated at 120 °C for 12-24 hours.

Upon cooling, the ampule is opened and the substrates are recovered and washed several times with various solvent solutions.

The silane vendor suggests a simpler, direct approach to bonding trichlorosilanes onto silicon (121). To anhydrous alcohol, sufficient silane reagent is added to make a 2-5% solution. This converts the chlorosilane to an alkoxysilane as depicted in the following reaction:



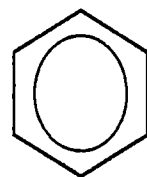
where R is the functional group of the silane (in this case, R = C₁₈- or C₆H₅-). The solution is warmed to 35 °C to promote completion of the reaction. Part of the HCl generated reacts with the alcohol to produce water which in turn results in the conversion of the alkoxysilanes to silanols:



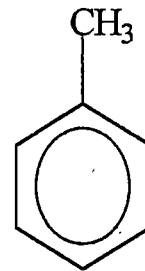
The silanols readily condense onto the substrate. Treated substrates are then cured at 110 °C for 10 minutes. This method is faster, uses less solvent solutions, and is safer than the deposition method described for aprotic conditions. Both visual and SEM inspection indicate that indeed this method deposits a film onto the substrate; therefore, this method was utilized for the remainder of the studies.

GC/MS analysis

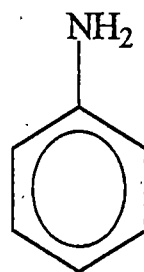
A series of standards were prepared containing the analytes of interest; i.e., benzene, toluene, aniline, and phenol (Figure 6.4). These compounds were selected because they represent a class of compounds (i.e., semivolatile organic



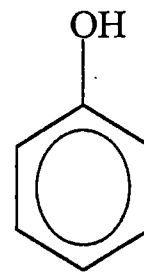
benzene



toluene



aniline



phenol

Figure 6.4: Structures of semivolatile organic compounds.

compounds) of interest to the Department of Energy as these types of compounds are found in abundance at many waste sites in need of characterization and remediation. These particular four compounds were chosen because they each have functional groups that represent characteristic groups described by McReynolds constants (126). McReynolds constants qualitatively describe retention characteristics of phases for various types of analytes. These constants are useful for predicting elution order, resolution, and selectivity of analytes from various classes of compounds. These constants are obtained by measuring the degree to which a phase retains probe compounds relative to the retention of these compounds on a non-polar phase (squalene). Some examples of probe compounds include pyridine (aromatic bases), nitropropane (nitro and nitrile derivatives), and 2-pentanone (aldehydes, ketones). These probe compounds are selected such that they represent classes of compounds with differing functional groups and, hence, differing chemical interactions. The following equation is utilized in calculating the Kovat's retention index (*i*) of compounds:

$$i = 100z + \frac{100|\log t'_r(i) - \log t'_r(<)|}{\log t'_r(>+1) - \log t'_r(<)} \quad (6.2)$$

where $t'_r(i)$ is the retention time of the compound of interest, $t'_r(<)$ is the retention time for the n-alkane eluted prior to the compound of interest, $t'_r(>+1)$ is the retention time of the n-alkane eluted after the compound of interest, and *z* is the carbon number of the n-alkane of retention $t'_r(<)$.

A series of compounds are analyzed on a non-polar column (squalene) and retention indices are determined. Next, these compounds are evaluated on other phases and, again, the retention indices are determined. The difference in these values (Δi) are calculated and used to determine McReynolds constants. These values are then used to qualitatively describe overall relative polarities of phases:

$$\Delta i_{overall} = \Delta i_{test\ compound\ x'} + \Delta i_{test\ compound\ y'} + \dots \quad (6.3)$$

Phases that provide Δi values between 0-100 are generally considered non-polar, values between 100-400 indicate moderate polarity of phases, and phases with values above 400 are considered highly polar.

McReynolds constants can also be used to compare expected selectivity of phases. It is generally assumed that phases that differ by +/- 10 units generally exhibit similar affinities. For example, in the following data, both PDEAS and LAC-2R-446 exhibit similar affinities for benzene:

<u>Phase</u>	<u>x' (benzene)</u>	<u>y' (butanol)</u>
PDEAS	386	555
LAC-2R-446	387	616

However, the values indicate that, relative to PDEAS, LAC-2R-446 exhibits a slightly higher affinity for butanol. In chromatographic application, alcohols would tend to be preferentially retained on the LAC-2R-446 phase (this ignores boiling point considerations). Similarly, this indicates that for the development of a sensor for alcohols, LAC-2R-446 would be the more suitable choice as the selective stationary phase.

A method to quantitate the four selected compounds by GC/MS analysis was developed and has previously been described in the experimental section and Appendix 1. With temperature programming, sufficient efficiency and resolution of these four compounds is obtained (Figure 6.5). A calibration plot to correlate integrated peak area to injected quantity was obtained by analyzing a series of standards (Figure 6.6). Note that the limit of quantitation is much better for benzene and toluene relative to aniline and phenol. This is due to the diminished S/N of these later-eluting compounds. The S/N ratio simply becomes too small to integrate peak areas for aniline and phenol once the injected quantity becomes less than 1 ng.

evaluation of affinity and selectivity of polymeric phases

Substrates were prepared and coated with OV-25, SP-2340, octadecyltrichlorosilane, and phenyltrichlorosilane as described. After exposing the prepared substrates to a 500 ppm aqueous solutions of the semivolatile organic analytes, extracting the adsorbed analytes with CH_2Cl_2 , and concentrating the extracts to 1 mL, the samples were analyzed by GC/MS. Results from these analyses are listed in Table 6.1.

Silicon chips that were cleaned with piranha solution yet had no phase deposited (blank) showed an appreciable affinity for benzene and toluene. This was reproducibly observed as a blank chip was included in every set of experiments performed. These results are not entirely surprising as these

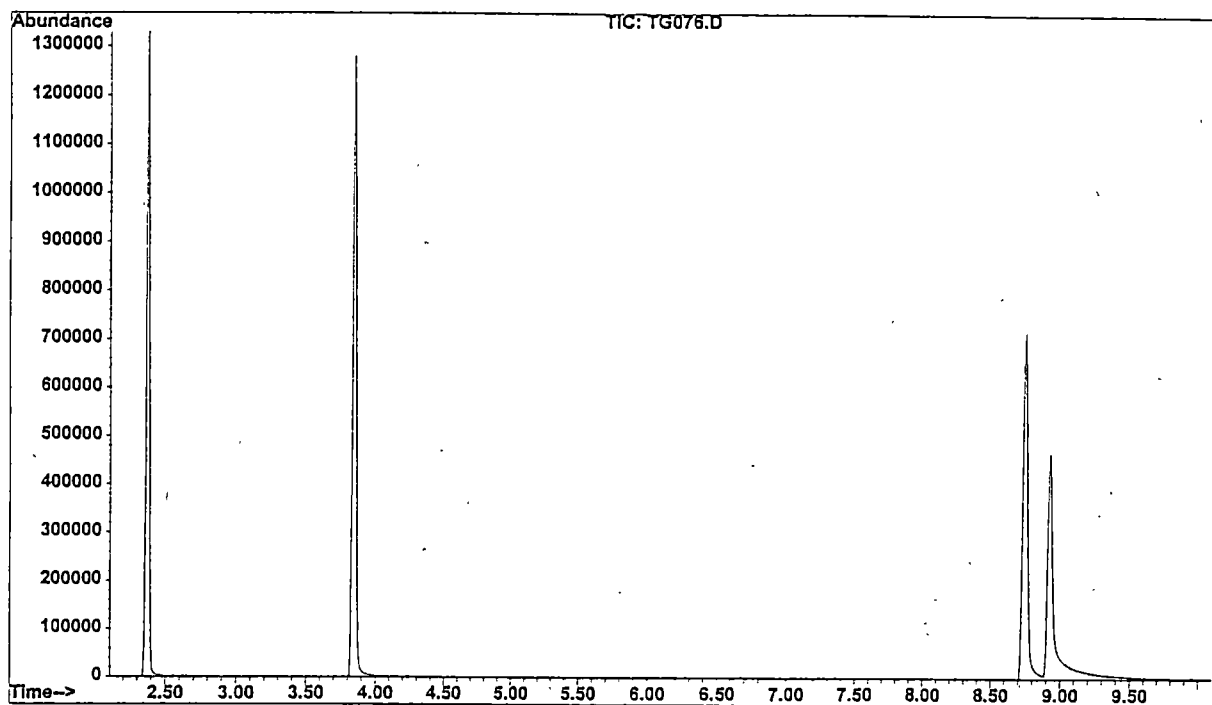


Figure 6.5: GC chromatogram of mixture of semivolatile organic compounds. Compounds (in order of elution): benzene, toluene, aniline, phenol.

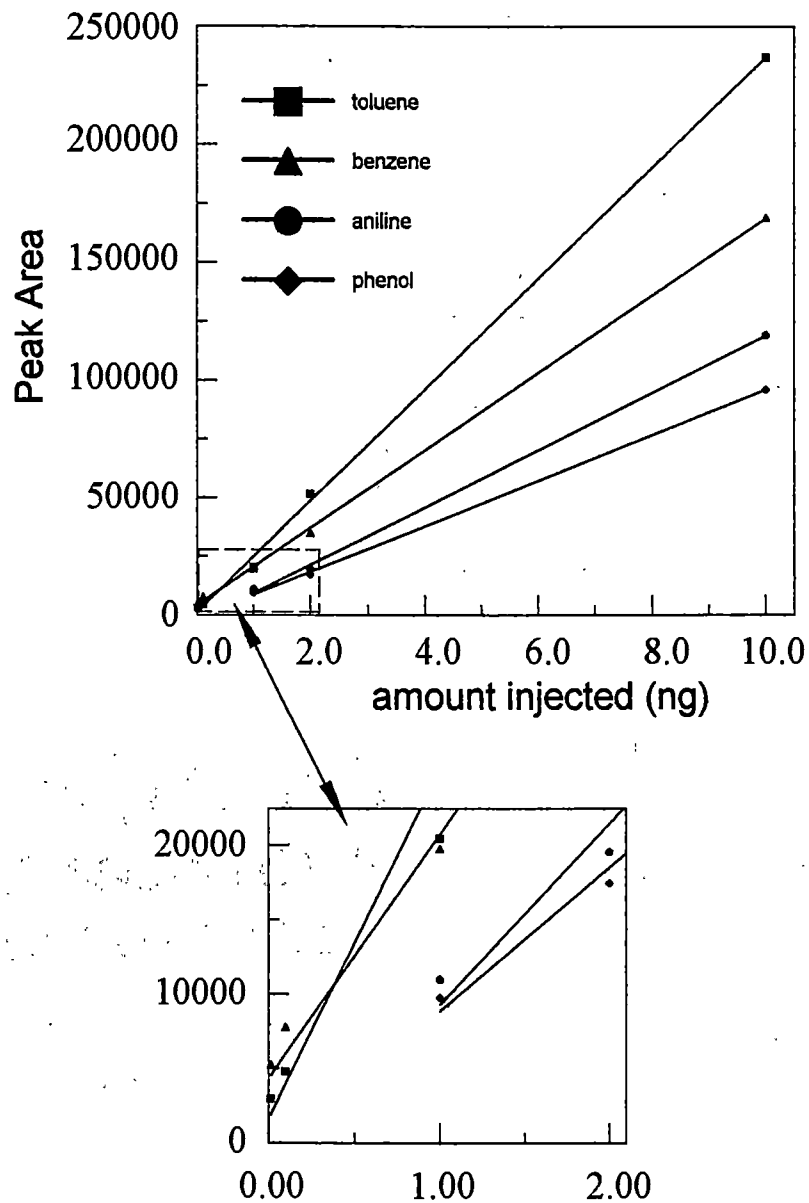


Figure 6.6: Calibration curve to correlate GC/MS peak area to quantity injected. Although some deviation from linearity is observed at low quantities injected, correlation coefficients were still quite good (r^2 for benzene = 0.9997; toluene = 0.9992; aniline = 0.9991; phenol = 0.9996).

Table 6.1: Affinity and Selectivity of Stationary Phases on Silicon Substrates

(ng detected; blq = below limit of quantitation)

	<u>benzene</u>	<u>toluene</u>	<u>aniline</u>	<u>phenol</u>
blank chip	2.9 (+/- 0.6)	8.2 (+/- 0.5)	blq	blq

substrates vapor-coated with GC phases

(a) 30 minute vapor-phase deposition;

(b) 3 hour vapor-phase deposition

	<u>benzene</u>	<u>toluene</u>	<u>aniline</u>	<u>phenol</u>
OV-25 (a)	3.1 (+/- 0.2)	8.4 (+/- 0.2)	7.4 (+/- 0.6)	6.1 (+/- 0.3)
OV-25 (b)	3.2 (+/- 0.3)	8.6 (+/- 0.2)	11.5 (+/- 0.3)	8.3 (+/- 0.3)
SP-2340 (a)	3.1 (+/- 0.1)	7.9 (+/- 0.2)	9.9 (+/- 0.4)	12.2 (+/- 0.4)
SP-2340 (b)	5.5 (+/- 0.5)	12.2 (+/- 0.5)	122.4 (+/- 9.8)	105.2 (+/- 7.1)

LC phases coated by bonding reaction

	<u>benzene</u>	<u>toluene</u>	<u>aniline</u>	<u>phenol</u>
octadecylsilane	2.9 (+/- 0.3)	27.4 (+/- 0.7)	blq	blq
phenylsilane	3.2 (+/- 0.4)	16.0 (+/- 0.5)	11.6 (+/- 0.9)	7.3 (+/- 0.6)

organic analytes also showed an appreciable affinity for glass silica fibers in earlier experiments with solid-phase microextraction fibers (75).

Coating substrates with OV-25 apparently did not result in a significant increase in the amount of benzene and toluene adsorbed. However, aniline and phenol did exhibit a modest affinity for this phase though these amounts adsorbed are very near the minimum quantitative limit of this method. Furthermore, increasing the phase deposition time by a factor of 6 did very little in increasing the amount of analyte adsorbed from solution.

Slightly better performance was observed for substrates coated with SP-2340. A modest increase in affinity for benzene and toluene is observed for the thicker film but more interesting to note is the very large enhancement in affinity for aniline and phenol by the thicker film. These results are in agreement with the McReynolds constants for these phases which suggest that SP-2340 does indeed have a higher affinity for polar analytes; the McReynolds values for SP-2340 are much higher than for OV-25 (126). Another interesting trend is that, as with OV-25, an improvement in selectivity for aniline also is apparent for the thicker film.

Both LC silane phases indicated a significant enhancement in selectivity for toluene relative to the blank specimen and the GC phases. This was particularly true for the octadecylsilane phase. This would be expected as this is the most non-polar phase and toluene is the most non-polar compound of the four analytes. For both of these LC phases, the affinity for aniline and phenol

was quite modest, especially for the octadecylsilane in which these analytes could not be identified.

The limited ellipsometry data provided is listed in Table 6.2. The vapor-deposition method was fairly precise in depositing equal amounts of OV-25 and SP-2340 onto the silicon substrates. Interesting to note is the fact that a 6-fold increase in deposition time only doubled the thickness of the deposited phase. This may indicate that there is a limit to vaporization of these GC phases. This preliminary data suggest that perhaps the maximum vaporization of this phase occurred within the first hour of deposition and that continued heating of the phase did not appreciably generate additional fumes. This limitation may be temperature dependent; that is, the starting vaporization temperature may have been too high and, thus, the majority of the sample was rapidly vaporized. Another possibility is that this process is limited by the amount of starting material. A small dish of only a few grams was placed in the vaporization oven so complete depletion of the volatile components may have readily occurred within the first hour. Perhaps a larger sample aliquot would have resulted in a thicker film.

Distribution coefficients were calculated and are also listed in Table 6.2. For SP-2340, there is a large increase in the distribution coefficient for the polar compounds (aniline and phenol) into this polar phase. For the other distribution coefficients, there does not appear to be any evidence indicating that a doubling of the film thickness doubles the uptake of analyte by these films. This suggests

Table 6.2: Film Thickness and Distribution Coefficients for GC Phases

A: film thickness (nm) of substrates vapor-coated with GC phases

	30 minutes	3 hours
OV-25	4.2 (+/- 0.1)	~ 8.4
SP-2340	3.6 (+/- 0.1)	~ 7.2

film on substrates coated for 3 hours showed a non-uniform refractive index; therefore, a definitive thickness measurement was not possible but appeared to be about twice as thick as the 30-minute films

B: distribution coefficients for substrates coated for (a) 30 minutes and

(b) 3 hours

	benzene	toluene	aniline	phenol
OV-25 (a)	3.3	8.8	4.9	4.1
OV-25 (b)	1.7	4.5	6.0	4.4
SP-2340 (a)	3.9	9.9	12.4	15.3
SP-2340 (b)	3.4	7.6	76.5	65.8

$$\text{distribution coefficients (D)} = \frac{\left(\frac{m_f}{V_f}\right)}{\left(\frac{m_s}{V_s}\right)}$$

where m_f and m_s are the mass amounts of analyte adsorbed on the film and in the probe solution; V_f and V_s are the volumes of the film (surface area x thickness) and the analyte solution being probed, respectively

that perhaps surface area rather than film thickness is most important in predicting the amount of analyte adsorbed by these stationary phases.

Conclusions

The goals of this research were to evaluate methods of phase deposition and to perform cursory evaluations of affinity and selectivity of a few selected phases for a few selected analytes. Clearly, SEM examinations indicate that the immobilization methods employed result in relatively uniform films. However, there is also evidence that some improvement is necessary. SEM micrographs still indicate small amounts of debris on the surface which indicate cleaner procedures are necessary during the cleaning, drying, deposition, and storage of coated substrates. Another possible method to utilize for substrate preparation is plasma cleaning (127). In this method, substrates are cleaned in a low-pressure chamber suitable to maintain an air, nitrogen, or oxygen plasma. Typical cleaning times are 15-20 minutes and remarkable reductions in contact angles have been reported (127). However, this method may roughen the surface of the substrate which would prove to be very problematic for cleaning delicate cantilevers used for microsensors.

Additional methods for preparing thin films may be evaluated. For example, spin-coating films onto substrates have been reported (128-130). In this technique, a solution is applied to the substrate and a relatively slow spinning rate (ca. 500 rpm) is applied to wet the surface. Next, a much faster spinning rate is applied (ca. 4000 rpm) in order to expel the bulk of the fluid. This rapid

spinning is maintained for several minutes as the solvent evaporates and leaves a thin, uniform film on the surface. Film thickness can be controlled by several factors including spin-rate, time of spinning, and the concentration and volume of the deposited solution (131). There are several factors which influence the effectiveness of this method. For example, a very clean surface is imperative to avoid many defects such as comets, chuck marks, edge effects, and striations (132). Also, the deposited solution must wet the surface completely or incomplete coverage can result (132). The geometric configuration of microcantilevers may preclude the use of spin-coating to coat these substrates.

Operating GC/MS in the SIM mode facilitated modest sensitivity but further improvements in sensitivity may be necessary if this method of analysis will be employed when this research is scaled down to the size required for cantilevers. Reducing the number of ions monitored by the quadrupole MS will improve detection sensitivity. Also, modifying the GC method to enhance efficiency and resolution will also result in improved sensitivity.

The preliminary data included here does indicate that the chemical nature of the phase does have an affect on the affinity and selectivity for this representative group of organic compounds. It was assumed that vaporization of the GC phases does not appreciably alter the chemical nature of the phase; that is, the vaporization of OV-25 results in a deposited film of the same chemical composition as the starting material. This assumption is based on the fact that the temperature used for vaporization was not above the maximum operating temperature specified by the vendor. To assess the validity of this assumption, a

profiling mass spectrometry method such as secondary-ion MS to characterize the deposited films would be desirable.

The ellipsometry data indicates that vapor-phase deposition does indeed deposit a thin film onto silicon substrates. Furthermore, the data may also suggest that surface area rather than film thickness may be more relevant in determining the amount of analyte adsorbed by the films. However, the distribution coefficients for aniline and phenol into the SP-2340 phase contradict this assumption. Clearly, further evaluation is necessary before a definitive discussion on surface area vs. film thickness can be presented.

Again, this was a cursory examination of a just a few phases and a few analytes. Using the developed methodology described in this chapter, additional phases of differing polarities can be examined. Careful examination of McReynolds constants may be used in selecting a particular GC phase for target analytes. Also, as different phases are selected for evaluations, so too can the selection of semivolatile organic analytes be expanded.

Although the reported affinity and selectivity of these phases was modest, it still suggests the feasibility of using these phases towards a generalized approach to sensing. Again, in a higher-order sensor, modest selectivity may be sufficient if spectroscopic characterization of the adsorbed species is also utilized. Clearly, further development and evaluation of this technology is warranted.

References

1. A. Tiselius, *Thesis*, Uppsala University, Uppsala, Sweden (1930)
2. T. Hager, *Force of Nature: The Life of Linus Pauling*, Simon & Shuster: New York, 1995, p. 333.
3. S. Hjerten *Arkiv. Kemi.* (1958) 13
4. S. Hjerten *Chromatogr. Rev.* 9 (1967) 122-125
5. R. Virtanen *Acta Polytech. Scand.* 123 (1974) 1-67
6. F.E.P. Mikkers, F.M. Evaraerts, T.P. Verheggen *J. Chromatogr.* 169 (1979) 11-20
7. J. Jorgenson, K.D. Lukacs *Anal. Chem.* 53 (1981) 1298-1302
8. T.M. Olefirowicz, A.G. Ewing in *Capillary Electrophoresis: Theory and Practice*; P.D. Grossman and J.C. Colburn, Eds.; Academic Press, Inc.: San Diego, 1992, pp 45-86.
9. S.C. Jacobson, R. Hergenroder, L.B. Koutny, J.M. Ramsey *Anal. Chem.* 66 (1994) 1114-1118
10. S.C. Jacobson, C.T. Culbertson, J.E. Daler, J.M. Ramsey *Anal. Chem.* 70 (1998) 3476-3480
11. Y.H. Lee, R.G. Maus, B.W. Smith, J.D. Winefordner *Anal. Chem.* 66 (1994) 4142-4149
12. D. Chen, N.J. Dovichi *Anal. Chem.* 68 (1996) 690-696
13. R. Weinberger in *Practical Capillary Electrophoresis*; Academic Press, Inc.: San Diego, 1993, pp 18-22.

14. P.W. Atkins in *Physical Chemistry*; W.H. Freeman: New York, 1990, pp 287.
15. J. Kennedy in *Analytical Chemistry, 4th ed.*; W.H. Freeman and Company: New York, 1990, pp 734.
16. R. Weinberger in *Practical Capillary Electrophoresis*; Academic Press, Inc.: San Diego, 1993, pp 61.
17. J.C. Giddings in *Unified Separation Science*; John Wiley & Sons, Inc.: New York, 1991, pp 91.
18. R. Weinberger in *Practical Capillary Electrophoresis*; Academic Press, inc.: San Diego, 1993, pp 200.
19. D.J. Rose, J.W. Jorgenson *Anal. Chem.* 60 (1988) 642-645
20. K.K.C. Yeung, C.A. Lucy *Anal. Chem.* 69 (1997) 3435-3441
21. S. Terabe, K. Otsuka, K. Ichikawa, Tsuchiya, T. Ando *Anal. Chem.* 56 (1984) 111-113
22. E.S. Yeung, W.G. Kuhr *Anal. Chem.* 63 (1991) 275A-282A
23. R. Weinberger in *Practical Capillary Electrophoresis*; Academic Press, Inc.: San Diego, 1993, pp 37-75.
24. J. Kennedy in *Analytical Chemistry, 4th ed.*; W.H. Freeman and Company: New York, 1990, pp 398.
25. J. Kennedy in *Analytical Chemistry, 4th ed.*; W.H. Freeman and Company: New York, 1990, pp 467.
26. D.F. Swaile, M.J. Sepaniak *Anal. Chem.* 63 (1991) 179-184
27. B.K. Clark, M.J. Sepaniak *J. Microcolumn Sep.* 5 (1993) 275-282

28. D.J. Rose, J. Jorgenson *J. Chromatogr.* 447 (1988) 117-131
29. R. Dadoo, L.A. Colon, R.N. Zare *J. High Res. Chromatogr.* 15 (1992) 133-135
30. A.L. Shapiro, E. Vinuela, J.V. Maizel *Biochem. Biophys. Res. Commun.* 28 (1967) 815-820
31. S. Hjerten *J. Chromatogr.* 270 (1983) 1-6
32. S. Hjerten *J. Chromatogr.* 347 (1985) 191-198
33. A.S. Cohen, B.L. Karger *J. Chromatogr.* 397 (1987) 409-417
34. P.D. Grossman, D.S. Soane *J. Chromatogr.* 559 (1991) 257-266
35. comment by J. Olechno at HPCE, 1989
36. E. Yeung in *High-Performance Capillary Electrophoresis: Theory, Techniques, and Applications*; M. Khaladi, Ed.; John Wiley and Sons, Inc: New York, 1998, pp 767-8.
37. M. Gilges, H. Husmann, M.H. Kleemib, S.R. Motsch, G. Schomberg *J. High Res. Chrom.* 15 (1992) 454-457
38. J.K. Towns, J. Bao, F.E. Regnier *J. Chromatogr* 599 (1992) 227-237
39. W. Nashabeh, Z.E. Rassi *J. Chromatogr.* 559 (1991) 367-383
40. M.H.A. Busch, J.C. Kraak, H. Poppe *J. Chromatogr. A* 695 (1995) 287-296
41. G.J.M. Bruin, J.P. Chang, R.H. Kulman, K. Zegers, J.C. Kraak, H. Poppe *J. Chromatogr.* 471 (1989) 429-438
42. M. Chen, R.M. Cassidy *J. Chromatogr.* 602 (1992) 227-234
43. E.N. Fung, E.S. Yeung *Anal. Chem.* 67 (1995) 1913-1921

44. D. Schmalzing, C.A. Piggee, F. Foret, E. Carrilho, B.L. Karger *J. Chromatogr. A* 652 (1993) 149-155
45. M. Strege, A. Lagu *Anal. Chem.* 63 (1991) 1233-1236
46. S. Hjerten, K. Kubo *Electrophoresis* 14 (1993) 390-395
47. H. Engelhardt, M.A. Cunat-Walter *J. Chromatogr. A* 716 (1995) 27-33
48. T.L. Rapp, W.K. Kowalchyk, K.L. Davis, E.A. Todd, K. Liu, M.D. Morris *Anal. Chem.* 64 (1992) 2434-2437
49. X. Huang, L.J. Doneski, M.J. Wirth *Anal. Chem.* 70 (1998) 4023-4029
50. S. Kaupp, R. Steffen, H. Watzig *J. Chromatogr. A* 744 (1996) 93-101
51. B.A. Siles, G.B. Collier *J. Capillary Electro.* 6 (1996) 313-321
52. T.J. Gibson, M.J. Sepaniak *J. Chromatogr. B* 695 (1997) 103-111
53. T.J. Gibson, M.J. Sepaniak *J. Capillary Electro.* 5 (1999) 73-80
54. M.A. Stebbins, J.B. Davis, B.K. Clark, M.J. Sepaniak *J. Microcol. Sep.* 8 (1996) 485-494
55. S.J. Hubert, G.W. Slater *Electrophoresis* 16 (1995) 2137-2142
56. J.L. Viovy, T. Duke *Electrophoresis* 14 (1993) 322-329
57. L. Stryer, *Biochemistry, 3rd Ed.*, W.H. Freeman and Co.: New York, 1988
58. A.E. Barron, H.W. Blanch, D.S. Soane *Electrophoresis* 15 (1994) 597-615
59. M.V. Olson *J. Chromatogr.* 470 (1989) 377-389
60. Y. Baba, T. Matsuura, K. Wakamoto, M. Tsuchiko *J. Chromatogr.* 558 (1991) 273-281
61. Y. Walbroehl, J.W. Jorgenson *J. Microcolumn Sep.* 1 (1989) 49
62. B.K. Clark, T. V-Dihn, M.J. Sepaniak *Anal. Chem.* 67 (1995) 680-684

63. J.A. Luckey, T.B. Norris, L.M. Smith *J. Phys. Chem.* 97 (1993) 3067-3071
64. M.S. Bello, R. Rezzonico, P.G. Righetti *Science* 266 (1994) 773-776
65. G.W. Slater, P. Mayer, P.D. Grossman *Electrophoresis* 16 (1995) 75
66. P.G. Righetti in *Capillary Electrophoresis in Analytical Biotechnology*, P.G. Righetti, Ed.; CRC Press: Boca Raton, 1996.
67. H.E. Schwartz, K.J. Ulfelder *Anal. Chem.* 64 (1992) 1737-1740
68. A.N. Glazer, H.S. Rye *Nature* 359 (1992) 859-861
69. H.S. Rye, S. Yue, D.E. Wemmer, M.A. Quesada, R.P. Haugland, R.A. Mathies, A.N. Glazer *Nucl. Acids Res.* 20 (1992) 2803-2812
70. H.S. Rye, A.N. Glazer *Nucl. Acids Res.* 23 (1995) 1215-1222
71. C. Carlsson, M. Jonsson, B. Akerman *Nucl. Acids Res.* 23 (1995) 2413-2420
72. H. Zhu, S.M. Clark, S.C. Benson, H.S. Rye, A.N. Glazer, R.A. Mathies *Anal. Chem.* 66 (1994) 1941-1948
73. D. Figeys, E. Arriaga, A. Renborg, N.J. Dovichi *J. Chromatogr. A* 669 (1994) 205-216
74. Y. Kim, M.D. Morris *Anal. Chem.* 66 (1994) 1168-1174
75. T.J. Gibson *unpublished results*
76. H.E. Schwartz, K. Ulfelder, F.J. Sunzeri, M.P. Busch, R.G. Brownlee *J. Chromatogr.* 559 (1991) 267-283
77. A. Guttman, N. Cooke *Anal. Chem.* 63 (1991) 2038-2042
78. S.M. Clark, R.A. Mathies *Anal. Chem.* 69 (1997) 1355-1363

79. W.F. Nirode, T.D. Staller, R.O. Cole, M.J. Sepaniak *Anal. Chem.* 70 (1998) 182-186
80. R. Weber *Helv. Chim. Acta.* 36 (1953) 424-434
81. X.C. Le, J.Z. Xing, Q. Wan, T. Carnelly, M. Ma, J. Lee, M. Weinfeld, S.A. Ledon *HPCE '99* (1999)
82. Y. Kiba, Y. Baba *HPCE '99* (1999)
83. A. Guttman, R. Nelson, N. Coocke *J. Chromatogr.* 593 (1992) 297-303
84. K. Hebenbrock, P.M. Williams, B.L. Karger *Electrophoresis* 16 (1995) 1429-1436
85. R.A. Mathies, X.C. Huang, M.A. Quesada *Anal. Chem.* 64 (1992) 2149-2155
86. B. Ekstrom, G. Jacobson, O. Ohman, H. Sjodin *Adv. Chromatogr.* 33 (1990) 1-9
87. C.S. Effenhauser, A. Paulis, A. Manz, H.M. Widmer *Anal. Chem.* 66 (1994) 2949-2955
88. B.B. Ward, A.R. Cockcroft, K.A. Kilpatrick *J. Gen. Microbio.* 139 (1993) 2285-2293
89. P.A.E. Piunno, U.J. Krull, R.H.E. Hudson, M.J. Damha, H. Cohen *Anal. Chem.* 67 (1995) 2635-2643
90. D.P. Allison, T. Thundat, K.B. Jacobson, L.A. Bottomley, R.J. Warmack *J. Vac. Sci. Technol. A* 11 (1993) 816-819
91. D.T. Breslin, J.E. Coury, J.R. Anderson, L. McFail-Isom, L.D. Williams, L.A. Bottomley, G.B. Schuster *J. Am. Chem. Soc.* 119 (1997) 5043-5044

92. B. Guo *Anal. Chem.* 71 (1999) 333R-337R
93. J. Janata, M. Josowicz, P. Vanysek, D.M. DeVaney *Anal. Chem.* 70 (1998) 179R-208R
94. W. Tan, Z.Y. Shi, S. Smith, D. Birnbaum, R. Kopelman *Science* 258 (1992) 778-781
95. D.J. Dobson, S. Saini *Anal. Chem.* 69 (1997) 3532-3538
96. A.L. Jenkins, O.M. Uy, G.M. Murray *Anal. Chem.* 71 (1999) 373-378
97. J. Lerchner, J. Seidel, G. Wolf, E. Weber *Sens. Actuators B* 32 (1996) 71-75
98. J. Janata, *Principles of Chemical Sensors* Plenum Press: New York, 1989
99. C. Raman-Suri, G.C. Mishra *Biosens. Bioelectron.* 11 (1996) 1199-1207
100. G. Sauerbrey *Z. Phys.* 155 (1959) 206-212
101. T.D. James, K.R.A.S. Sandanayake, R. Iguchi, S. Shinkai *J. Am. Chem. Soc.* 117 (1995) 8982-8987
102. A.P.d. Silva, H.Q.N. Gunaratne, A.T.M. Kane, G.E.M. Maguire *Chem. Lett.* 2 (1995)
103. T. Ishiji, K. Kudo, M. Kaneko *Sens. Actuators, B* 22 (1994) 205-210
104. Q. Chang, J. Sipor, J.R. Lakowicz, G. Rao *Anal. Biochem.* 232 (1995) 92-97
105. T.D. James, K.R.A.S. Sandanayake, S. Shinkai *Nature* 374 (1995) 345-347
106. R. Wang, U. Narang, N. Prasad, F.V. Bright *Anal. Chem.* 65 (1993) 2671-2675

107. M.T. Cygan, G.E. Collins, T.D. Dunbar, D.L. Allara, C.G. Gibbs, C.D. Gutsche *Anal. Chem.* 71 (1999) 142-148
108. W. Schramm, S.H. Paek, G. Voss *Immunomethods* 3 (1993) 93-103
109. F.L. Dickert, S. Thierer *Adv. Mater.* 8 (1996) 987-990
110. H.W. Hellinga in *Protein Engineering: Principles and Practice*; J.L. Cleland and C.S. Craik, Eds.; Wiley-Liss: New York, 1996, pp 369-398.
111. J. Raba, H.A. Mottola *Crit. Rev. Anal. Chem.* 25 (1995) 1-42
112. M. Yang, M.E. McGovern, M. Thompson *Anal. Chim. Acta* 346 (1997) 259-275
113. G. Gillen, S. Wight, J. Bennett, M.J. Tarlov *Appl. Phys. Lett.* 65 (1994) 534-536
114. G. Wittstock, R. Hesse, W. Schuhmann *Electroanalysis* 9 (1997) 746-750
115. P. Tejedor, F. Briones *Appl. Phys. Lett.* 64 (1994) 936-938
116. J.R. Barnes, R.J. Stephenson, C.N. Woodburn, S.J. O'Shea, M.E. Welland, T. Rayment, J.K. Gimzewski, C. Gerber *Rev. Sci. Instrum.* 65 (1994) 3793-3798
117. J.R. Barnes, R.J. Stephenson, M.E. Welland, C. Gerber, J.K. Gimzewski *Nature* 372 (1994) 79-81
118. V.T. Binh, N. Garcia, A.L. Levanuk *Surf. Sci. Lett.* 301 (1994) 224-228
119. F.L. Dickert, U.P.A. Baumler, H. Stathopoulos *Anal. Chem.* 69 (1997) 1000-1005
120. P.G. Datskos, M.J. Sepaniak *DOE Proposal* (1998)

121. B. Arkles in *Silicon, Germanium, Tin and Lead Compounds, Metal Alkoxides, Diketonates and Carboxylates: A Survey of Properties and Chemistry, 2nd Ed.*; Gelest, Inc.: Tullytown, PA, 1998, pp 88-89.
122. F. Pintchovski, J.B. Pricw, P.J. Peavey, K. Kobold *J. Electrochem. Society* 126 (1979) 1428-1433
123. J.H. Moon, J.W. Shin, S.Y. Kim, J.W. Park *Langmuir* 12 (1996) 4621-4624
124. H.C. Lee, R.E. Gaensslen *Advances in Fingerprint Technology* CRC Press: Boca Raton, FL, 1994
125. B. Buszewski, A. Jurasek, J. Garaj, L. Nondek, I. Novak, D. Berek *J. Liquid Chrom.* 10 (1987) 2325-2336
126. copyrighted information provided by Supelco, Bellefonte, PA, USA
127. J.W. Grate, R.A. McGill *Anal. Chem.* 67 (1995) 4015-4019
128. E. Wang, M.E. Meyerhoff, V.C. Yang *Anal. Chem.* 67 (1995) 522-527
129. D.L. Ellis, M.R. Zakin, L.S. Bernstein, M.F. Rubner *Anal. Chem.* 68 (1996) 817-822
130. M.D. Petit-Dominguez, H. Shen, W.R. Heineman, C.J. Seliskar *Anal. Chem.* 69 (1997) 703-710
131. D. Meyerhofer *J. Appl. Phys.* 49 (1978) 3993-3997
132. D.P. Birnie, www.mse.arizona.edu/faculty/birnie, 1994

Appendix

Method information for GC/MS method TGAROM3.M

HP6890 GC METHOD

OVEN

Initial temp: 40 °C

Initial time: 2 minutes

Equilibration time: 0.50 min

Ramps:

#	Rate	Final temp	Final time
1	5.00	55	0.00
2	10.00	75	0.00
3	2.00	85	0.00
4	20.00	200	0.00
5	0.0 (Off)		

Post temp: 0 °C

Post time: 0.00 min

Run time: 17.75 min

FRONT INJECTOR (MANUAL)

Mode: splitless

Initial temp.: 250 °C (on)

Pressure: 7.1 psi (on)

Purge flow: 50.0 ml/min

Purge time: 0.00 min

Total flow 53.8 ml/min

Gas type: Helium

COLUMN 1

Capillary column

Model Number: HP 19091S-433

HP-5MS 5% Phenyl Methyl Siloxane

Max temperature: 325 °C

Nominal length: 30.0 m

Nominal diameter: 250.00 µm

Nominal film thickness: 0.25 µm

Mode: constant flow

Initial flow: 1.0 ml/min

Nominal init pressure: 7.1 psi

Average velocity: 36 cm/sec

Inlet: Front Inlet

Outlet: MSD

Outlet pressure: vacuum

SIGNAL 1

Data rate: 20 Hz

Type: test plot

Save data: Off

Zero: 0.0 (Off)

Range: 0

Fast Peaks: Off

Attenuation: 0

THERMAL AUX 1

Use: MSD Transfer Line Heater

Description: Transfer Line

Initial temp: 270 °C

Initial time: 0.00 min

#	Rate	Final temp	Final time
1	0.00 (Off)		

FRONT INJECTOR (NOT INSTALLED)

HP5973 MSD METHOD

=====

Acquisition mode: SIM

Solvent delay: 2.00 min

Resulting EM voltage: 1152.9

GROUP 1

Resolution: high

Ions: Mass, 94.0; Mass, 93.0; Mass, 91.0; Mass, 78.0

MS Quad: 106 C

MS Source: 230 C

Vita

Tim Gibson was born in Inverness, Florida in 1967. He was raised in the nearby town of Dunnellon and graduated from Dunnellon High School in 1985. After serving in the US Army, he returned to Florida to attend the University of West Florida where, in 1992, he graduated with a B.S. in Chemistry/Biochemistry. He was employed at the US EPA research laboratory in Gulf Breeze, Florida, for two years before moving to Knoxville in 1994 to begin his graduate studies at the University of Tennessee under the direction of Michael J. Sepaniak. Upon earning his Ph.D. in Chemistry in July 1999, he will be employed at Magellan Laboratories, Research Triangle Park, North Carolina.